Louisiana State University
LSU Digital Commons

LSU Doctoral Dissertations | Graduate School

April 2020

Phytosampling of Ambient Air Particulate Matter (PM) -New Method of PM-Associated Pollution Characterization

Chuqi Guo
Louisiana State University and Agricultural and Mechanical College

Follow this and additional works at: https://digitalcommons.lsu.edu/gradschool_dissertations

Recommended Citation

Guo, Chuqi, "Phytosampling of Ambient Air Particulate Matter (PM) -New Method of PM-Associated Pollution Characterization" (2020). *LSU Doctoral Dissertations*. 5209.
https://digitalcommons.lsu.edu/gradschool_dissertations/5209

This Dissertation is brought to you for free and open access by the Graduate School at LSU Digital Commons. It has been accepted for inclusion in LSU Doctoral Dissertations by an authorized graduate school editor of LSU Digital Commons. For more information, please contactgradetd@lsu.edu.

PHYTOSAMPLING OF AMBIENT AIR PARTICULATE MATTER (PM) - NEW METHOD OF PM-ASSOCIATED POLLUTION CHARACTERIZATION

A Dissertation

Submitted to the Graduate Faculty of the
Louisiana State University and
Agricultural and Mechanical College
in partial fulfillment of the
requirements for the degree of
Doctor of Philosophy

in

The Department of Environmental Sciences

by
Chuqi Guo
B.S., Tianjin University of Technology, 2014
May 2020

ACKNOWLEDGEMENTS

I would like to express my gratitude and appreciation to my advisor, Dr. Slawo Lomnicki, who offered me this great opportunity to join his group and be an LSU tiger. I am so grateful to him for all his guidance and mentoring throughout my whole journey to pursue a doctoral degree. I would like to thank and acknowledge the guidance and support from my committee members: Dr. Kevin Armbrust, Dr. Margaret Reams and Dr. Shaomian Yao. Thank you all for your valuable time to serve on my committee.

Much appreciation also to Dr. Stephania Cormier and Dr. Tammy Dugas for their help on my research and to LSU Superfund Research Center for providing me a lot of good opportunities to learn more things from different trainings and to communicate with other researchers in the field.

I am grateful to Dr. Lavrent Khachatryan for all the valuable suggestions in my research, Dr. Albert Leo N. dela Cruz for helping me start my project, Dr. Farhana Hasan for always being there to answer any of my questions, Dean Lay for explaining everything about the instrument with great patience, Dr. Xia Guan for not only helping me in my research but being a good friend and caring about my life, and Dr. Ajit Ghimire for sharing everything he knows generously. I am also thankful to Dr. Phillip Potter, Dr. Rafael Cueto, Thomas Blanchard, Ms. Charlotte G. St. Romain, and all my colleagues in LSU Superfund Research Center and the Department of Environmental Sciences. I am so glad that I have met you and worked with you during my Ph.D. journey.

I would like to acknowledge the financial support from National Institute of Environmental Health Sciences and LSU Superfund Research Center.

Finally, I would like to thank my family and my friends for all your support and encouragement. I cannot even imagine being here and accomplishing my Ph.D. without all of you.

TABLE OF CONTENTS

LIST OF ABBREVIATIONS

PM	Particulate Matter
COPD	Chronic Obstructive Pulmonary Disease
PAHs	Polycyclic Aromatic Hydrocarbons
CHCs	Chlorinated Hydrocarbons
BHCs	Brominated Hydrocarbons
EPFRs	Environmentally Persistent Free Radicals
ROS	Reactive Oxygen Species
2-MCP	2-Monochlorophenol
1,2-DCB	1,2-Dichlorobenzene
ENMs	Engineered Nanomaterials
SOD	Superoxide Dismutase
CAT	Catalase
CNS	Central Nervous System
RCRA	U.S. Federal Resource Conservation and Recovery Act
NESHAP	National Emission Standards for Hazardous Air Pollutants
EPA	Environmental Protection Agency
CAA	Clean Air Act
MACT	Maximum Achievable Control Technology
SEM	Scanning Electron Microscope
EDS	Energy Dispersive X-ray Spectroscopy
EPR	Electron Paramagnetic Resonance
DPPH	2,2-diphenyl-1-picrylhydrazyl

DMPO	5,5-dimethyl-1-pyrroline N-oxide
BMPO	5-tert-butoxycarbonyl-5-methyl-1-pyrroline N-oxide
PBS	Phosphate Buffered Saline
GC	Gas Chromatography
MS	Mass spectrometry
EI	Electron Ionization
CI	Chemical Ionization
ESI	Electron Spray Ionization
SIM	Selective Ion Monitoring
MRM	Multiple Reaction Monitoring Scan
BEAS-2B	Human Bronchial Epithelial Cells
ATP	Adenosine Triphosphate
AMP	Adenosine Monophosphate
ICP	Inductively Coupled Plasma
OES	Optical Emission Spectrometry
RF	Radio Frequency

ABSTRACT

Ambient air particulate matter (PM) has been documented to be a contributor to a lot of pollution-related health effects. Due to the common anthropogenic origin, PM could be an effective vehicle to carry and deliver many toxic materials, including environmentally persistent free radicals (EPFRs) and polycyclic aromatic hydrocarbons (PAHs) into the human body, thus significantly raise the health risk of PM exposure. Studies of ambient air PM potentially bear artifacts stemming from the collection methods. We investigated the effects of collection methods on the ambient air PM composition and developed a static collection method relying on the particle entrapment by the plant's leaf through electrostatic interactions and surface trichomes ("phytosampling"). This method allows for easy particle recovery from the matrix, collection under natural environmental conditions, and enables a dense collection network to represent spatial pollutants distribution more accurately. The experimental results show that the new "phytosampling" method is an effective method to collect PM from ambient air. And the PM retrieving process does not compromise the leaf integrity. On phytosampling collected PM, we detected relatively more potassium and calcium, the larger contribution of oxygen-centered EPFRs, different decay behavior, more consistent PAHs distribution between PM sizes, and less toxicological effects in cell viability test compared to the standard sampling method PM samples. These results indicate that the phytosampling method could prevent some unpredictable changes during PM collection, and collected PM will be more representative as the PM that the general public is exposed to. However, phytosampling cannot evaluate the absolute PM concentration in the air, so it serves as an excellent supplementary tool to work in conjunction with the standard PM collection method. This method has been successfully applied to field studies.

CHAPTER 1. INTRODUCTION

1.1. Particulate Matter

1.1.1. Background of Particulate Matter and Its Health Impacts

Particulate matter (PM) is one of the National Ambient Air Quality Standards (NAAQS) criteria pollutants. According to the size fractions, airborne particles are characterized as particles whose aerodynamic diameter (d_a) is between 10 μm and 100 μm, coarse particles ($d_a \leq 10$ μm), fine particles ($d_a \leq 2.5$ μm) and ultrafine particles ($d_a \leq 0.1$ μm)[1,2]. Upon inhalation, particles smaller than 10 μm deposit at different parts of human respiratory tract according to their size fractions[3,4], with ultrafine particles are able to translocate through circulation systems to various organs, and even to the brain[5,6].

Ambient air particulate matter (PM) is one of the major contributors to the pollution-related health effects. The data from the World Health Organization shows that about three million deaths were attributed to the ambient air PM globally in 2012. 87% of these deaths occurred in the countries with low or middle income, and around 6% of total deaths are children under five years with acute lower respiratory diseases[7]. Moreover, their model also shows that 92% of the world population were experiencing a higher $PM_{2.5}$ exposure level than WHO Air Quality Guidelines (annual mean (10 $\mu g/m^3$))[7]. Numerous studies have shown that the exposure to PM, especially to fine ($d_a \leq 2.5$ μm) and ultrafine ($d_a \leq 0.1$ μm) particles are responsible for morbidity and mortality of some respiratory and cardiovascular diseases, including asthma, pneumonia, chronic obstructive pulmonary disease (COPD), lung cancer and cardiac arrhythmias[4,8–13]. To control the fine particle emission and mitigate the health impacts due to the inhalation of $PM_{2.5}$, different countries and organizations have their air quality standard concerning $PM_{2.5}$. Table 1.1 compares the current $PM_{2.5}$ air quality standard among the United States[14], the World Health Organization (WHO)[15],

the European Union (E.U.)[16], and the People's Republic of China[17]. Besides the health impact, PM also has some ecological influences such as affecting global radiative budget[18,19] and visibility[19,20].

Table 1.1. Comparison of $PM_{2.5}$ air quality standard among the U.S., WHO and China.

	U.S.	WHO	E.U.	China
Annual	Primary: 12.0 μg/m^3	10 μg/m^3	25 μg/m^3	Grade-I[a]: 15 μg/m^3
	Secondary: 15.0 μg/m^3			Grade-II: 35 μg/m^3
24 hr	35 μg/m^3	25 μg/m^3		Grade-I: 35 μg/m^3
				Grade-II: 75 μg/m^3

[a]: Grade I & II are corresponded to ambient air functional zones. Grade-I applies to the zones that require special protection, including nature reserves. Grade-II applies to general zones, including residential area, commercial area, industrial area, and rural area.

*: None of these countries/organizations has standard for ultrafine particles ($PM_{0.1}$).

1.1.2. Sources and Compositions of PM

PM is non-homogenous materials with varying chemical compositions, which are often determined by their origins. PM could be emitted by natural sources such as volcanic eruptions, wildfire, sea spray, and soil dust or result from condensation/reaction of atmospheric components[2]. However, with the decreasing size of PM, the contribution of anthropogenic-born PM is increasing and 70% of $PM_{2.5}$ and >90% of $PM_{0.1}$ result from combustion processes[21–24], including vehicle exhaust and industrial. Some indoor activities such as cooking and cigarette smoking also contribute to the emission of PM. PM is composed of inorganic ions, organic and elemental carbons, crust elements, and metals[19]. Fine and ultrafine particles are effective vehicles for several toxic materials related to a lot of pulmonary and cardiovascular diseases. They could carry and deliver polycyclic aromatic hydrocarbons (PAHs), oxidized forms of polycyclic aromatic hydrocarbons (Oxy-PAHs), chlorinated hydrocarbons (CHCs), brominated hydrocarbons (BHCs), toxic metals, and environmentally persistent free radicals (EPFRs) generated in combustion processed with the presence of redox-active metals[25,26].

1.2. Environmentally Persistent Free Radicals (EPFRs)

1.2.1. Introduction to Environmentally Persistent Free Radicals (EPFRs)

Environmentally persistent free radicals (EPFRs) are a kind of surface-stabilized pollutant that has a much longer life span than normal concerned free radicals[22,27–29] and is therefore environmentally persistent. Most of the fine and ultrafine particles are formed from combustion processes, and EPFRs can be mainly generated through the interaction of transition metal oxide with substituted aromatic compounds on the surface of particles[22,26,30] in the post flame zone and cool zone of a combustion system. These EPFRs associated particles can remain in the atmosphere for a long time and travel for a long distance, which increased the risk of inhalation exposure. The toxicity of EPFRs stems from their persistence in the environment and the ability to generate reactive oxygen species (ROS)[31]. These ROS, such as hydroxyl (•OH), peroxyl (RO_2•), and alkoxyl (RO•) radicals, could induce oxidative stress in biological systems[32–35]. A lot of studies have been done on adverse health effects of PM exposure, however many of the studies presented an oversimplified view of PM as just a carrier of toxic compounds in the beginning, disregarding synergistic effects between PM components resulting in new chemical quality or species. The EPFRs, which is the species resulting from exactly such interaction, started to draw more attention as an overlooked pollutant carried on PM in recent years. And more and more epidemiological studies concerning human exposure to EPFRs on PM were performed to help understand the mechanism of toxicity of EPFRs in biological systems.

1.2.2. Formation and Types of EPFRs

EPFRs have been found in different materials both naturally exist, such as biomass and coal[36,37], and as the products of thermal processes, such as fly ash and soot[38,39]. Considering that the combustion processes are the main source of PM and EPFRs generation, Cormier et al.

illustrated the conditions and areas of the nanoparticles and free radicals generation in a combustion process by the chemical reaction zone theory[40]. In this theory, a combustion process contains four thermal zones: 1. Preflame zone (fuel zone, wide temperature range from ambient to 1200 ºC); 2. Flame zone (>1200 ºC); 3. Postflame zone (1200-600 ºC); 4. Cool zone (<600 ºC). In zone 1, a lot of new reaction intermediates are created. Zone 2 is where most reactions are undergoing that organics covert to their stable thermal products, and vaporized metal and chlorins are generated. In zone 3, many radical-molecule reactions occur. And a lot of pollutants, such as polycyclic aromatic hydrocarbons (PAHs) and brominated hydrocarbons (BHCs), are formed and the vaporized metals condense to the surface of PM. In zone 4, which has a lower temperature, the surface-mediated reactions with transition metals to form EPFRs occur. And the temperature is not high enough to destroy the new-formed pollutants[40]. Although the concept of the persistent free radicals was first introduced in 1950s[41] and detected by Pryor and co-workers in 1970s[42,43], the more detailed and prevailing mechanism of the EPFRs formation has been proposed by Dellinger's group[29]. Based on the calculations and the results of experiments, they proposed that the EPFRs formation mainly contains three stages: physisorption, chemisorption, and electron transfer and delocalization (Scheme 1.1 uses 2-monocholorophenol as a precursor example). In the cool zone of a combustion process, substituted aromatic compounds would physisorb to the surface of a transition metal oxide, and then the chemisorption takes place as eliminating a water and/or hydrogen halide molecule. The final stage is the reduction of the metal and formation of surface-associated EPFRs through the electron transfer to the metal. The unpaired electron on the EPFRs could delocalize resulting in EPFRs with different centers. This mechanism has been verified by following laboratory studies using different molecule precursors, including phenol, hydroquinone, catechol, 2-chlorophenol, monochlorobenzene, and 1,2-dichlorobenzene under

various reaction temperature conditions ranging from 50 ºC to 400 ºC[22]. On the basis of the lab condition test results, CuO (redox potential, catalyst of dioxin formation[44,45] and abundance of Cu in PM[46]) has been picked to be impregnated to the cabosil fumed silica (fine particle size and inert substrate) and exposed to the vapor of 2-monochlorophenol or 1,2-dichlorobenzene (dioxin precursors[22,47–49]. 2-MCP is a typical product of thermal waste treatment[47] and 1,2-DCB is a common compound used in the industrial processed[50]). And through this procedure, surrogate EPFRs containing particles had been made in the lab and applied to several studies to evaluate the toxicological effects of EPFRs containing particles[47,50,51]. Besides this prevailing mechanism, Vejerano et al. proposed another mechanism to try to explain EPFRs' formation under the following conditions: with non-substituted aromatic compounds, without the presence of transition metal and when interacting with ZnO (electron move from metal oxide to the organic compounds)[52]. This new mechanism is applied to the EPFRs formation on the engineered nanomaterials (ENMs) in a combustion or a thermal treatment process. And it is proposed based on the fact that these ENMs are showing a "metallic" characteristic that has lower band gap energy compared to the general EPFRs formed on nanoparticles that supported by a larger particle in combustion systems[52]. This new mechanism provides a new prospect for EPFRs research, but it still requires more studies to be supported.

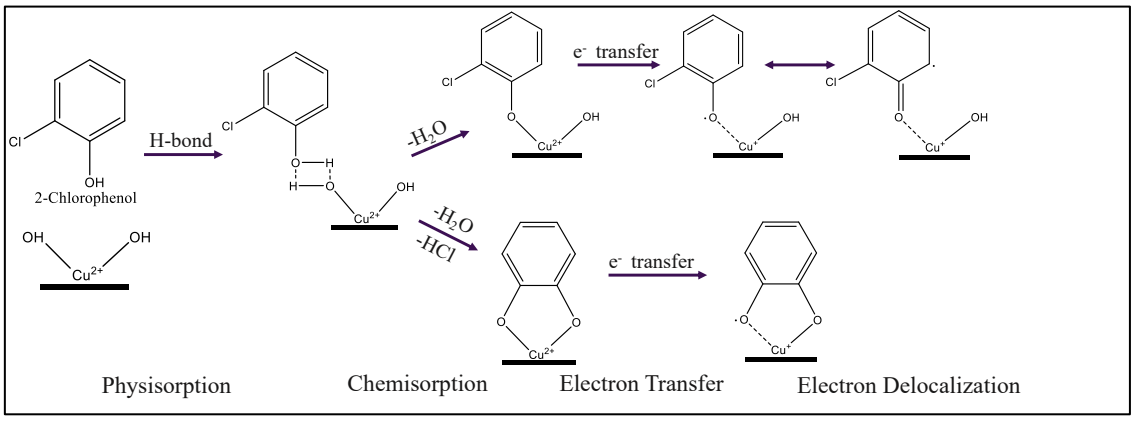

Scheme 1.1. Proposed mechanism of EPFRs formation (2-monochlorophenol on Cu(II)O/Silica)[48,56,136].

Different precursors interact with transition metal oxide and form various EPFRs. The structure of the absorbate, together with the property of absorption site under certain conditions, determine the structure of the newly-formed EPFRs and their different reactivities[22,29]. Because of the delocalization of the unpaired electron, the EPFRs could be carbon-centered or oxygen-centered. And the g-factor of different types of EPFRs, which indicates the nature property of an electron, will not be the same. A higher g-factor indicates that the unpaired electron is closer to an oxygen atom. For carbon-centered radicals, such as phenyl radicals, g-factors are < 2.0030 while for oxygen-centered radicals, such as semiquinone radicals, g-factors are > 2.0040[22,28,29,53,54]. The g-factor of EPFRs from an environmental sample is usually in between, and the spectra of the radicals are broadened, indicating that the unpaired electron is not exclusively centered on carbon or oxygen atoms or the samples contain several different radicals.

1.2.3. Generation of ROS and Cytotoxicity

EPFRs have been proved to generate reactive oxygen species (ROS) such as hydrogen peroxide (H_2O_2), superoxide anion radicals ($O_2•^-$), and hydroxyl radicals (•OH) through several different studies, including an HPLC-based scavenging assay[31], spin-trapping processes[32], and comet assay[33], with application of well-known antioxidant enzymes: superoxide dismutase (SOD)

and catalase (CAT). SOD and CAT could consume superoxide and hydrogen peroxide, respectively. So the decreased detection of ROS generated in the system treated by SOD and CAT in all foregoing studies confirmed the ROS redox cycle[31–33]. The simplified ROS generation redox cycle is shown in Scheme 1.2. Once the EPFRs enter this redox cycle, they can reduce O_2 to produce superoxide, which then, through dismutation, will form hydrogen peroxide. Then at the presence of metal ion on the surface, the Fenton reaction takes place to produce hydroxyl radicals. At the same time, the oxidized form of EPFRs will be reduced back to the initial radicals by the reducing agents in the biological systems[32,33,55–57]. So in this way, ROS could be continuously generated through the cycle. Based on the calculations in the study conducted by Khachatryan et al., after 140 mins of incubation, one EPFR could generate about ten hydroxyl radicals[32]. These surface-associated ROS could induce oxidative stress in the biological system and damage DNA, lipid, and proteins in a living cell[56,58,59]. Considering about high yield of ROS by the redox cycle of EPFRs, a lot of in vitro and in vivo studies have been done on the cytotoxicity and the toxicological effects to the organs and even the whole living body to evaluate the potential health effect of human exposure to the EPFRs containing particles[46,47,50,51,60,61]. Cardiac[60,62–64] and pulmonary[47,50,51,65,66] dysfunction due to inhalation exposure of EPFRs carried PM had been identified, and recent studies focusing on the relationship of PM exposure and the central nervous system (CNS)[67–71] provided a new direction that there may be a causal relationship of EPFRs with neurodevelopment defects.

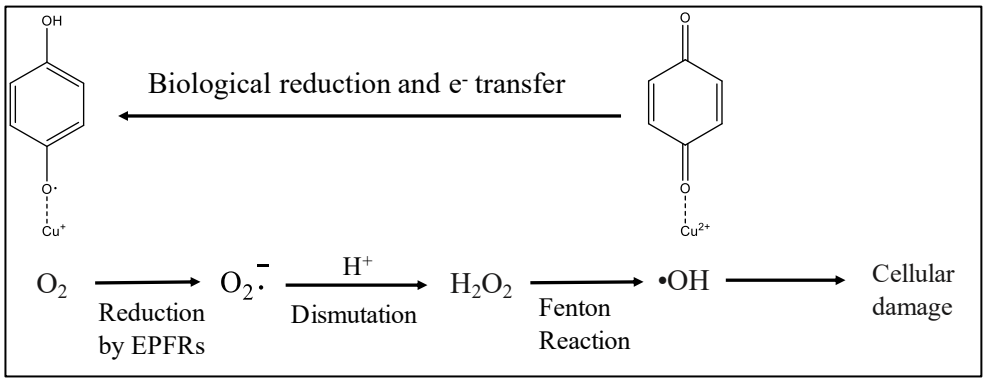

Scheme 1.2. Simplified ROS generation redox cycle.

1.3. Polycyclic Aromatic Hydrocarbons (PAHs)

Polycyclic aromatic hydrocarbons (PAHs) are a group of organic compounds that are comprised of two or more aromatic rings. PAHs are naturally existing in coal, tar, oil, and creosote and could be generated in the incomplete combustion processes[72]. Among all PAHs generation contributors, incomplete combustion (naturally and anthropogenically) is the largest source for PAHs in the environment[72,73]. Human activities, including biomass burning, waste incinerators, vehicle emissions, and some industrial processes (e.g., coal gasification, steel manufacturing, and asphalt manufacturing), are the dominant source of PAHs production[72,74,75]. PAHs are ubiquitously present in the ambient environment. Some small PAHs (2-rings and some 3-rings) are soluble in water, which makes them the pollutants in drinking water[76]. And PAHs with 2-4 rings are also volatile so that they can distribute in the air in a gas form[77]. Most PAHs (> 5 rings) are generally insoluble in water and have low vapor pressure and high boiling and melting points[72,77]. These bigger PAHs tend to adsorb to the soil, sediment, and ambient air particles.

The general public can be exposed to PAHs through inhalation, ingestion, and dermal contact. Cigarette smoke, biofuel burning, and exposure to the PAHs polluted air or PAHs containing PM, polluted drinking water, eating vegetables containing PAHs through bioaccumulation or PM deposit, and even grilled meat are important routes for PAHs exposure.

Short-term exposure in occupational studies shows that PAHs could cause nausea, vomiting, skin and eye irritations and diarrhea[78]. However, the chronic effect of long-term PAHs exposure is at a greater concern since it is related to cancer, cardiovascular diseases, and adverse effects on fetal growth[79–84]. When PAHs enter human body, several steps of metabolic transformation will occur. Most of the metabolites will be excreted through urine and feces[85], but some reactive metabolites such as diol epoxides, PAH radical cation, and ortho-quinone can form adducts with DNA and proteins which then makes certain PAHs mutagenic and carcinogenic[86–88]. Cytochrome enzymes play an important role in these PAHs activation pathways[87,88].

The anthropogenic PM is characterized by high content carbonaceous materials, including PAHs. Many studies had been done on PM-associated PAHs and evaluated the human health risk[89–94]. Around 90% of PAHs in ambient air are anthropogenic[95,96] and are a common constituent of fine and ultrafine particulate. Due to the common anthropogenic origin, EPFRs and PAHs share the same transport vehicle i.e., PM [73,93,97–99], so PM-associated PAHs were also analyzed in this research.

1.4. Hazardous Waste Incineration

Hazardous waste refers to the waste that potentially poses a higher risk on human health and the environment. In the United States, the U.S. Federal Resource Conservation and Recovery Act (RCRA) manages hazardous waste. As discussed earlier, the generation of PM, especially fine and ultrafine particles, and EPFRs usually occurs in the post-flame zone and cool zone of a combustion process typically during an incineration process[40]. Hazardous waste incineration as a hazardous waste thermal destruction treatment technology is an important way to destroy a large part of the hazardous components and reduce the volume of hazardous waste. It is a widely applicable technology that is proved to be effective[100]. Besides EPFRs and PAHs, other toxic

substances, such as dioxins and lead, could also be part of the emission from the incinerator. So, to make sure that all the emissions from hazardous waste incinerators meet a certain standard that poses no significant risk to public health is very important. Flue gas scrubbing is the crucial step to meet the requirement[100].

The latest version of the National Emission Standards for Hazardous Air Pollutants (NESHAP) for hazardous waste combustors was finalized by Environmental Protection Agency (EPA) and was effective since Oct. 28, 2008. The rule was set under the guidance of the Clean Air Act (CAA) and reflected the maximum achievable control technology (MACT). Referring to 40 CFR 63.1219(b)(7) and 63.1220(b)(7)(i), the particulate matter standard for new incinerators is 0.0016 grains per dry standard cubic foot (gr/dscf)[101].

CHAPTER 2. ANALYSIS TECHNIQUES

In this research, two PM collection methods have been applied. The details of each method are discussed and compared in chapter 4. Samples were analyzed for surface morphology and elements, EPFRs characteristics, the potential for hydroxyl radical and superoxide generation, PAHs concentration, and cell exposure viability. The techniques used in this research are introduced in this chapter.

2.1. Morphology and Surface Elements Analysis

The leaf surface morphology and the surface elements of retrieved PM have been analyzed by Scanning Electron Microscope (SEM) and Energy Dispersive X-ray Spectroscopy (EDS).

2.1.1. Principle of SEM-EDS

SEM is a technique to obtain surface morphology pictures of samples through the interaction of an electron beam with sample surface atoms. Typically, the electron beam hits the surface atoms, and the secondary electrons will be emitted and detected. And based on the numbers of detected secondary electrons at the different parts of the scanning raster, namely, signal intensity, the SEM pictures can be generated with the morphology information. SEM could obtain pictures for 2D and 3D materials with nanometer-scale resolutions[102].

EDS is an analytical technique through which the elemental composition of the sample could be obtained. The electron beam hits the sample and may excite an electron in the inner shell. This electron will be ejected and a hole will be created. When the electron which has higher energy on the outer shell fills the hole, the energy difference between two shells will be emitted as an X-ray and be detected. Besides the elemental spectra, an elemental map could also be generated to show the element distribution in a selected area[102].

2.1.2. Instrument Settings for SEM

Collected leaf surface microstructure has been analyzed using JEM 6610LV Scanning Electron Microscope (SEM) at an accelerating voltage of 5-10 kV before and after PM retrieving. A 10 mm × 10 mm piece had been cut from the center of the leaf and fixed on the sample holder with double-sided adhesive carbon tape.

PM collected by different methods has been analyzed by the Quanta™ 3D DualBeam™ FEG FIB-SEM system. The PM samples were mounted to the sample holder by using a piece of double-sided adhesive carbon tape and coating with platinum. The accelerating voltage for analyzing is 20 kV, and EDS provided information on elemental compositions.

2.2. EPFRs Characteristics

2.2.1. Principle of Electron Paramagnetic Resonance (EPR)

EPR is a spectroscopic technique used to study samples containing unpaired electrons. As an elementary particle, the electron has intrinsic angular momentum, which is parameterized by spin quantum number ($s=\frac{1}{2}$). It can generate a magnetic field because of spin and have a magnetic moment. When there is no external magnetic field, the orientation of electrons is random. But once an external magnetic field is applied, the magnetic moment will align electrons in two directions to the field: parallel ($m_s = \frac{1}{2}$) or antiparallel ($m_s = -\frac{1}{2}$). Parallel state (α) is always a lower energy state, while the antiparallel state (β) is a higher energy state. This spilt of energy state at the presence of a magnetic field is calls the Zeeman effect (Figure 2.1.). The energy of the two states is calculated as:

$$E = m_s\, g\, \mu_o\, B_o, \qquad \text{(Equation 2.1.)}$$

Where: μ_o is Bohr magneton ($\mu_o = 9.27 \times 10^{-24}$ J T^{-1}); B (Tesla) is the magnetic field; and g is the g-factor. In EPR, the microwave is providing energy to electrons in the parallel state (α), and once the energy equals the energy difference between two states, namely:

$$\Delta E = h\nu = g\ \mu_o\ B_o, \qquad \text{(Equation 2.2.)}$$

Where h is the Planck's constant ($h = 6.63 \times 10^{-34}$ J·s); ν (Hz) is the frequency of the incident microwave, the electron will absorb the energy and jump to the high energy antiparallel state. This changing of electron spin between the energy states is known as resonance.

Typically, the microwave frequency is fixed, and the magnetic field is changing until the resonance takes place, and usually, the first derivative of the absorption spectrum is measured. So, according to the equation above, under a certain magnetic field and microwave frequency, the g-factor is a constant and provides the information of the electron structure. Besides the applied external magnetic field, electrons are also affected by the local magnetic field generated by neighboring atoms or molecules and change the g-factor due to the changing of the angular momentum. For example, with the association of the unpaired electron with an atom that has a non-zero nuclear spin, the hyperfine interaction will occur[103].

In Figure 2.2, the upper spectrum is the first derivate spectrum usually recorded by EPR, and the lower one is the absorption spectrum. g-factor is obtained as the maximum of the absorption curve, and the peak width ΔHp-p is the distance between crest and trough. Both g-factor and ΔHp-p depend on the radical types in the sample.

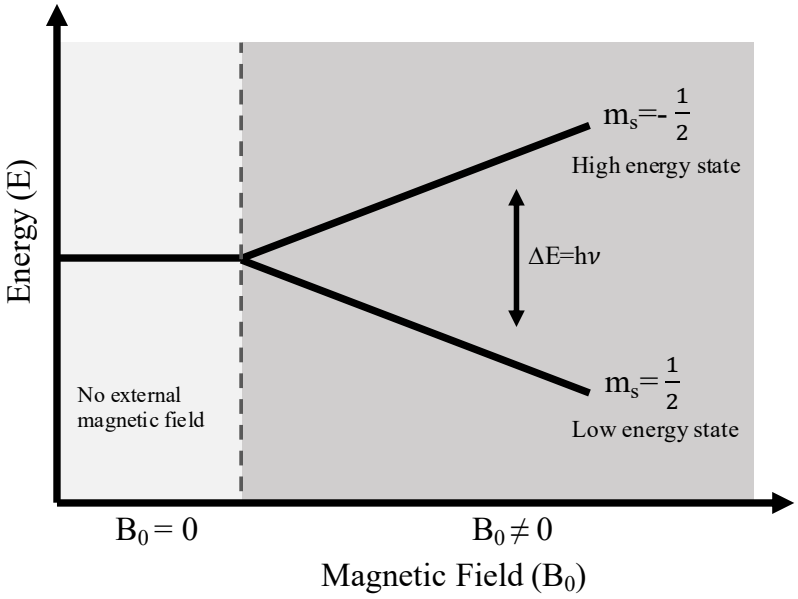

Figure 2.1. The Zeeman effect. m_s is the spin quantum number. h is the Planck's constant (h = 6.63 x 10^{-34} J·s); ν (Hz) is the frequency of the incident microwave.

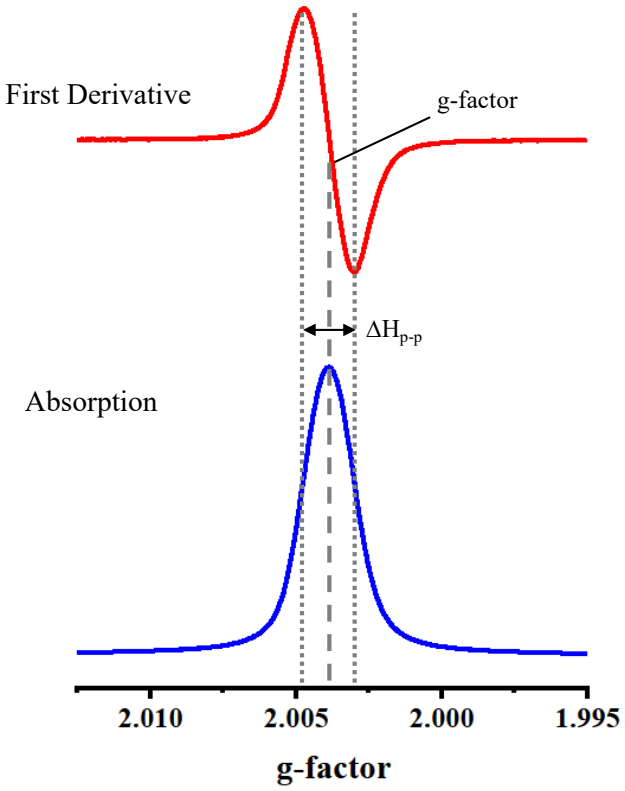

Figure 2.2. EPR first derivative and absorption spectra. ΔHp-p is the peak width of the absorption spectra.

2.2.2. Instrument Settings for EPR

All PM samples were characterized for the EPFRs content by EPR using a Bruker EMX 10/2.7 EPR spectrometer (X-band) equipped with a dual cavity. The parameters of free radical signal measurements were based on William's paper[57] and were applied to all particles' measurements. These parameters were as follows: 2.03 mW power; modulation amplitude of 4.0 G; sweep width of 100 G; time constant of 40.96 ms corresponding to a conversion time of 163.84 ms; sweep time of 167.77 s; receiver gain of 3.56×10^4; and three scans. EPFRs concentration was calculated by comparing the area of the peak to a 2,2-diphenyl-1-picrylhydrazyl (DPPH) standard.

2.3. Simulated Sample Aging

A study focusing on the decay behavior of EPFRs in $PM_{2.5}$ has been conducted before, and three decay patterns -fast decay, slow decay, and no decay have been identified[28]. In this research, a sample aging study has been conducted after the particles had been retrieved from the medium to simulate the collection conditions of two methods under a laboratory set up. The same sample has been divided into two groups, and particles were left in the EPR tube for an easier measurement. The first group of samples was subjected to air purged at a constant flow rate of 0.8 mL/s and labeled as active aging, simulating the collection condition of HV PM sampler. The second group was exposed to the air and only subjected to air diffusion and called passive aging, simulating the phytosampling condition. We compared the EPFRs concentration and EPFRs speciation changes under different conditions along time.

2.4. Hydroxyl Radicals and Superoxide Radicals Generation by PM

EPFRs could generate ROS, which will induce oxidative stress in the biological systems[33]. In this research, we adapted the procedure of using spin traps to detect the generation of hydroxyl radicals (•OH) and superoxide radicals ($O_2^{\bullet -}$) from a paper published by Khachatryan et al.[32].

2.4.1. Background of Spin Trapping Experiment

Spin trapping study is to use a spin trap reagent to react with the short-lived radicals to form more stable spin adducts which can be detected and measured by EPR. Spin trap reagents are nitrone or nitroso compounds and will form more stable radical adducts with typical spectrum patterns that are detectable and easily characterized by EPR. The most widely used spin trap is 5,5-dimethyl-1-pyrroline N-oxide (DMPO), and the DMPO-hydroxyl adduct has a 4-line spectrum pattern in EPR measurement. Another spin trapping reagent 5-tert-butoxycarbonyl-5-methyl-1-pyrroline N-oxide (BMPO) is usually used to detect the generation of superoxide radicals which serves as a precursor to generate hydroxyl radicals in the EPFRs redox cycle. Although DMPO can also react with superoxide radicals, the half-life of DMPO-superoxide adduct is very short ($t_{1/2}$= 45 s). And the DMPO-superoxide adduct will quickly decay to DMPO-hydroxyl adduct. In order to detect the generation of superoxide radicals, BMPO has been used, and the half-life of BMPO-superoxide adduct is much longer and measurable in EPR ($t_{1/2}$=23 mins)[104,105]. The detection of superoxide radicals is characterized by the shoulders on the two center peaks of the BMPO-superoxide adduct 4-line spectrum.

2.4.2. Spin Trapping Experiment Protocol

The procedure of measuring hydroxyl radicals generated by EPFRs using DMPO is as follows. 2 mg of PM sample was added into 1 mL phosphate buffered saline (PBS) solution at pH 7.4. Two sets of PBS solutions were used for each sample: purged with pure N_2 for 5 mins to remove dissolved oxygen (control) and purged with pure O_2 for 5 mins. PM suspensions were vortexed for 10 mins. 10 μL was taken out for analysis. 10 μL of freshly made 3M 5,5-dimethyl-1-pyrroline-N-oxide (DMPO) was added into the sample and sample solution was diluted with additional PBS to 190 μL. 20 μL from final 200 μL suspension was probed into spin-free capillary

tube (Fisher brand), and EPR spectra was measured with the following instrumental parameters: 10.18 mW power; modulation amplitude of 0.8 G; sweep width of 100 G; time constant of 40.96 ms corresponding to a conversion time of 163.84 ms; sweep time of 167.77 s; receiver gain of 5.02 $\times 10^5$; and two scans. The spectra of DMPO-OH adduct were recorded after 10 mins, 30 mins, and every hour up to 6-7 hours. All 4-line peaks were considered for spin quantitation with the peak area calculated as the $\Delta Hp\text{-}p^2$ multiplied by relative intensity. The area result of each peak for every data point was summed, and all data points were plotted in one graph. The difference of hydroxyl radical concentration between the sample group and the control group indicated the potential of PM sample to generate hydroxyl radicals.

2.5. PAHs Extraction and Concentration Analysis

2.5.1. Gas Chromatography-Tandem Mass Spectrometry (GC-MS/MS)

Gas Chromatography (GC) is an analytical technique used to separate volatile compounds. The mobile phase in gas chromatography is carrier gas, while the stationary phase could be liquid or solid packed on the inner wall of the column. And the column is mounted in an oven in which the temperature ramp could be setup. Separation occurs based on the interaction of the analyte molecules with the mobile phase and the stationary phase. With the moving of the carrier gas with analyte molecules, the adsorption strength of various molecules to the stationary phase results in the different elute time of analyte molecules from the column, and this time is called retention time of the compound. A detector connected to the end of the column can monitor and analyze the compounds.

Mass spectrometry (MS) is a technique that measures the mass-to-charge ratio (m/z) of ions. Once the analyte enters the mass spectrometer, it will be ionized, and some molecules will break into charged fragments, and then these fragments can be separated based on their mass-to-

charge ratio. As ionization is an important process for mass spectrometry, there are different ion sources available for various sample types. For example, electron ionization (EI) and chemical ionization (CI) are suitable for gaseous samples, while electron spray ionization (ESI) is usually chosen for liquid biological samples. There are two typical methods to analyze ion fragments in a mass spectrometer: full scan and selective ion monitoring (SIM). In the full scan, all fragments in the target range are detected, and the full spectrum could be recorded. This method is usually used to determine unknown compounds in the sample, and the peaks in the spectrum could be compared to the database for compound qualification. The SIM method only monitors those fragments that are interested so that it could reach a lower detection limit.

GC could be connected to different detectors considering the sample characteristics and the research needs. Gas chromatography-mass spectrometry (GC-MS) is widely applied in many fields, including environmental sciences, criminal forensics, chemical engineering, food industry, medicine, and so on, for detection, identification, and quantification even trace amount of substances in the sample[106,107]. When another phase of mass fragmentation has been added, a GC-tandem MS or GC-MS/MS system has been built. This system is very useful in detecting a low-level substance in a high background matrix. In this research, a GC-MS/MS system Agilent 7980B/7000C Triple Quad System was used to analyze the ambient air PM samples. A triple quadrupole mass spectrometer consists of two quadrupole mass filters (Q1 and Q3) and a quadrupole collision cell (q2) in between. This triple quadruple configuration enables four scan modes by changing the fixed or scanning status of the two mass filters. These four modes are product ion scan, precursor ion scan, neutral loss scan, and multiple reaction monitoring scan (MRM). Product ion scan (Q1 fixed, Q3 scanning) can detect all the fragment ions of a selected precursor ion. Precursor ion scan (Q1 scanning, Q3 fixed) can find out all the precursors have

certain fragment ion. Neutral loss scan (Q1 scanning, Q3 scanning) monitors all pairs of ions that have the same m/z difference, and multiple reaction monitoring scan (MRM) (Q1 fixed, Q3 fixed) can find a precursor/product pair specifically. In the study, electron ionization is used, and MRM mode is the major method used to qualify and quantify the PAHs in the airborne fine and ultrafine particles collected by HV PM samplers and phytosampling. Figure 2.3 is a schematic overview of MRM mode[108].

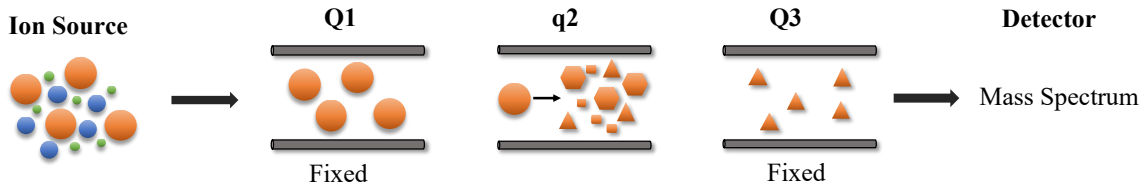

Figure 2.3. Schematic overview of MRM mode[108]. Q1 and Q3 are two quadrupole mass filters. q2 is a quadrupole collision cell.

2.5.2. PM Extraction and PAHs Analysis

Selected PM samples retrieved from matrixes were subjected to PAHs analysis. Samples were extracted with dichloromethane (≥99.9%, MilliporeSigma) to obtain PAHs. Samples were placed in a 5 ml glass centrifuge tube (Pyrex), and 3 mL of dichloromethane was added. Samples were then vortexed for 2 hrs 45 mins by Vortex Genie 2 (Daigger) and sonicated for 15 mins (FS-20 ultrasonic, Fisher Sci.). Suspensions were next centrifuged for 2 hrs (Drucker Diagnostics). The supernatant was collected, dried under a gentle nitrogen flow, and redissolved in 200 µL of dichloromethane (≥99.9%, MilliporeSigma).

Samples were analyzed by GC-MS/MS (Agilent 7980B/7000C Triple Quad System) with a capillary GC column HP-5ms (30 m × 250 µm × 0.25 µm) and compared with the standard, i.e. mixed native PAH solution (Willington Laboratories): Naphthalene, 2-Methylnaphthalene, Acenaphthylene, Acenaphthene, Fluorene, Phenanthrene, Anthracene, Fluoranthene, Pyrene,

Benzo[c]fluorene, Cyclopenta[c,d]pyrene, Benz[a]anthracene, Chrysene, 5-Methylchrysene, Benzo[b/k/j]fluoranthene, Benzo[e]pyrene, Benzo[a]pyrene, Perylene, Indeno[1,2,3-c,d]pyrene, Dibenz[a,h]anthracene, Benzo[g,h,i]perylene, Dibenzo[a,l]pyrene, Dibenzo[a,e]pyrene, Dibenzo[a,i]pyrene, Dibenzo[a,h]pyrene. 1 μL of extract was injected into GC-MS/MS system with the split ratio of 10:1. Multiple reaction monitoring (MRM) method was used for PAHs quantitation. Details of the GC-MS/MS method are provided in Table 2.1.

Table 2.1. GC-MSMS parameters for PAHs analysis.

	Parameters
Model	Agilent 7980B/7000C Triple Quad system
Mode	Multiple reaction monitoring (MRM)
Method	Electron ionization
Column	Agilent J&W HP-5ms
Dimensions	30 m × 250 μm × 0.25 μm
Carrier Gas	Helium, 1.2 mL/min
Injection	Split, split ratio: 10:1, 1 μL, 230 °C
Oven Program	60 °C for 1min, 60 °C to 100 °C at 20 °C/min and hold for 1min, 100 °C to 220 °C at 5 °C/min and hold for 10min, 220 °C to 230 °C at 5 °C/min and hold for 8 min, , 230 °C to 300°C at 5 °C/min and hold for 8 min. Total run time 70 mins.
Detector	Ion source 230 °C, Transfer line 290 °C

2.6. Luminescence ATP Assay on Human Bronchial Epithelial Cells (BEAS-2B)

PM exposure through inhalation is correlated to a lot of respiratory diseases[9,11], and as an important component that can generate ROS, the cytotoxicity of EPFRs is worth studying. Several in vitro and in vivo studies have identified toxicological effects of radicals containing PM using surrogate EPFRs containing particles made in the lab. For example, Paul et al. found that exposure to the radicals containing PM caused lysosomal membrane permeabilization, lipid peroxidation, and epithelia-to mesenchymal transition (EMT) on human brachial epithelial cells (BEAS-2B)[109]. Balakrishna et al. identified the cytotoxicity of radicals containing PM to BEAS-2B through lipid

peroxidation and influence on inflammatory cytokines expression[110]. In this research, a cell viability test concerning the cytotoxicity of EPFRs on PM has been conducted on human brachial epithelial cells (BEAS-2B) by luminescence ATP assay. The cells were exposed to the airborne PM as well as a surrogated sample synthesized in the lab, and the dose-response relationships of cells to both types of PM were compared.

2.6.1. Surrogate EPFRs Containing PM Synthesis

The procedure of synthesizing surrogate EPFRs containing PM was adapted from studies of Balakrishna et al[110]. Based on the proposed EPFRs formation mechanism introduced earlier, a transition metal oxide, a substituted aromatic compound, and an appropriate supporting matrix are needed in the suitable condition to synthesize the EPFRs containing PM. In this study, we chose to introduce 0.25% CuO to the ultrafine silica powder (Cab-O-Sil® fumed silica, <200 nm) as our PM surrogate and dose 2-monochlorophenol (2-MCP) and 1,2-dichlorobenzene (DCB) to the particles at 230 °C to form EPFRs on the surface of the PM surrogate.

To make 0.25% CuO/SiO_2 PM surrogate, copper (II) nitrate hemi(pentahydrate) has been introduced into silica powder using the incipient wetness method. The incipient wetness is also known as capillary impregnation, and it is relied on the capillary action to draw metal solution into the pores of the supporting matrix. After the calcination, the volatile part is removed, leaving metal composition in the pores. The mixture of hemipentahydrate and silica powder was stirred and then dried at 120 °C in the oven for 12 hrs. After grinding through the rotation with beads on a Rotavap, sieved through a 63 μm mesh and dried in the oven again, particles were calcinated at 450 °C for 6 hrs, and PM surrogate is ready to use.

Chemisorption process occurred through dosing 2-monochlorophenol (2-MCP) and 1,2-dichlorobenzene (DCB) under vacuum to the surface of the surrogated PM by using a customized

vacuum exposure system. The system is consist of a vacuum pump to maintain vacuum, a pressure gauge to monitor system vacuum, a dosing port as the vapor source of MCP or DCB, an equilibrium chamber to maintain vapors and connect to the reactor, two reactors mounted in a ceramic heater to keep the reaction temperature, and two EPR tubes connected to the upper side of the reactor for an easier PM transfer and EPR measurement. The system was first evacuated to 10^{-2} torr, and the CuO/SiO_2 particles were heated in situ at 450 °C for 1 hr to remove any possible organic contaminants. Then the temperature of the system was lower to 230 °C, and the port connected to the pump was closed, CuO/SiO_2 particles were dosed under the vapor for 6 mins. After dosing, the system was evacuated to 10^{-2} torr again to remove excess MCP or DCB, and EPFRs contained PM surrogate was cooled down to room temperature and subjected to EPR measurement to test for radical signals. The surrogate samples made use this method were marked as MCP-230 and DCB-230 in later experiments.

2.6.2. BEAS-2B Cells Culture and Exposure Viability Test

BEAS-2B cells were cultured in the cell medium (Corning® DMEM/Hams F-12 50/50 mix, sodium bicarbonate, glutamine, antibiotics, and fetal bovine serum) and maintained in 25 cm^2 flasks (T25) in the incubator under 37 °C, 5% CO_2. A 1:5 split ratio was applied to passage cells every four days when replacing with new culture media (passaging time was determined in the beginning before they reach confluency). Heathy growing cells in a T25 flask were split and transferred to a 96-well plate (the designed layout is shown in Figure 2.4.). The wells on edges were filled with PBS solution, the second column was left for control, and the 11^{th} column was blank. This layout design could mitigate the edge effects due to the uneven evaporation rate of culture medium on the whole plate during incubation. After cells were transferred in, the plate was incubated for four days, and the confluency of the cells was checked under the microscope to make

sure they were full of the well and ready to be exposed to PM. Once the PM has been retrieved from the sampling matrix and a surrogate sample has been made, they were immediately subjected to EPR measurement. All the PM used in the cell viability test were measured by EPR for EPFRs characteristics. And four PM concentration levels (10 μg/μL, 2.5 μg/μL, 1μg/μL and 0.1 μg/μL, corresponding to 310 μg/cm^2, 77.6 μg/cm^2, 31 μg/cm^2, and 3 μg/cm^2 to the surface area of each well) had been picked for a relative wide test range. Every four columns of the plate were grouped together for four levels' solution from one sample. Cells also grew in the control wells that were not exposed to PM. Blank wells only contained medium without cells. 500 μL of particle stock solution with a concentration of 10 μg/μL had been made in PBS, and then this stock solution had been sonicated with an ultra-sonicator (QSONICA, Q125) for few second to break the particle aggregates and fully suspend them in the PBS. Gradient concentration level solutions were made from stock with the dilution of culture medium. Aspirated and discarded the old culture medium from each well and added back 5 ml of new culture medium to planned sample exposure wells and 100 mL to blank and control wells. Added 10 μL of the different concentration levels of PM solutions in the designated wells and 90 μL medium in order (obtained six replicates for each exposure level). Added 100 μL additional PBS to the edge wells and incubated the plate for 24 hrs. After incubation, the old medium, together with the PM solution, was aspirate out and discarded, and cells in the well were rinsed twice with PBS. A luminescence ATP assay (CellTiter-Glo® Luminescent Cell Viability Assay, Promega) was applied to test the live cells through the detection of Adenosine Triphosphate (ATP) molecule, which is only present in metabolic active cells. The principle of this assay is through the reaction of beetle luciferin with ATP and O_2 under the catalyzation of luciferase and Mg^{2+} to produce oxyluciferin, Adenosine Monophosphate (AMP), CO_2, and release luminescence signal.

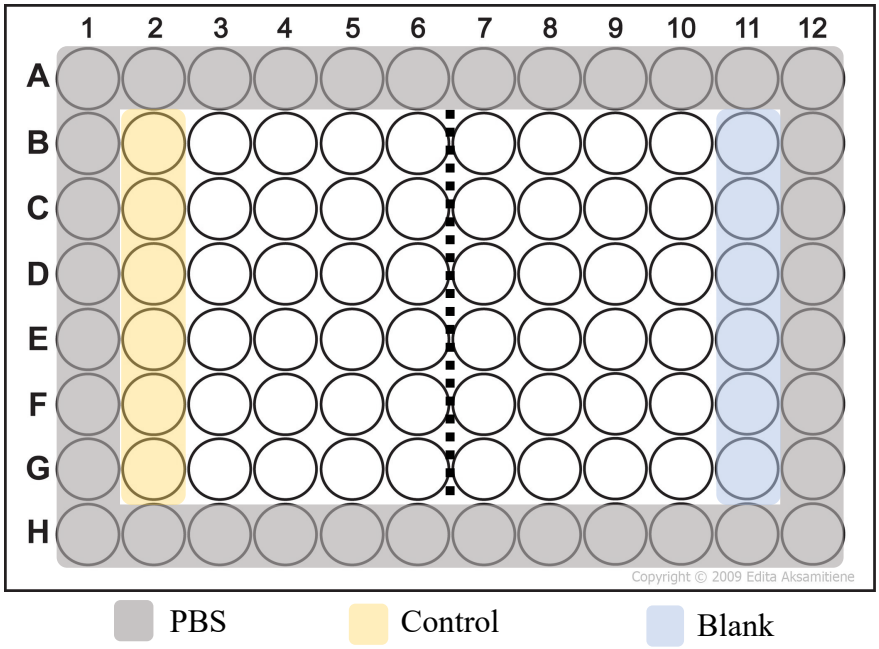

Figure 2.4. Plate layout used in the cell viability test.

2.7. Microwave Digestion and Inductively Coupled Plasma Optical Emission Spectrometry

Inductively Coupled Plasma Optical Emission Spectrometry (ICP-OES) is a multi-element analytical technique and is the preferred method to analyze trace metals in the samples. When a sample solution is drawn by a peristaltic pump into the instrument and converted into a fine aerosol spray in a nebulizer, larger droplets are drained away to the waste while the finer droplets are directed into the plasma torch. The plasma is generated in a quartz torch, which is surrounded by a radio frequency (RF) coil. Once turned on, the high-power RF creates an electromagnetic field in which the gas (usually Ar) is ignited, and the ionization of sample molecules is initiated. The plasma vaporizes the sample and excites the atoms and ions, and the characteristic light is emitted. This characteristic light then passes into a spectrometer, and a specific wavelength for each element is separated and measured. The light intensity for each different wavelength is quantified by using a calibration curve from standard to get the concentration data of an element[111,112].

Microwave digestion is the method used to decompose the samples before analyzing them by ICP-OES. PM samples are digested in the strong acid under microwave irradiation[113]. In this research, the Sineo MDS-6G microwave digestor with eight vessels has been used to digest PM and cellulose filter samples in a 7:1 mixture of nitric acid (68%-71%, TraceMetal Grade, Fisher Scientific) and H_2O_2 (30%). And the digestion program is as follows: 130 °C for 10 mins, then 150 °C for 5 mins, and finally 180 °C for 15 mins. Once the samples are fully digested, they are diluted to a less than 10% acid sample solution and analyzed by VISTA-MPS CCD Simultaneous ICP-OES (wavelength coverage: 175-785 nm).

2.8. Statistical Test

Analysis of Variance (ANOVA) is a statistical test method that can be used to compare the means among groups. ANOVA was first proposed and introduced by Ronald A. Fisher in 1918[114]. Conducting ANOVA test is based on several assumptions: the deviations of observations within groups should be independent, identical and normally distributed; each treatment group is sampled independently; the variance of each treatment group is the same (homogeneity). The null hypothesis (H_0) tested in ANOVA is that means of all populations are the same, while the alternative hypothesis (H_1) is that at least one population mean is different. The variances come from the treatment effect (between group variance) and random error (within group variance). These two variances, together with sample sizes, determine the equality of the population means. F-test was conducted in ANOVA, and F test statistics provide the information of significant treatment differences. To calculate F test statistics, between treatments variance (SStreatment) and within treatment group variances (SSerror) need to be calculated first as:

$$SStreatment = \Sigma\, n_j\, (\bar{x}_j - \bar{x})^2 \qquad \text{(Equation 2.3.)}$$

$$SSerror = \Sigma\, (x_i - \bar{x}_j)^2 \qquad \text{(Equation 2.4.)}$$

Where $\bar{x}_j$ is group mean, $\bar{x}$ is the overall mean, x_i is an individual observation, and n_j is the sample size in each group.

And the between treatments mean square (MStreatment) and within treatment group mean square (MSerror) are obtained with their degree of freedom (dfbetween, dferror),

$$\text{MStreatment} = \frac{\text{SStreament}}{\text{dfbetween}} = \frac{\text{SStreament}}{\text{m}-1} \quad \text{(Equation 2.5.)}$$

$$\text{MSerror} = \frac{\text{SSerror}}{\text{dfwithin}} = \frac{\text{SSerror}}{\text{n}-\text{m}} \quad \text{(Equation 2.6.)}$$

Where m is the number of groups and n is the number of independent observations. So, the F test statistics is:

$$\text{F} = \frac{\text{MStreament}}{\text{MSerror}} \quad \text{(Equation 2.7.)}$$

If there are no differences between treatment groups, the F statistics will be 1. From F statistics and its F distribution, one could find out the probability value (p-value). If this p-value is smaller than a pre-specified significance level (usually 0.05), the null hypothesis will be rejected, and there are significant differences among tested groups.

In this research, one-way ANOVA was applied to test the effects of different sample collection methods and collection locations to a certain sample characteristic, and the p-value was chosen to be 0.05.

CHAPTER 3. RESEARCH HYPOTHESIS AND OBJECTIVES

As one of the six criteria pollutants, particulate matter has been proved to relate to many diseases. The toxicity of PM is in terms of the particle size and the chemical compositions (or pollutant load). Because fine and ultrafine particles are able to deposit in the alveolar region and even be translocated to other organs, they serve as effective vehicles to deliver toxic materials and significantly raise the human exposure risks. Among all these toxic substances, EPFRs and PAHs are two important components that are almost ubiquitous in combustion generated PM, thus worth to study. EPFRs can be considered as an emerging contaminant since they have existed in the environment for a long time, and there is a rising concern about their potential risks[115]. EPFRs could generate ROS and induce oxidative stress in the biological systems, and certain PAHs are carcinogenic and mutagenic. So, to collect and study EPFRs/PAHs-associated PM is important to evaluate the exposure health risks of the general public to the airborne PM.

The prevailing PM collection method is to use PM samplers, but it bears some artifacts and has some limitations. For example, it is not easy to recover the particles from collection matrixes for further analysis. The collected PM is not subjected to exactly the same environmental conditions as those suspended PM that human is exposed to. Moreover, setting up a sampler is expensive, and using it requires professional training. Hence, the applications of the sampler in a dense network for a more accurate evaluation of spatial PM distribution are limited. Therefore, we are trying to develop and solid another method to solve these problems in this research. A new phytosmapling method using leaves as a passive PM sampler has been developed to overcome the drawbacks of the prevailing high volume air samplers. The hypothesis of this research is that the sampling methods will affect the chemical compositions of the fine and ultrafine particles.

To test this hypothesis, the research is divided into three parts with three specific objectives. The first objective is to develop the new phytosampling method and test the feasibility and the effectiveness of it. This objective was approached by optimizing the method details and comparing EPFRs characteristics, the potential of ROS generation, PAHs compositions, and the cytotoxicity between the PM collected from phytosampling and prevailing high volume PM sampler. The second objective is to evaluate the application of the phytosampling method to field studies. The phytosampling method has been applied to a study in Memphis, Tennessee, with more than a hundred sampling sites to investigate the spatial distribution of EPFRs concentration to provide information of potential radical explore "hot spot" within the city. And the method was also applied to a field study in New Orleans, Louisiana, concerning the PM associated pollutant emissions from a ship cargo terminal. The third part is the application of a high volume PM sampler to collect PM samples during the tailgate parties in the football season to evaluate the influence of human behavior on short-term PM emissions.

CHAPTER 4. DEVELOPMENT OF PHYTOSAMPLING METHOD

For the regulatory and research purposes, PM is collected from ambient air using special sampling devices. Most commonly, the particle concentration in the air is determined through the mass change of the collection matrix. Major drawbacks of such method include the difficulty of particle retrieval for further analysis if needed, and altered environmental conditions during the sampling process (i.e., excessive air flow, changed lighting conditions compared to ambient air or prolonged time lapse during collection) that may affect some properties and compositions of the sample. The network density of the sampling devices is also a factor in the accurate evaluation of the local PM distribution.

It has been shown that the urban forest has the function to remove air pollutants[116–120], including PM[2]. PM removal from ambient air by plants is based on the "enhanced" deposition mechanism on leaves, i.e., through electrostatic interactions and entrapment by trichomes (Figure 4.1.). This phenomenon creates a potential for the development of "phytosampler" for ambient air PM collection. Though such method will not be able to accurately define the PM concentration in ambient air, it can be an excellent supplementary tool for chemical characterization of PM, and through referencing with PM concertation in the air (evaluated by other methods) translate to chemical exposure. Phytosampling offers more flexibility in spatial resolution (such as creating a dense sampling network), reduced cost, no instrument set-up, easier particle recovery, more volatile organics could be kept without the high volume air flow pulling through the sample and particles will be exposed to the same solar and atmospheric conditions as those suspended in air. However, the efficiency PM collection will vary a lot from different plant species and be influenced by weather conditions.

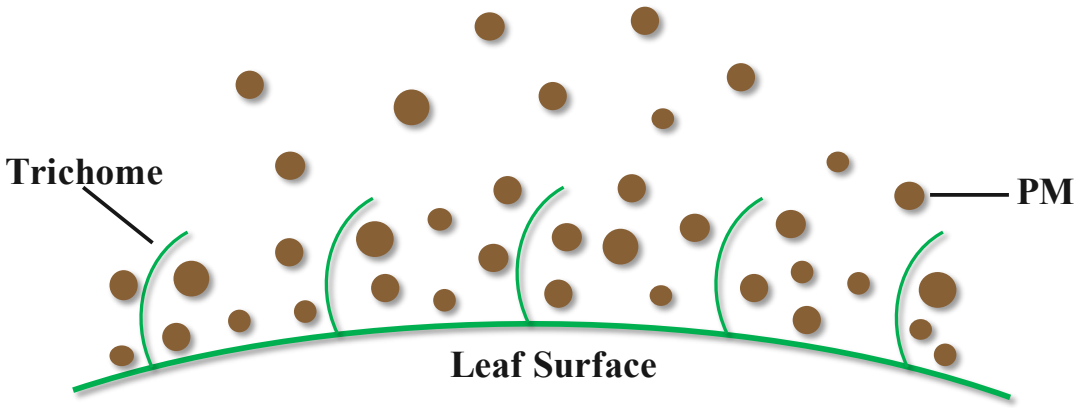

Figure 4.1. Particles are trapped by trichomes when they deposit on the leaf surface.

In this research, fine particles and ultrafine particles were collected using both prevailing high volume (HV) PM sampler and new phytosampling collection methods. The speciation and concentration of EPFRs on PM have been analyzed and compared. Spin trapping experiment has been conducted on particles from different sources to evaluate the hydroxyl radical generation potential. After retrieving from collection matrixes, PM has been extracted by dichloromethane, and polycyclic aromatic hydrocarbons (PAHs) on PM samples have been analyzed and compared between two collection methods. The comparison results of selected pollutants present on the PM collected from different methods could help to establish the feasibility of phytosampling as a supplementary tool for PM pollution studies.

4.1. Phytosampling Method

Phytosampling is a method that uses leaf surface to collect PM. In this research, PM was retrieved from the plant leaves in the Baton Rouge, LA area to develop and test the viability of the phytosampling method. Three common to Louisiana plant species were selected, and fresh leaves of those plants were collected for preliminary experiments around the campus of Louisiana State University, Baton Rouge, LA. The three tree species are *Ligustrum japonicum* (Japanese privet), *Callicarpa americana* (American beautyberry), and *Camellia japonica* (Japanese camellia). The sampling locations are provided in Table 4.1 and Figure 4.2.

Table 4.1. Sampling locations.

Sampling site	GPS Coordinates	Plant Species	Site Characteristics
SP #1	30.396734, -91.177729	*Ligustrum japonicum* (Japanese privet)	The corner of an intersection where traffic provided an important source for PM.
SP #2	30.413446, -91.182333	*Callicarpa americana* (American beautyberry)	A busy bus stop on LSU campus.
SP #3	30.409424, -91.177341	*Camellia japonica* (Japanese camellia)	Next to a department building on LSU campus.
HV #1	30.410441, -91.176964	High volume (HV) PM sampler	On the roof of a seven-story building on LSU campus.

Figure 4.2. Sampling sites in Google Earth.

Only healthy-looking leaves with similar size at shoulder high were collected and stored in ziplock bags. After collection, samples were immediately transferred to the laboratory for PM retrieval, and all leaves were treated within 6 hours after collection. The total leaf surface area was measured using grid paper. Next, leaves were transferred to beakers containing deionized water in the amount sufficient to cover all leaves except petiole (approximately 100 mL water). Leaves were then sonicated by ultrasonic FS-14 (Fisher Scientific) for 30 s followed by leaves removal and transfer of water containing retrieved particles to vacuum filtration assemblies. Larger size particles were removed on a 3.0 μm pore size prefilter (Pall Corporation), and filtrate containing particles < 3 μm was collected (P_3). Filtration using 0.7 μm pore size A/D glass fiber filter (Pall Corporation) or a 0.2 μm polyethersulfone membrane sterile syringe filter (VWR brand) produced

filtrate suspensions containing particles < 0.7 μm (P_{07}) and < 0.20 μm (P_{02}), respectively. Filtrates were next subjected to freeze drying (lyophilizer, Labconco Co., model #7740020), and corresponding particle size fractions were collected, weighed, and ready to be analyzed. This PM retrieving procedure is shown in Figure 4.3.

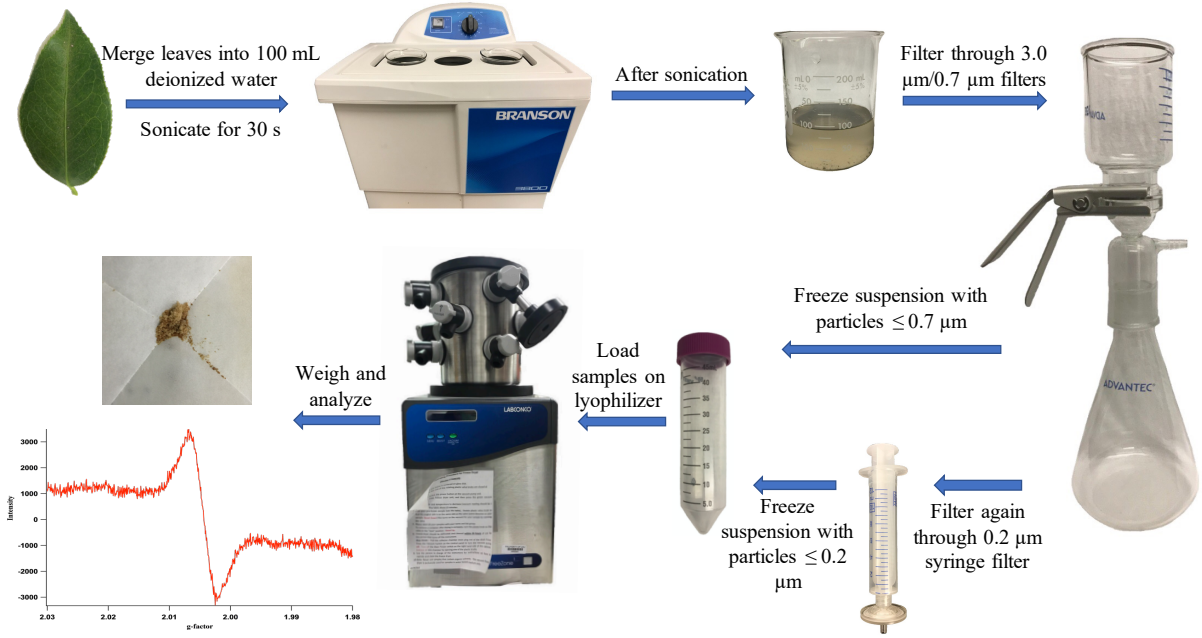

Figure 4.3. Phytosampling method to collect PM.

The efficiency of capturing PM by different plant species depends on the features of their leaf surface and varies with the change of the environmental conditions. There are published studies that focused on the ability of different plant species on retaining airborne PM[121–125]. The average efficiency of PM collection (μg/cm^2 leaf surface) in this study from each plant species is presented in Table 4.2. The results for P_{07} are from preliminary experiments. Considering the site characteristics and availability of plants, site SP #1 with P_3 and P_{02} had been chosen for more extensive studies.

Table 4.2. Average collection efficiency of three plant species.

μg/cm^2 leaf surface	*Ligustrum japonicum* (SP #1)	*Callicarpa americana* (SP #2)	*Camellia japonica* (SP #3)
P_{07}	4.24 (7 collections)	11.63 (4 collections)	2.87 (5 collections)
P_{02}	2.88 (16 collections)	/	/
P_3	4.03 (9 collections)	/	/

4.2. High Volume (HV) PM Sampler

$PM_{2.5}$ and $PM_{0.1}$ were collected by a high volume (HV) PM sampler (BGI 900 High Volume Cascade Impactor) fitted with three stages of the impactor (PM_{10}, $PM_{2.5}$, and $PM_{0.1}$), polyurethane foam (PUF) filter as impacting matrix and ultrafine fiber filter as the residual stage. A cascade impactor works based on the principle of Cascade Impaction, in which certain size fraction of the total particulate matter will pass the designed orifice under specific air flow. So, particles collected on each stage are normally distributed in size, with a median of stage designed size. Using PUF filter, which has larger pores and lower density than traditional filters as the collection matrix largely reduces the bounce-off losses of PM, increases the collection capacity, and enables easier particles retrieval for analysis on particulate only[126].

The sampler was set up on the roof of Choppin Hall, Louisiana State University (marked as HV#1 in Figure 4.2. and Table 4.1.), which is a seven-story building. The sizes of PUF filter for three collection stages are: PUF for PM_{10} - inside diameter 3.5 inches, outside diameter 6.5 inches, actual measured D_{50} 9.5 μm; PUF for $PM_{2.5}$ - inside diameter 4.5 inches, outside diameter 5.5 inches, actual measured D_{50} 2.5 μm; PUF for $PM_{0.1}$- inside diameter 4.75 inches, outside diameter 5.25 inches, actual measured D_{50} 0.17 μm. Before collection, PUF filters were prepared by sequential washing with Milli-Q water, hexane (≥95%, MilliporeSigma), methanol (≥99.8%, BDH), and dichloromethane (99.9%, MilliporeSigma) under 1-hour sonication each. After cleaning, PUF filters were covered and left overnight to dry, and cleaned PUF filters were stored

at 4 °C in plastic bags before use. The air sampling rate of 900 L/min was checked by a BGI High Volume Calibrator before each sampling, and PM was collected continuously for two weeks. After collection, PUF filters were cut into 1 cm^2 pieces and tapped to retrieve free falling particles ($PM_{0.1}$ TAP and $PM_{2.5}$ TAP). These particles were weighed to be analyzed separately. The remaining particles in the matrix were retrieved by sonication in water: filter pieces were put into a beaker with 50 mL Milli-Q water and sonicated for 10 minutes, filters were removed, and the water suspension was immediately frozen using dry ice and acetone mixture and beakers were then loaded to the lyophilizer (Labconco Co., model #7740020) until dry and corresponding particles were collected ($PM_{0.1}$ FD and $PM_{2.5}$ FD), weighed, and ready to be analyzed. Table 4.3 compared the features of high volume (HV) PM sampler with the phtosampler. A picture of the BGI 900 High Volume Cascade Impactor is shown in Figure 4.4.

Table 4.3. Comparison of the new phytosampling method and high volume (HV) PM sampler method.

BGI 900 High Volume Cascade Impactor	Phytosampler (leaves)
Collection time: 2 weeks	Collection time: flexible from 1 day after the rain up to next rain
Collection major steps: PUF filter cleaning; Sampler setting up; Flow rate checking; Sample collection; Particles extraction.	Collection major steps: Leaves collection and environment condition recording; Leaves area measurement; Washing and sonication; Filtration; Freeze Drying.
PM size: normally distributed with a median of stage designed size.	PM size: < filter size (filter cut-off).

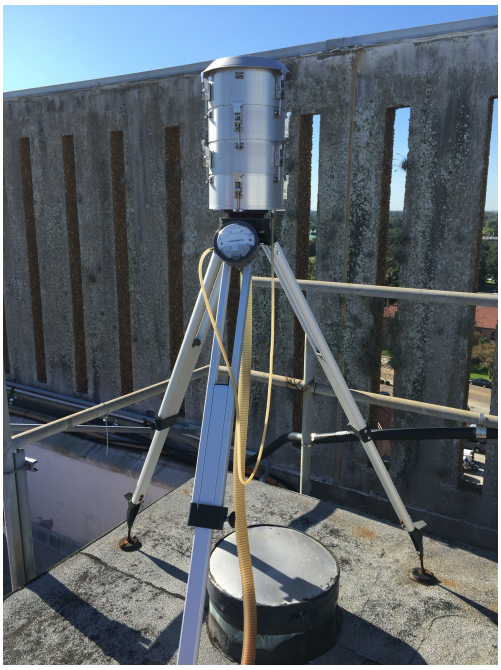

Figure 4.4. BGI 900 high volume cascade impactor.

4.3. Leaf and PM Surface Morphology and Elements Analysis Comparison

The PM retrieving procedure from the leaves surface includes sonication of collected leaves. Compromising leaf integrity may affect the outcome of the process and introduce the experimental artifacts. Scanning Electron Microscope (SEM) has been used to analyze the leaf surface before and after the PM retrieving (Figure 4.5.). These pictures show the stomata and trichomes on leaf surface both before and after the treatment, and the number of particles captured on the leaf surface reduced after the retrieving with no damage to the structure of the leaf surface.

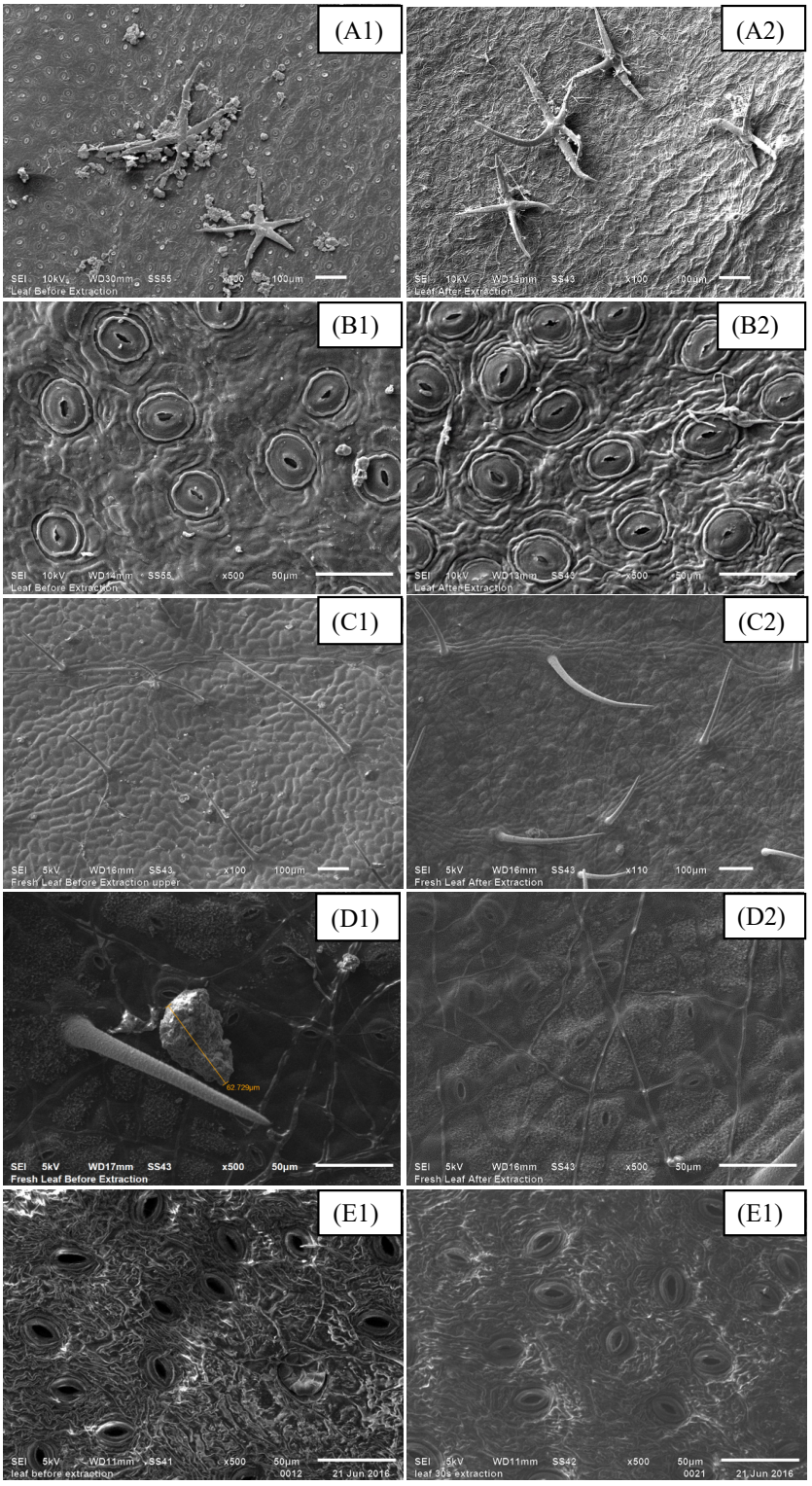

Figure 4.5. SEM results on leaf surface before (A1, B1, C1, D1 and E1) and after (A2, B2, C2, D2 and E2) the PM retrieving from two species. (A and B are from the leaves of *Hedera helix* (the common ivy), which were collected from Memphis, Tennessee for our previous study. C-E are from the leaves of *Ligustrum japonicum* (Japanese privet).

The SEM results in Figure 4.6 show typical PM morphology, and fine and ultrafine particles are always present as an aggregate of a lot of small particles. The Energy Dispersive X-ray Spectroscopy results of retrieved particles from both HV PM sampler ($PM_{0.1}$ TAP, $PM_{0.1}$ FD, $PM_{2.5}$ TAP, and $PM_{2.5}$ FD) and phytosampling methods (P_{02} and P_3) are shown in Figure 4.7. The spectrum next to each sample figure is an example of the spectroscopy result and shows all the elements that we analyzed. Elemental carbon and oxygen accounted for a majority of elements in the samples from both collection methods. However, C, O, and Pt are also background elements due to the utilization of carbon tape and platinum coating for sample fixing. Thus, the actual content of those elements cannot be established with this method. We have normalized remaining elements data and presented as inset graphs with the average from several samples in analysis areas. The results show higher sodium, silicon, aluminum, sulfur, and chlorine contents in the HV samples, while potassium and calcium were higher in phytosampled samples. It is, however, worth noting that nitrogen and sulfur were also prominent in P_{02} samples from phytosampling method. These elements are commonly detected in ambient PM, and nitrogen and sulfur are mainly from nitrates and sulfates, which are the most abundant inorganic components of secondary PM in the ambient air.

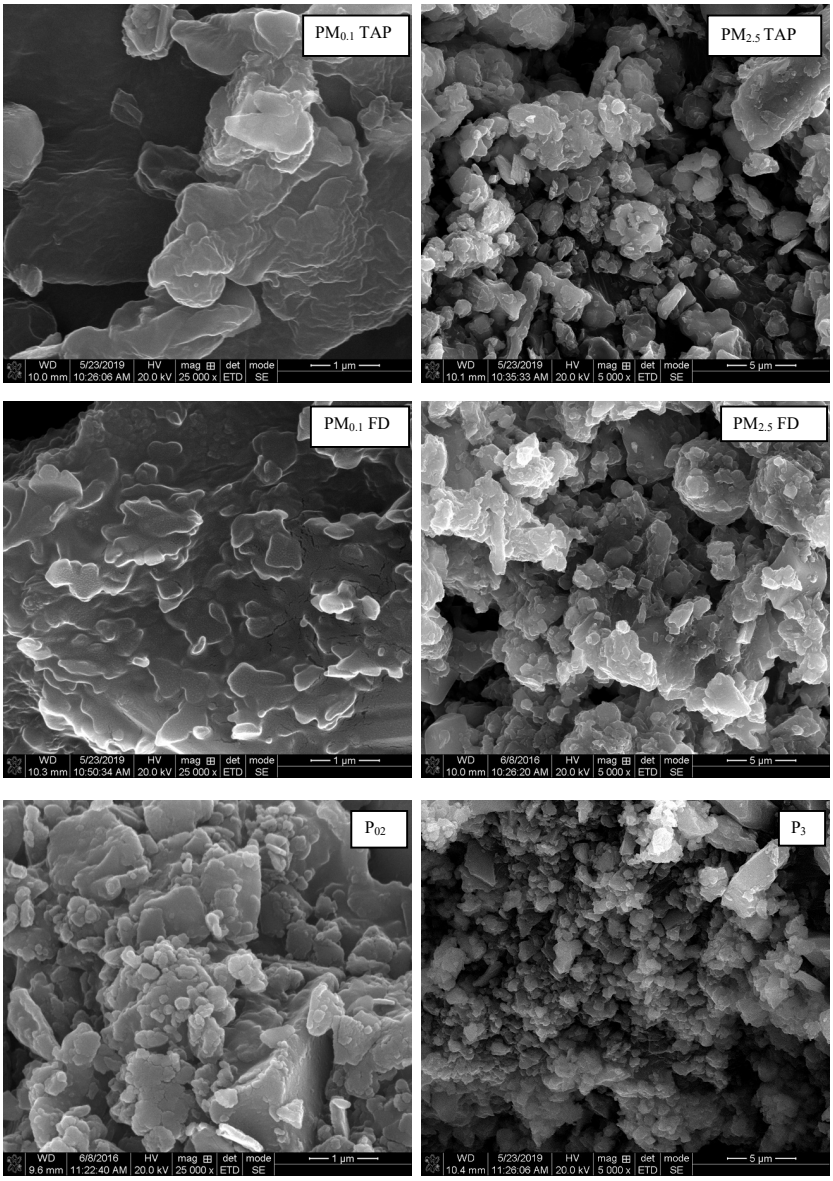

Figure 4.6. Scanning electron microscope images of retrieved particles from both HV PM sampler ($PM_{0.1}$ TAP, $PM_{0.1}$ FD, $PM_{2.5}$ TAP and $PM_{2.5}$ FD) and phytosampling method (P_{02} and P_3).

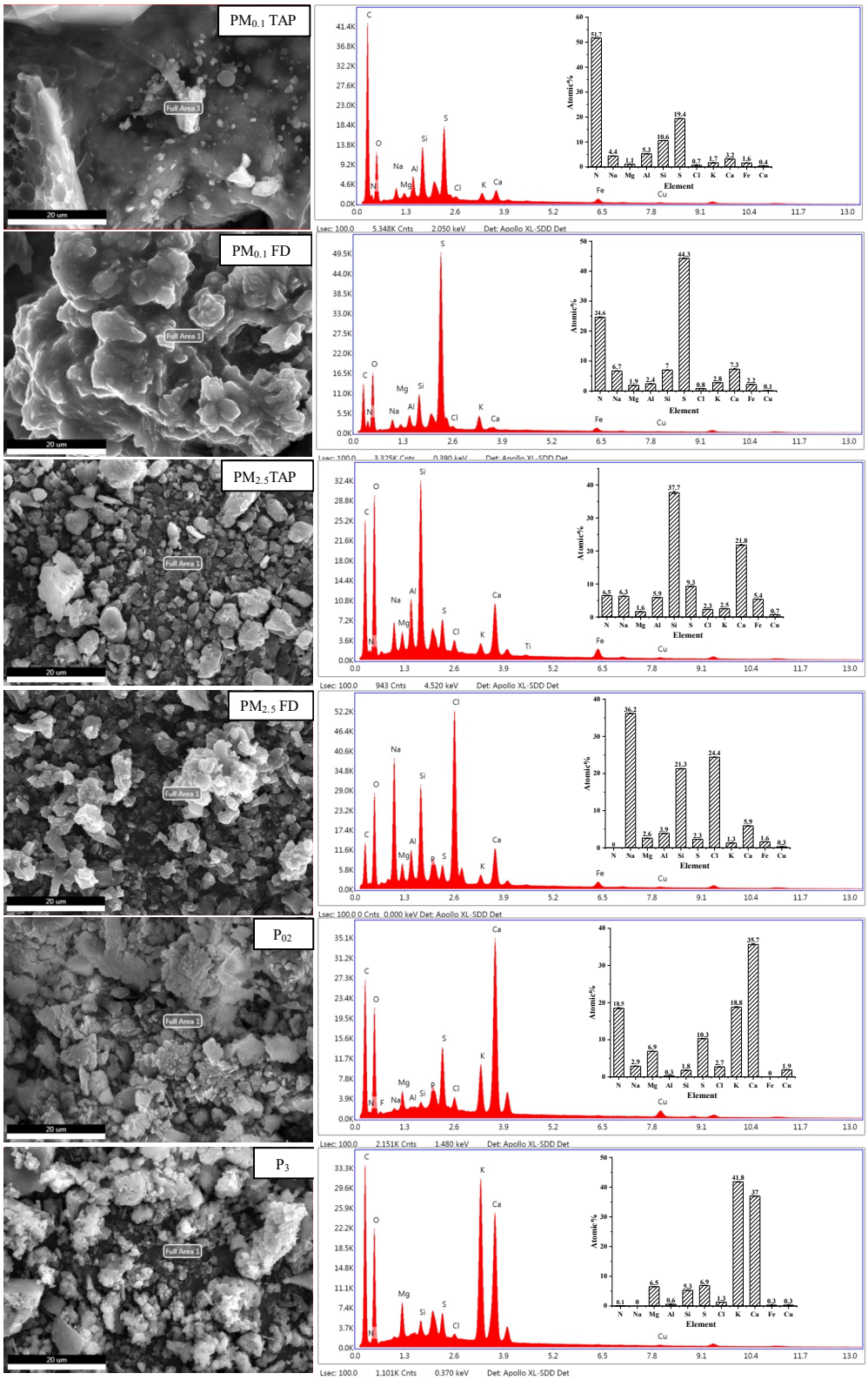

Figure 4.7. Energy dispersive x-ray spectroscopy results of retrieved particles from both PM sampler ($PM_{0.1}$ TAP, $PM_{0.1}$ FD, $PM_{2.5}$ TAP and $PM_{2.5}$ FD) and phytosampling method (P_{02} and P_3).

4.4. EPFRs Characteristics Analysis and Comparison

EPFRs concentration and characteristics of PM samples were measured and compared between two collection methods. The g-factor, ΔHp-p, and EPFRs concentration were averaged for P_{02} (16 batches), P_3 (9 batches), $PM_{0.1}$ TAP (8 retrievable batches), $PM_{0.1}$ FD (11 batches), $PM_{2.5}$ TAP (7 retrievable batches) and $PM_{2.5}$ FD (10 batches).

The average g-factors of all samples are in the range of 2.0030-2.0050. The values closer to 2.003 is indicative of more carbon-centered radicals, while higher g-factors (2.004 and above) is typical for oxygen-center EPFRs[22]. The g-factor of EPFRs on phytosampled PM (>2.0045) is statistically significantly higher ($p<0.01$) compared to those collected by HV PM sampler (<2.0040), while the g-factor of EPFRs from same collection method but different PM sizes is not statistically significantly different from each other (Figure 4.8. (A)). Therefore, EPFRs on "phytosampled" PM contain a larger contribution of oxygen-centered EPFRs compared to PM from HV PM samplers. This supports our hypothesis that the collection method affects EPFRs characteristics (and potentially other chemical changes). We posit that using air sampler (particularly for a long collection period) results in a change of environment of PM on the matrix (no sunlight, high air-solid exchange ratio due to high flow of air), thus impacting suspended particles. On the contrary, PM deposited on the leaves is exposed to conditions that resemble more those of PM suspended in the air.

To investigate the impact of sample treatment during PM recovery from the matrix, we compared a fraction of PM tapped out of the collection matrix with that removed by sonication followed by freeze drying. We found that applied treatment does not significantly impact EPFRs and elemental composition (the observed variation in the elemental composition can account for

heterogenicity of PM samples). For both types of samples, ΔHp-p is similar, between 6.9 and 7.7, and indicates a presence of carbon- and oxygen-centered EPFRs mixture.

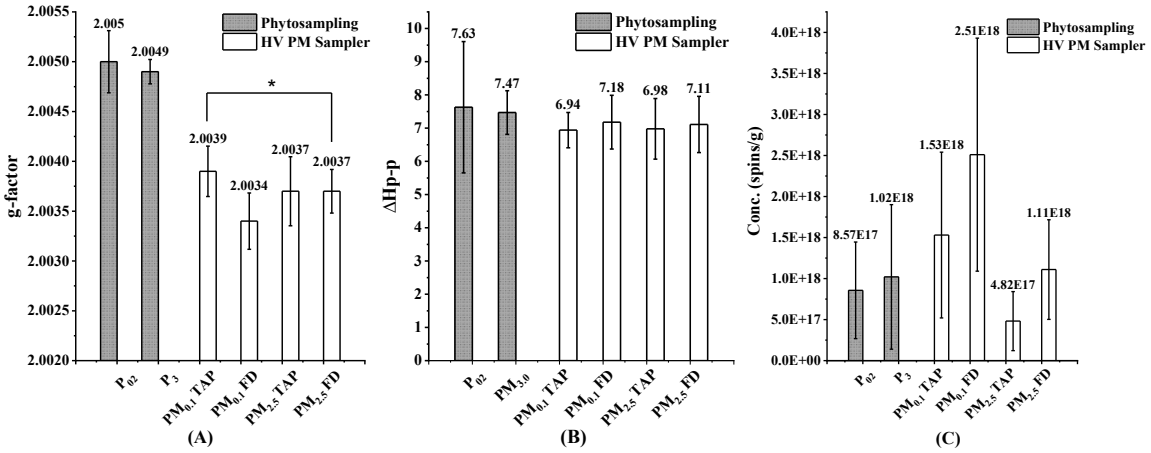

Figure 4.8. Average g-factor (A), ΔHp-p (B) and spins concentration (C) of EPFRs on $PM_{2.5}$, $PM_{0.1}$, P_{02}, and P_3. * is indicating for significant difference by ANOVA ($p<0.01$).

No relationship between EPFRs concentration with PM size was detected for samples collected by the phytosampling method (Figure 4.9.). However, for HV PM sampler collected samples, $PM_{0.1}$ always contains higher EPFRs concentration than $PM_{2.5}$. We believe that the differences in EPFRs with PM size below 2.5 micron diameter is a result of inherent PM size artifact in an impactor. EPFRs are typically associated with PM of combustion origin, which is below 2.5 μm in size. In cascade impactor, particles collected on each stage are normally distributed in size, with a median of stage designed size. Thus, the collection stage for $PM_{2.5}$ will also collect larger and heavier particles, which are more typical to erosion, dust, and sand, not containing EPFRs. With the decreasing nominal size of the collection stage, the contribution of those large particles is decreasing significantly. This is in line with other observations[27,127] that related increased EPFRs concentration on smaller PM with higher carbon content. The phytosampling method, in contrast, is a filter size cutoff method which will only collect particles with the size below the filter size.

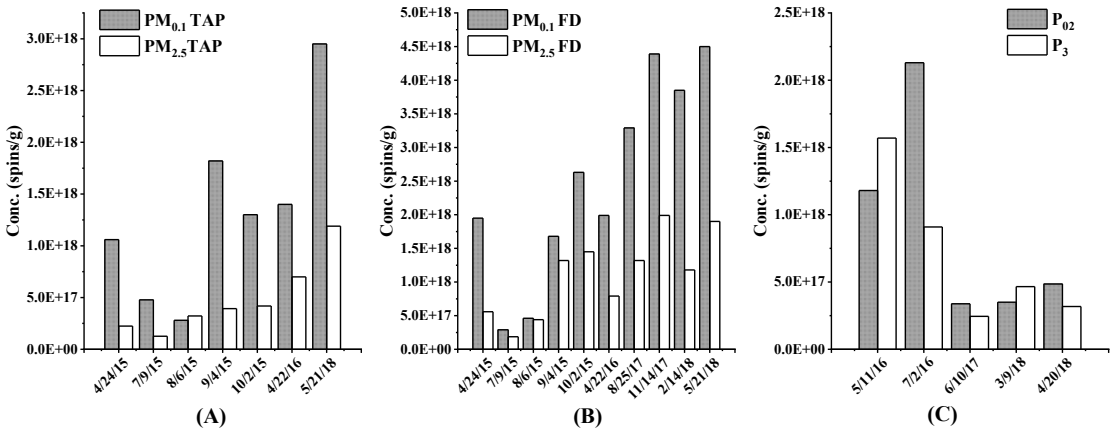

Figure 4.9. Comparison of spins concentration of EPFRs on $PM_{2.5}$, $PM_{0.1}$, P_{02}, and P_3 within the same collection batch. A is the comparison of EPFRs spins concentration between $PM_{0.1}$ TAP and $PM_{2.5}$ TAP collected from HV PM sampler. B is the comparison of EPFRs spins concentration between $PM_{0.1}$ FD and $PM_{2.5}$ FD collected from HV PM sampler. And C is the comparison of EPFRs spins concentration between P_{02} and P_3 collected from phytosampling method.

4.5. Simulated Sample Aging Analysis

The simulated sample aging study is to mimic the condition of HV PM sampler (active) and phytosampling (passive) in a laboratory setup. The results are shown in Figure 4.10. A significant difference in EPFRs changing behavior between HV samples and phytosamples was observed. In general, HV samples have shown an over-time decay behavior, described by others[28,128], with EPFRs lifetime ranging from 63-167 days depending on the mode of aging (forced air flow – active aging or diffusion air contact – passive aging). On the contrary, phytosamples have shown an increasing EPFRs concentration with time to reach a steady state level (with trending concentration downwards after prolonged aging). Interestingly, for HV samples, g-factor remains relatively constant, while decreasing with aging for phytosamples. Based on these observations, we have concluded that EPFRs in natural environment are formed by oxidation leading to oxygen-centered EPFRs (higher g-factor) and at the same time decay and convert to carbon-centered EPFRs. This is why during aging, though the g-factor on phytosampled

EPFRs is declining (increasing contribution of C-centered EPFRs), overall radical concentration is increasing. On the contrary, HV PM samples provide a snapshot of PM further in time (due to prolonged exposure to high air flow in the sampler) where g-factor is already much lower, and no formation of new EPFRs is observed. Due to the two-week collection time, the captured aging start point for HV PM sampler samples is more comparable to the point at 300-400 hrs in the phytosampling PM aging studies where it is approaching the steady and decay phase.

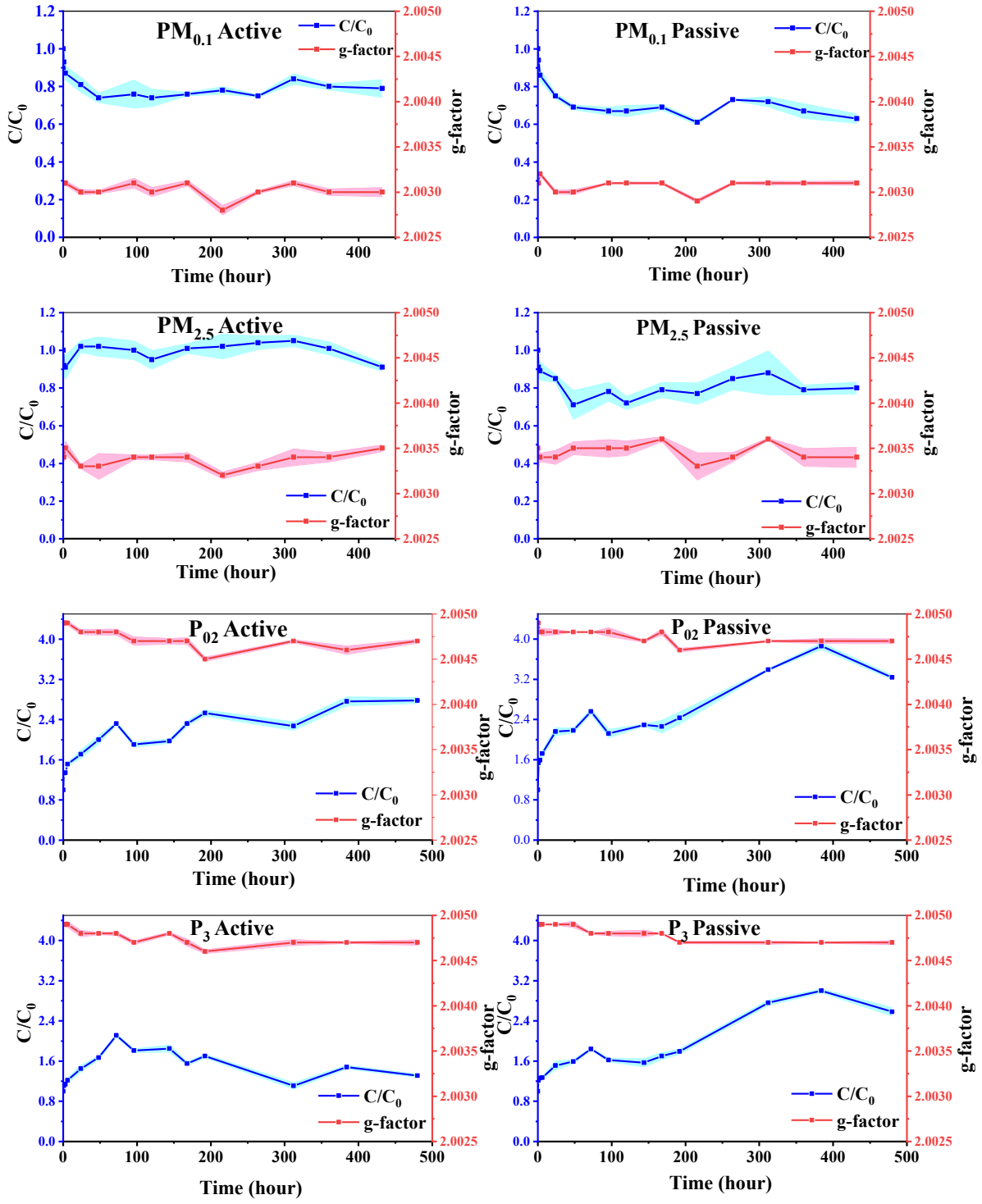

Figure 4.10. Comparison of spins concentration (blue) and g-factors (red) of EPFRs on PM from both collection methods under different aging conditions (active and passive). $PM_{0.1}$ and $PM_{2.5}$ were collected from HV PM sampler while P_{02} and P_3 were collected by phytosampling method.

4.6. Hydroxyl Radical and Superoxide Generation by EPFRs

Since the toxicity of EPFRs is associated with the generation of ROS, a spin trapping study was conducted to quantify the production of hydroxyl radicals. Two spin trapping reagents had been used to test the generation of ROS in phosphate buffered saline solution (PBS). 5,5-dimethyl-1-pyrroline-N-oxide (DMPO) was used to trap hydroxyl radicals, and the difference of DMPO−OH adduct concentration between results under O_2 presence and N_2 presence is the generation of hydroxyl radicals by EPFRs (Figure 4.11.). This kind of difference was observed from both HV air samples and phytosamples. Average hydroxyl radical production among eight measurements in 300 mins for $PM_{0.1}$ FD and $PM_{2.5}$ FD are 0.14 nmol/μg and 0.03 nmol/μg. And the average hydroxyl radical production among five measurements in 400 mins for P_{07} is 0.16 nmol/μg. These concentrations are corresponding to the following hydroxyl radical generation potential: for $PM_{0.1}$, 1 EPFR generated 19 •OH; for $PM_{2.5}$, 1 EPFR generated 9 •OH; and for P_{07}, 1 EPFR generated 18 •OH. From this result, the generation of hydroxyl radicals by PM collected from both methods is at a similar level and in line with the results published by Khachatryan et al. that after 140 mins of incubation, one EPFR could generate about ten hydroxyl radicals[32]. However, the difference of hydroxyl radical generation under two experimental conditions cannot always be identified on every sample, which may result from different chemical compositions of particles and short half-life of hydroxyl radical, so that this concentration level reported here could only be regarded as a reference value. The experiment procedure also needs to be optimized and more experiments are required.

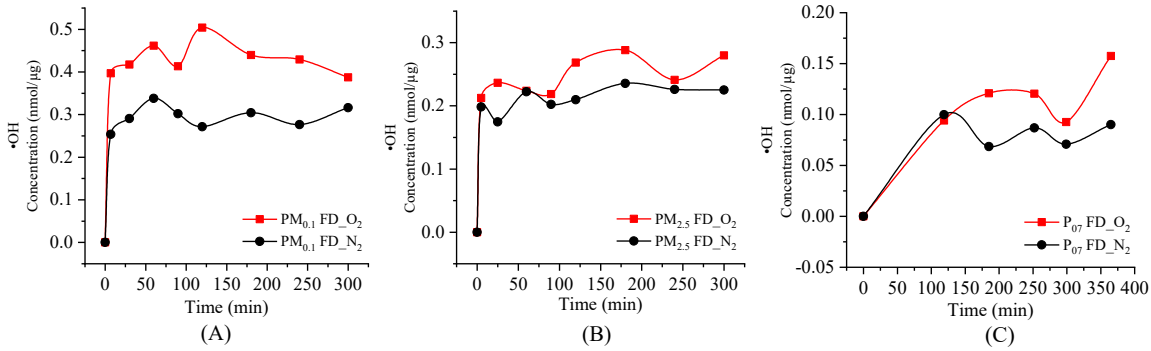

Figure 4.11. Hydroxyl radical generation curve under presence of N_2 and O_2. A is the experiment result conducted on $PM_{0.1}$ FD collected by HV PM sampler. B is the experiment result conducted on $PM_{2.5}$ FD collected by HV PM sampler. And C is the experiment result conducted on P_{07}, which was collected by phytosampling method.

Another spin trapping reagent 5-tert-Butoxycarbonyl-5-methyl-1-pyrroline-N-oxide (BMPO) was used to trap superoxide radicals, which is the precursor of hydroxyl radicals according to the redox cycle showed by Dellinger et al.[56]. Xanthine oxidase will catalyze the reaction of xanthine with oxygen and water to produce uric acid and superoxide radicals, and this reaction is always used as a standard for superoxide radical generations. BMPO superoxide adduct spectrum has two shoulders on the two center peaks, as shown in the xanthine reaction spectrum in Figure 4.12. The features for superoxide radicals on the spectra from tested PM samples and the surrogate model EPFRs samples (MCP230) are not very clear, meaning that we can only detect the hydroxyl radical signals in our procedure settings.

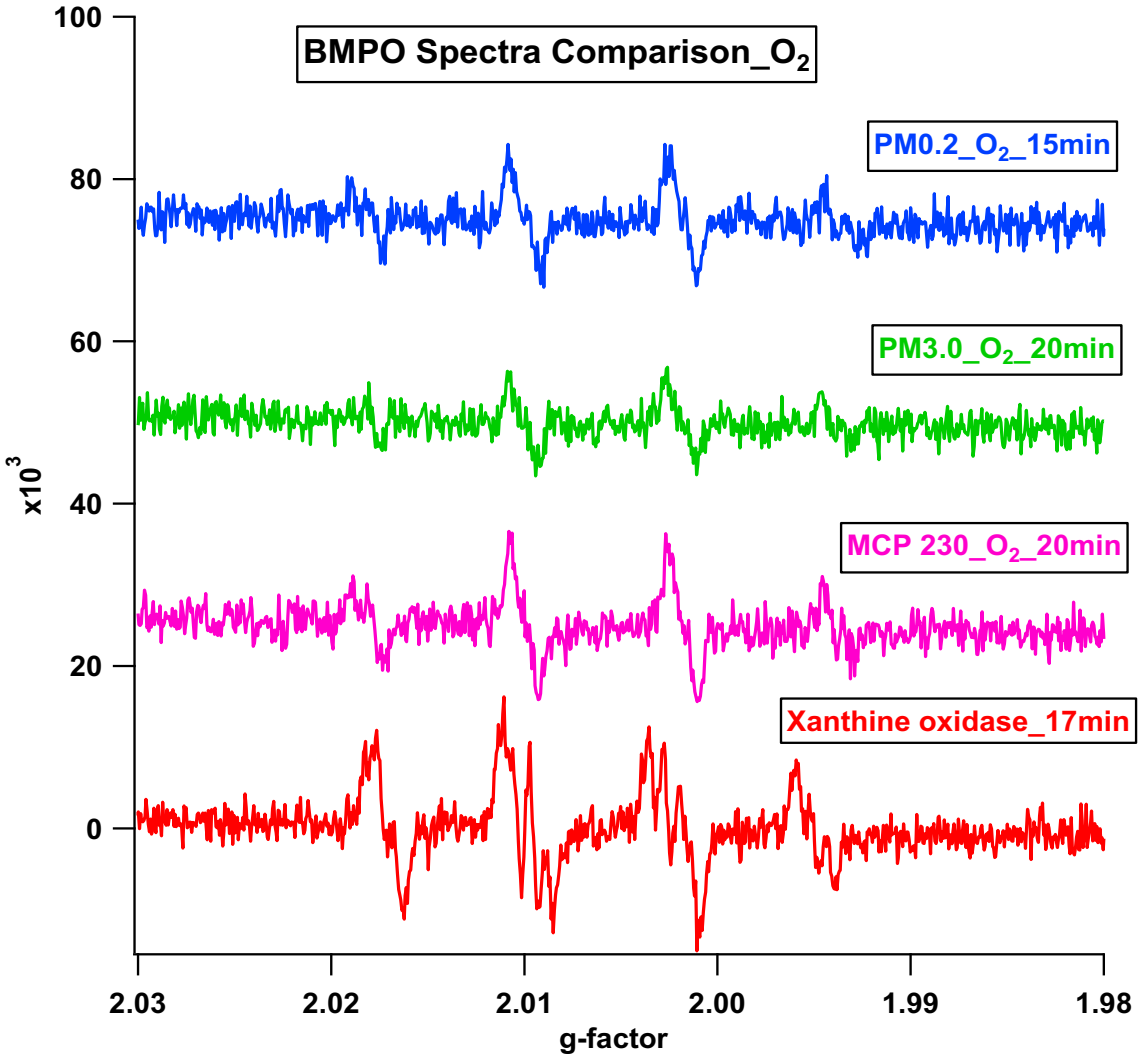

Figure 4.12. Spectra of BMPO adduct from PM samples and xanthine.

4.7. PAHs Concentration Comparison

Three batches of PM from the HV PM sampler and two batches of PM from phytosampling had been extracted and analyzed for PAHs contents. For phytosamples, larger particle size (P_3) contains in both cases more PAHs compared to ultrafine samples (P_{02}) (Figure 4.13. (B)). This is in contrary to HV samples, where smaller PM contains typically more PAHs (Figure 4.13. (A)). This result is anticipated and due to the difference in collection methods – phytosamples represent all particles with a diameter below filter cutoff size, thus P_3 includes all

PAHs associated with smaller particles. But this is not the case for HV samples, which represent a normal distribution of particle sizes with shifting median.

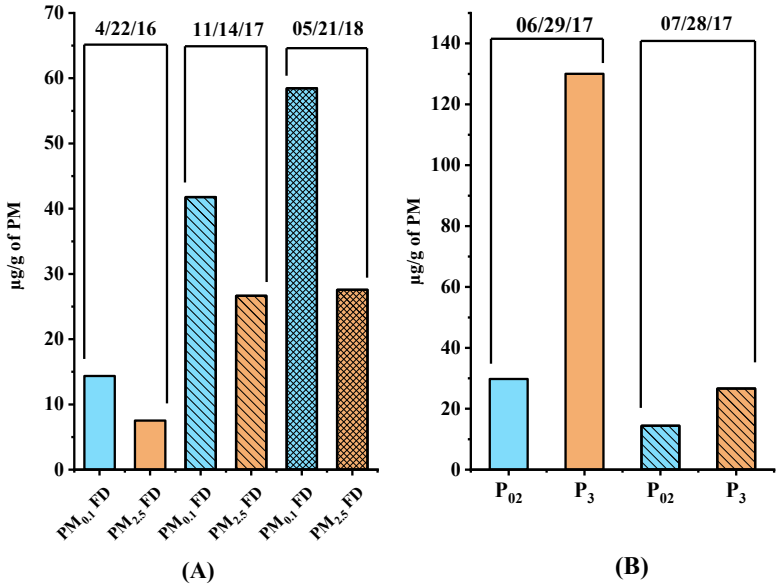

Figure 4.13. Concentration of total PAHs on PM from PM sampler (A) and phytosampling (B).

The normalized percentage concentration of PAHs to the total PAHs has been shown in Figure 4.14. Specific PAH profile for both sizes (P_{02} and P_3) of phytosamples were very similar (Figure 4.14. (A)), dominated by the presence of Perylene, Benzo[b/k/j]fluoranthene, Anthracene, Benzopyrenes, and to lesser extent Fluoranthene and Dibenz[a,h]anthracene. For HV samples (Figure 4.14 (B)), a distinct difference is noticed in PAH profiles with the changing size: $PM_{2.5}$ samples contain relatively higher amount of lighter PAHs (4 or fewer rings, profile dominated by Pyrene, Fluoranthene, and Phenanthrene), while $PM_{0.1}$ contain more heavier PAHs (more than 5 rings, profile dominated by Indeno[1,2,3-c,d]pyrene and Benzo[g,h,i]perylene]). The sample collected on 05/21/2018 appears to show a different pattern in both $PM_{0.1}$ and $PM_{2.5}$ sizes and indicated a different source of PM. In fact, this sample resembles more phytosamples in respect of specific PAH profile. Though no sufficient data is available, it is possible that this resemblance is associated with the seasonal change in PAHs profile (this specific HV sample and both

phytosamples were all collected in the summer months, while other HV samples were collected in cooler months).

It is not possible at this point to explain the differences in the PAHs profile between $PM_{0.1}$ and $PM_{2.5}$, considering that such differences are not observed for phytosamples. One can speculate that it might be associated with the combination of the collection method and the vaporization of lighter PAHs from smaller particles (high surface-volume ratio). This finding, however, underscores the advantage of phytosampling over impactors for chemical speciation characterization associated with PM in ambient air.

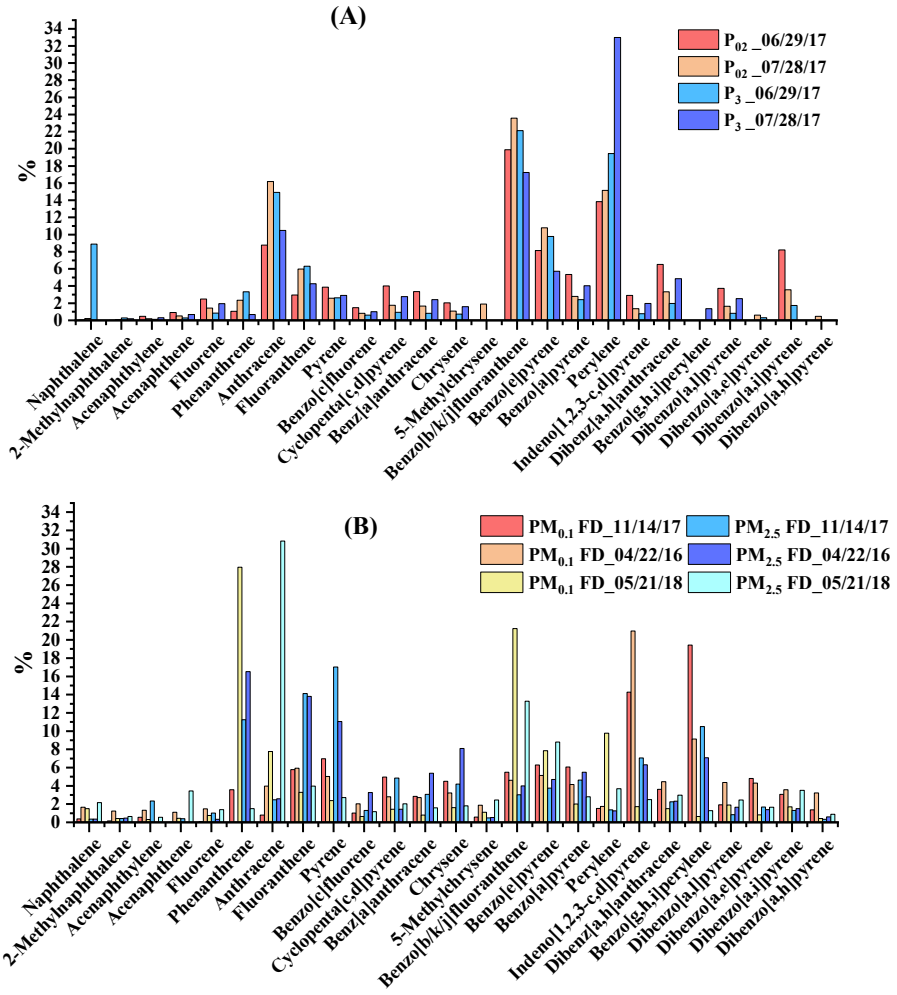

Figure 4.14. Comparisons of PAHs concentration on PM from both collection methods between similar particle sizes. A compares the PAHs profiles between P_{02} and P_3 from two collections by phytosampling method. B compares the PAHs profiles between $PM_{0.1}$ FD and $PM_{2.5}$ FD from three collections by HV PM sampler.

4.8. Cell Viability Test

BEAS-2B cells were exposed to PM collected from both methods and surrogate MCP-230, DCB-230 particles. All results are normalized to the blank and plotted as particle exposure level to cell viability. $PM_{0.1}$ and $PM_{2.5}$ show different dose-response relationships (Figure 4.15.). $PM_{0.1}$ has a linear dependence of dose-response, while $PM_{2.5}$ shows an exponential dose-response. These two types of PM behave differently in our test. Cell viability to the exposure to $PM_{0.1}$ drops slower

in the low PM concentrations and faster when concentration increased. However, cells have a faster response at the lower dose of $PM_{2.5}$ and then stays stable or respond much slower.

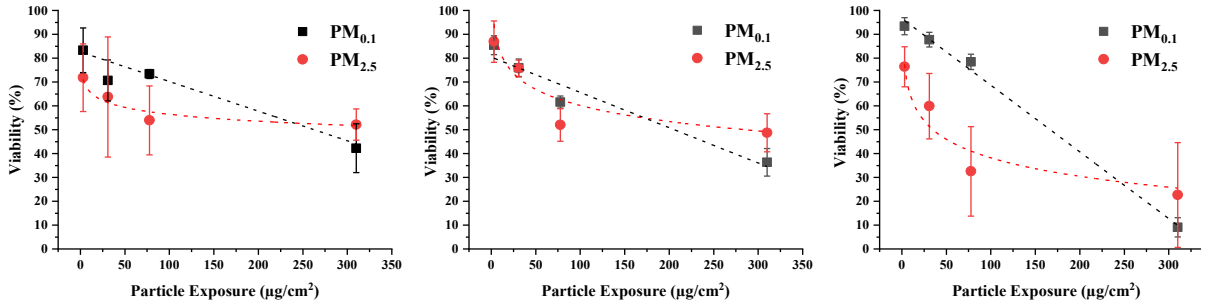

Figure 4.15. All three panels show similar trend of cell viability test results from three batches of $PM_{0.1}$ and $PM_{2.5}$ samples collected by HV PM sampler. $PM_{0.1}$ has a linear dose-response while $PM_{2.5}$ shows an exponential dose-response.

Figure 4.16 evaluates the correlation between cytotoxicity and the g-factors of EPFRs. For $PM_{0.1}$ shown in the A1 and A2 panels, two samples with similar radical concentrations (black and blue curves) have similar response patterns; however, one sample (red curve) shows much lower toxic dose (TD50). And panel A2 plots their g-factors, and this sample has a much higher g-factor, which indicates that oxygen-centered radicals put more stress to the cells. Panel B1 and B2 are the results comparing three $PM_{2.5}$ samples. Cell viability response curves all show exponential dose-dependence, and two samples behave similarly (black and blue curves), while the one with the highest g-factor shows the more toxicological effect (red curve). The relationships of g-factor and slope in these samples (panel B2) are not very clear, indicating that the toxicity could be a result depends on both concentration and g-factor of radicals.

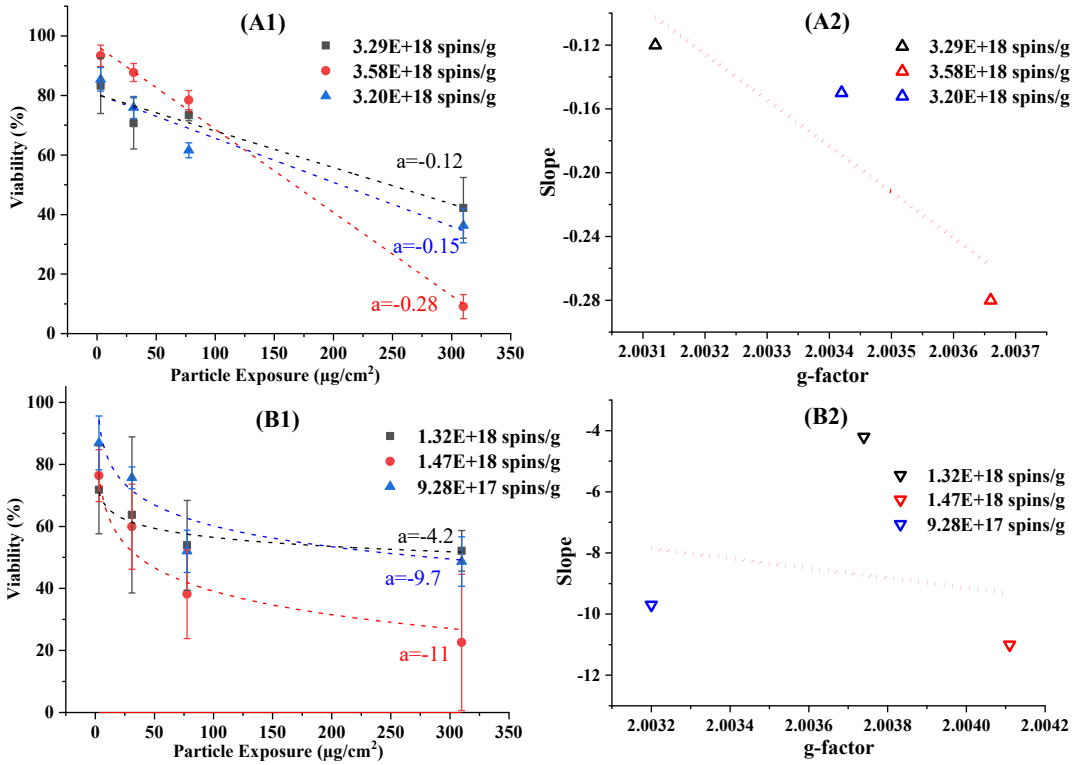

Figure 4.16. Correlation of the dose-response curve slope and sample g-factor for HV PM samples. A1 and A2 are results for $PM_{0.1}$ while B1 and B2 are results for $PM_{2.5}$.

Figure 4.17 shows the dose-response curve fitting for phytosamples. Both P_{02} and P_3 show a linear dependence. All four samples have close g-factors (2.0047). The toxicological effects of P_{02} and P_3 resemble more of $PM_{0.1}$ from HV PM sampler which is anticipated due to their common combustion origin. In panel A, two P_{02} samples also have similar concentrations, so they behave alike. In panel B, the parallel dependence line with the same slope could be a result of the concentration difference.

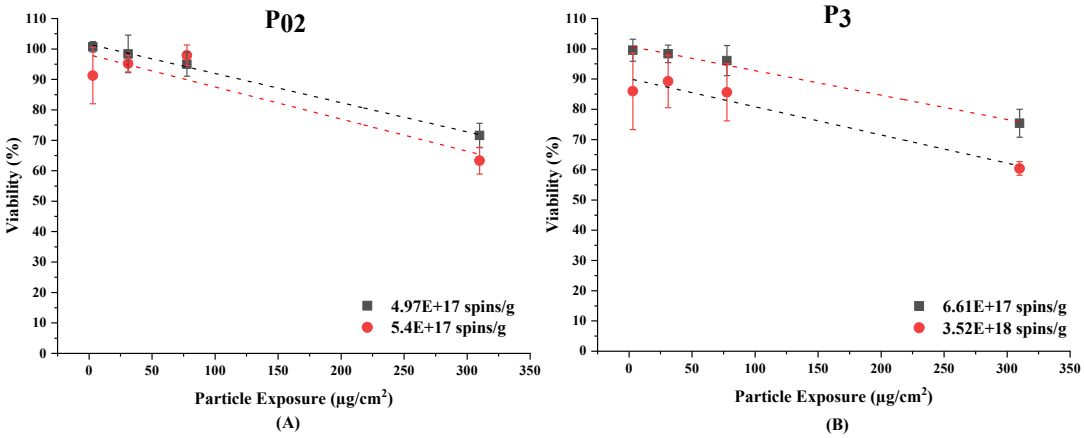

Figure 4.17. Both P_{02} (A) and P_3 (B) show linear dose-response relationships.

Simulated aging PM exposure study could provide information to asses if EPFRs concentration has any effect on the toxicity change of the EPFRs. We used the same simulated active/passive aging method to treat PM, as discussed earlier, and exposed BEAS-2B cells to aged particles. Figure 4.18 panel A shows the dose-response of cells to fresh and aged $PM_{0.1}$. The radical concertation drops almost 50% after aging, but there is no significant change in g-factors in both aging patterns (change within 0.0001, and data for g-factor is not shown). The toxicological effect was eased on aged samples with similar curve slope except that the first two points of active samples have some problems and are not reliable. This result is consistent with the previous finding that sample radical concentrations shift the position of the dose-response curve, but the slopes of the curve (potential for toxicological effects) stay similar when their g-factors are close. Panel B is a set of $PM_{2.5}$ samples fitting exponential curves. The trend is similar, not considering the active sample, which has some data point exceeding 100%. Panel C shows the results for P_{02} and panel D for P_3. In both cases, g-factor change after aging is within 0.0001. The cell response curves to these two phytosamples based on the radical concentration changes generally follow the same trend as observed in HV air sampler samples. So, in summary, g-factor could change the slope of dose-response curve, and concentration will result in a shifted position on dose-dependence curve.

More experiments are needed to confirm the toxicological effects of the radicals on PM to the BEAS-2B cells.

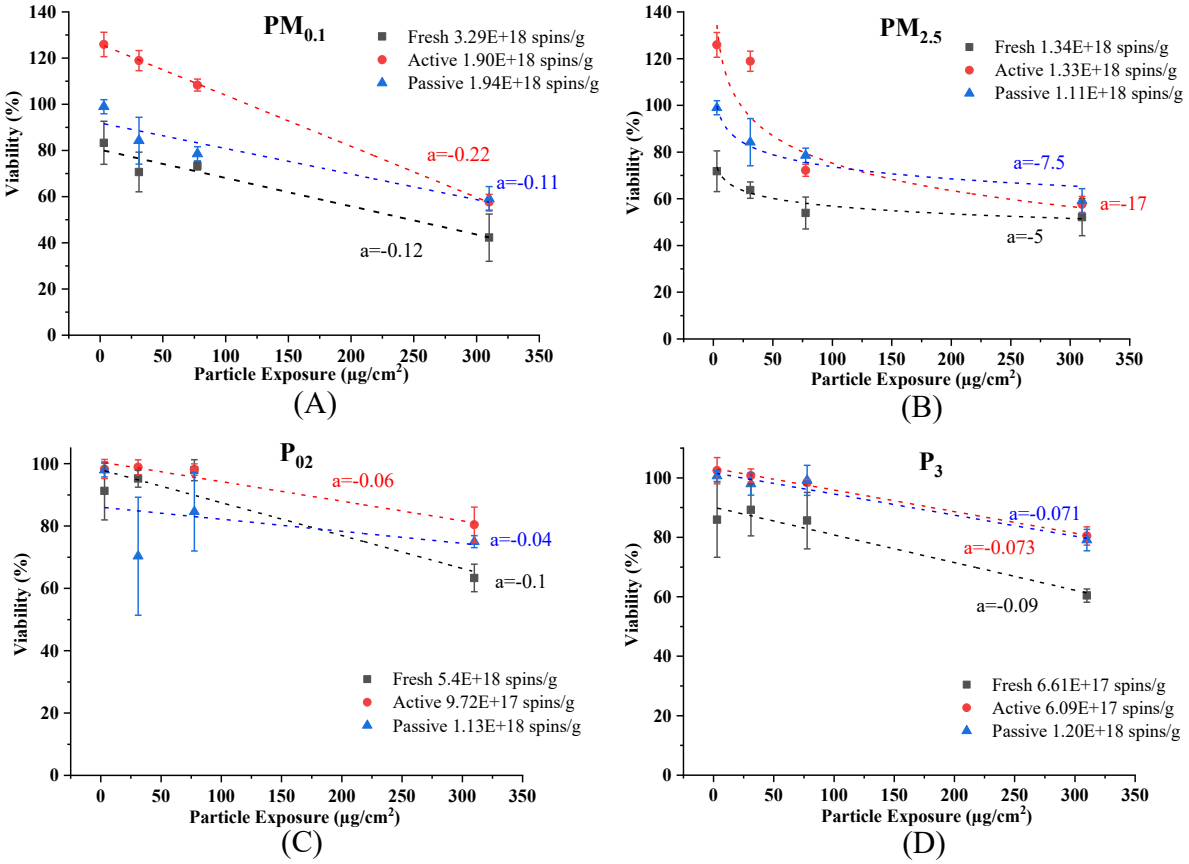

Figure 4.18. Comparison of dose-response relationship of fresh PM samples with aged PM samples from both HV PM sampler (A and B) and phytosampling methods (C and D). The slope of each dose-response curve is denoted as "a" in the figure.

The PM cytotoxicity from the ambient PM samples could also be a result from chemicals other than EPFRs presented on the surfaces of PM. To fully understand the effect of EPFRs, we conducted the cell viability test on surrogate MCP-230, DCB-230 particles and compared all the environmental samples that show linear relations to the cell exposure results of MCP-230 and DCB-230. The radical concentrations of environmental samples are generally 1-2 order magnitude higher than the surrogate samples. Figure 4.19 shows that the behavior on ambient air PM and the surrogate samples are very similar. However, the phytosampling samples show the least

toxicological effects with the highest g-factor and radical concentrations than HV samples and surrogate samples. The sampling methods did change the chemical composition of the PM, which will influence the toxicological effects of particles. Comparing phytosamples with surrogate samples that only contain EPFRs, there could be a possibility that some other mechanisms protect cells when exposed to phytosamples. But more replicated studies are needed to acquire more information to explain this phenomenon.

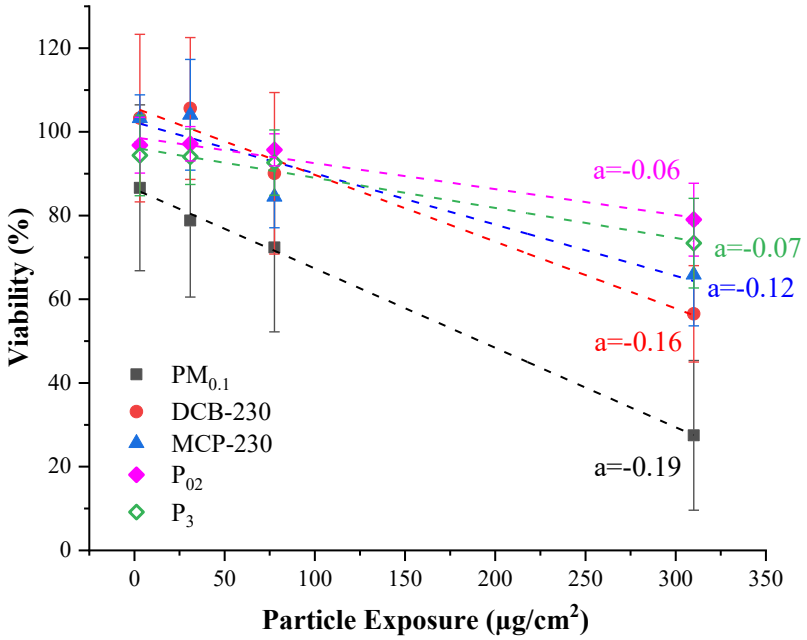

Figure 4.19. Comparison of dose-response relationship of environmental PM samples with surrogate MCP-230 and DCB-230 particles. The slope of each dose-response curve is denoted as "a" in the figure.

CHAPTER 5. PHYTOSAMPLING APPLICATIONS IN THE FIELD STUDIES

5.1. A Scalable Field Study in Memphis, Tennessee[1]

In this study, the phytosampling method has been applied to investigate the spatial patterns of EPFRs g-factor and concentration in Memphis, TN. Due to the spatially heterogeneous over a wide study area, the two official $PM_{2.5}$ monitoring sites (one in the downtown and the other in the east) set up by the Tennessee Department of Environment and Conservation could not capture the spatial variability of EPFRs g-factor and concentrations. So phytosampling was chosen to collected leaves contaminated by on-road mobile emissions to capture regional variability of the EPFRs and evaluate the community exposure in Memphis, TN. A field study was designed to measure the EPFRs on ambient PM collected by the phytosampling method and identify potential health risks to the Memphis community using Geographic Information System (GIS) and high spatial resolution Global Positioning System (GPS) technologies.

5.1.1. Sampling Sites Description

As the largest city in Tennessee, Memphis, located at Shelby County, is a major hub for river, highway, railroad, and air transportations, and several air pollutant emission hot spots have been identified in the north and south of the city[129–131]. This emission information was incorporated into the sampling site selection. Leaf samples were collected three days later following a rain from November 9th to 11th, 2015. A 32.9 × 28.4 km sampling grid with 188 samplings sites has been created with a link to the environmental characteristics, ambient pollution situation, and health

[1] Part of this chapter is reprinted with permission from Oyana, T. J., Lomnicki, S. M., Guo, C., & Cormier, S. A. (2017). A scalable field study protocol and rationale for passive ambient air sampling: a spatial phytosampling for leaf data collection. *Environmental science & technology*, *51*(18), 10663-10673. Copyright 2017. American Chemical Society.

outcomes. Sampling sites were located randomly in the area so that the sample site distribution could be representative for emission hot spots and important exposure factors. The sampling sites are shown in Figure 5.1. Due to the unexpected rain on November 12th, which washed off particles in the air, leaves from various tree species were collected from 107 sites (60% coverage) for analysis. Samples were transferred to the lab, and PM smaller than 3.0 μm (P_3) were retrieved from leaf surface by sonicating leaves in deionized water for 30 s and passing through a filtration assembly with 3.0 μm supported membrane filters followed by freeze drying as described before.

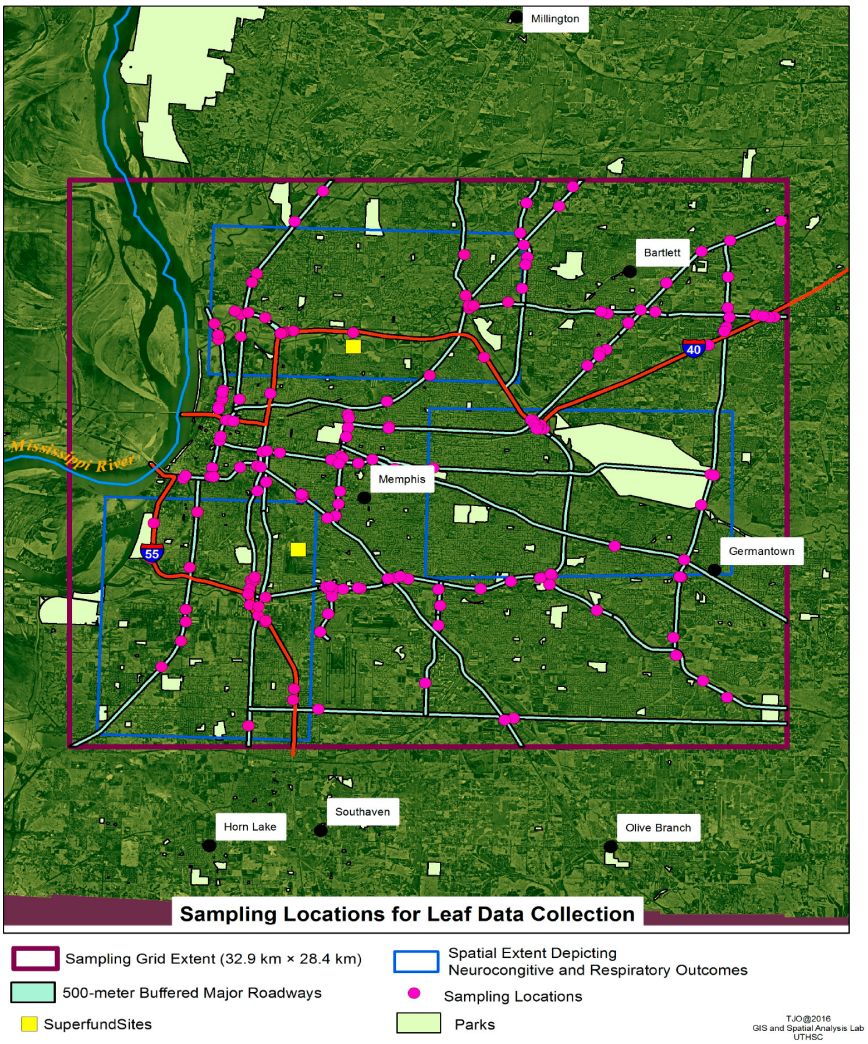

Figure 5.1. Sampling sites for leaves collection in Memphis. Blue boxes indicate the areas with health outcomes.

5.1.2. Spatial EPFRs Profile Analysis

EPFRs characteristics for all samples obtained by EPR were analyzed and presented on the map using a number of visualization techniques. All planned sampling sites were spread in seven geographical areas (downtown, midtown, east, north, northeast, south, and southeast Memphis) with five areas got samples collected (no samples in southeast and northeast). These collection sites involved key ambient pollution exposure factors, such as on-road mobile emissions, residence characteristics, and industrial sources. South Memphis is a major industrial area. The leaf capture efficiency for PM from different sampling sites varied a lot as we expected (0.3-41.7 μg/cm^2), but there are no significant differences between any of five regions and the overall average collection efficiency across the areas is 6.81 μg/cm^2. EPFRs concentrations were quantified in spins/g and also showed the variation across the areas with the range of 1.14×10^{17}-3.68×10^{19}. Based on the EPFRs concentration, samples are categorized into three bins: low EPFRs concentration (below 7.99×10^{17} spins/g), medium (7.99×10^{17}–1.99×10^{18}), and high (1.99×10^{18} and above) corresponding to low, moderate and high EPFRs laden samples. These three categories were plotted in Figure 5.2.

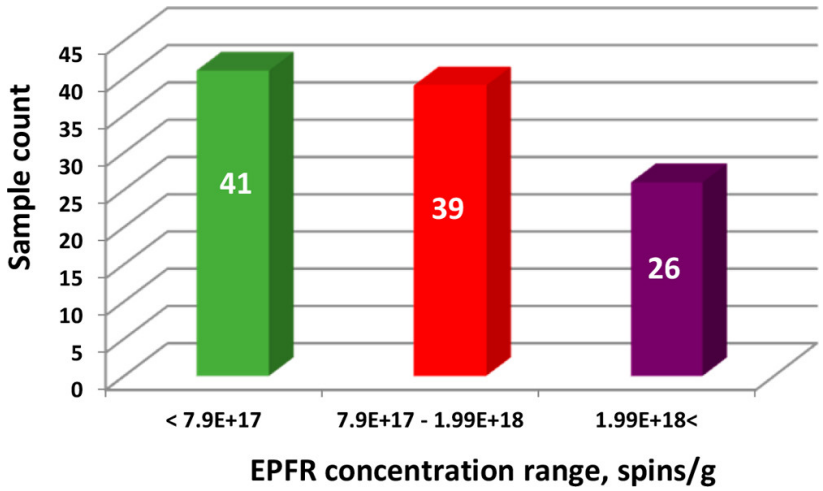

Figure 5.2. Three sample categories based on EPFRs concentration.

The g-factor indicating the radical species for these three categories are 2.00442, 2.00475, and 2.00482, respectively. And a trend between g-factor and radical concentration has been observed from Figure 5.3 that higher g-factor is associated with higher radical concentrations. The higher the g-factor, the more oxygen-centered radicals[22], which are typical from PM produced under incomplete combustion conditions.

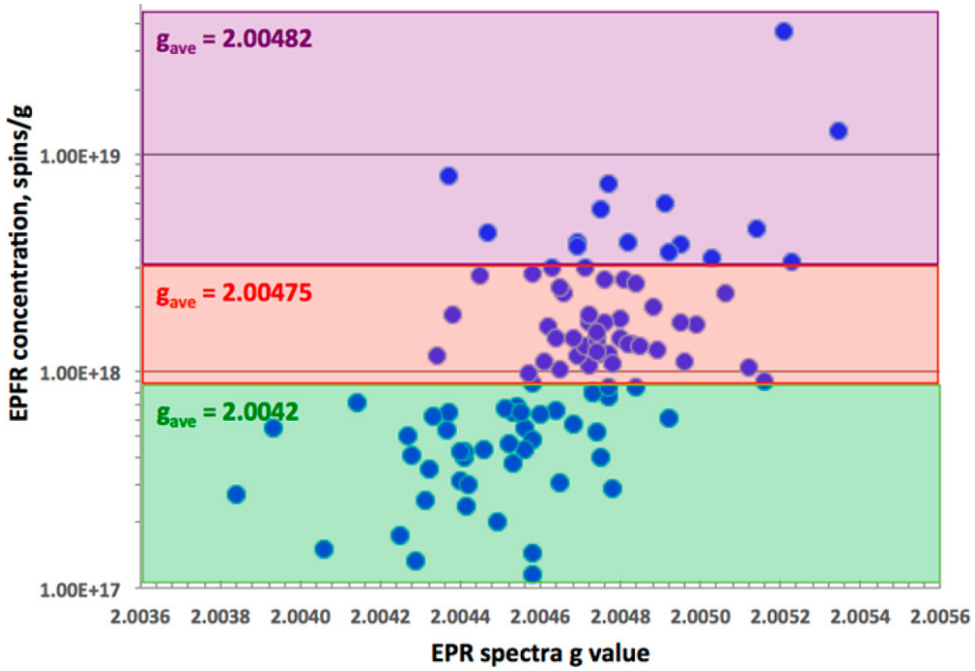

Figure 5.3. Correlation of g-factor and EPFRs concentration in three sample categories. Correlation parameters: R^2=0.38, p=0.00006.

Figure 5.4 mapped the three categories of data and color-coded them to show a spatial distribution pattern. The highest EPFRs concentrations are observed in the south, downtown, and north near major ambient pollution sources. And the top ten EPFRs concentrations are discovered in the south (5), downtown (3), and north (2) of Memphis while the lowest concentrations are found in some parts of midtown and the east. In the high EPFRs concentration areas, the main ambient sources are mobile emission and major industrial sites, but the land use characteristics also include commercial and residential areas. From this data, we can predict regional EPFRs concentration distributions.

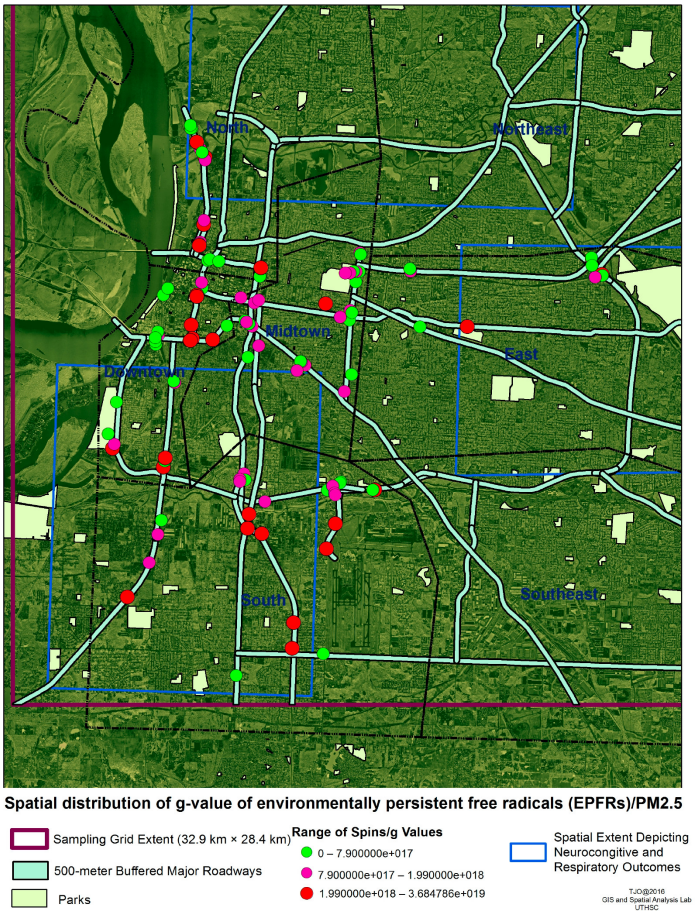

Figure 5.4. Spatial distribution of EPFRs concentration on PM samples.

Based on the radical concentration of PM samples, four spatial profiles are derived from ordinary kriging techniques[129,132–134] by Tonny J. Oyana, and the characteristics of each file are summarized in Table 5.1. Profile 2 is significantly different from profile 4 ($p = 0.00000553$) and profile 3 ($p = 0.0075$), but any other two profiles are not significantly from each other ($p>0.05$). The data summarized in Table 5.1 shows that PM pollution, here indicated by EPFRs concentration, is not uniformly distributed within the entire city, and our phytosampling method is practicable to identify local "hot spot" with potentially higher exposure risks, which can be later linked to PM concentration in the ambient air measured by other methods and integrated into health outcomes.

Table 5.1. Characteristics of the four spatial profiles.

	Profile 1	Profile 2	Profile 3	Profile 4
Conc. range	1.14×10^{17} - 7.36×10^{17}	7.36×10^{17} - 1.23×10^{18}	1.2×10^{18} - 3.29×10^{18}	3.29×10^{18}- 1.2×10^{19}
Mean conc.	$5.11\times10^{17}\pm$ 3.83×10^{17} SD	$1.02\times10^{18}\pm$ 8.74×10^{17} SD	$3.09\times10^{18}\pm$ 5.44×10^{18} SD	$6.61\times10^{18}\pm$ 8.23×10^{18} SD
Land use	Mainly vacant, recreational/golf course, roadways, and a few industrial facilities	Mainly commercial, roadways, residential, and industrial facilities	Mainly commercial, roadways, residential, and industrial facilities	Mainly roadways, major transportation hub, and industrial facilities
Population	Total: ~50,000, about 20.2% white, 79.6% African Americans (AA), and others 0.2%	Total: ~240,000, about 35.8% white, 62.5% AA, and others 1.7%	Total: ~220,000, about 21.5% white, 78.3% AA, and others 0.2%	Total: ~17,000, about 7.1% white, 82.2% AA, and others 0.7%
Area and population density	12.9 km^2, 3900 people/km^2	100.8 km^2, 2400 people/km^2	146.6 km^2, 1500 people/km^2	2.8 km^2, 6100 people/km^2
Cover areas	Parts of downtown, northeast, midtown, and southeast	A large portion of midtown, east, and portions in northeast	A large portion of the south, north, and small portions in midtown	Mainly situated in the south
2015 annual average daily traffic (AADT)	357,510 vehicles	1,839,273 vehicles	3,275,950 vehicles	153,159 vehicles

Figure 5.5 presents a color-coded map of four spatial profiles, a box plot of these spatial profiles, and a tile plot for $PM_{2.5}$ Daily Air Quality Index in early November 2015 from EPA. From the map, south and north area, which have slightly over 52% of traffic burden, show higher concentrations of EPFRs on PM. Profile 4 indicates an EPFRs concentration "hot spot."

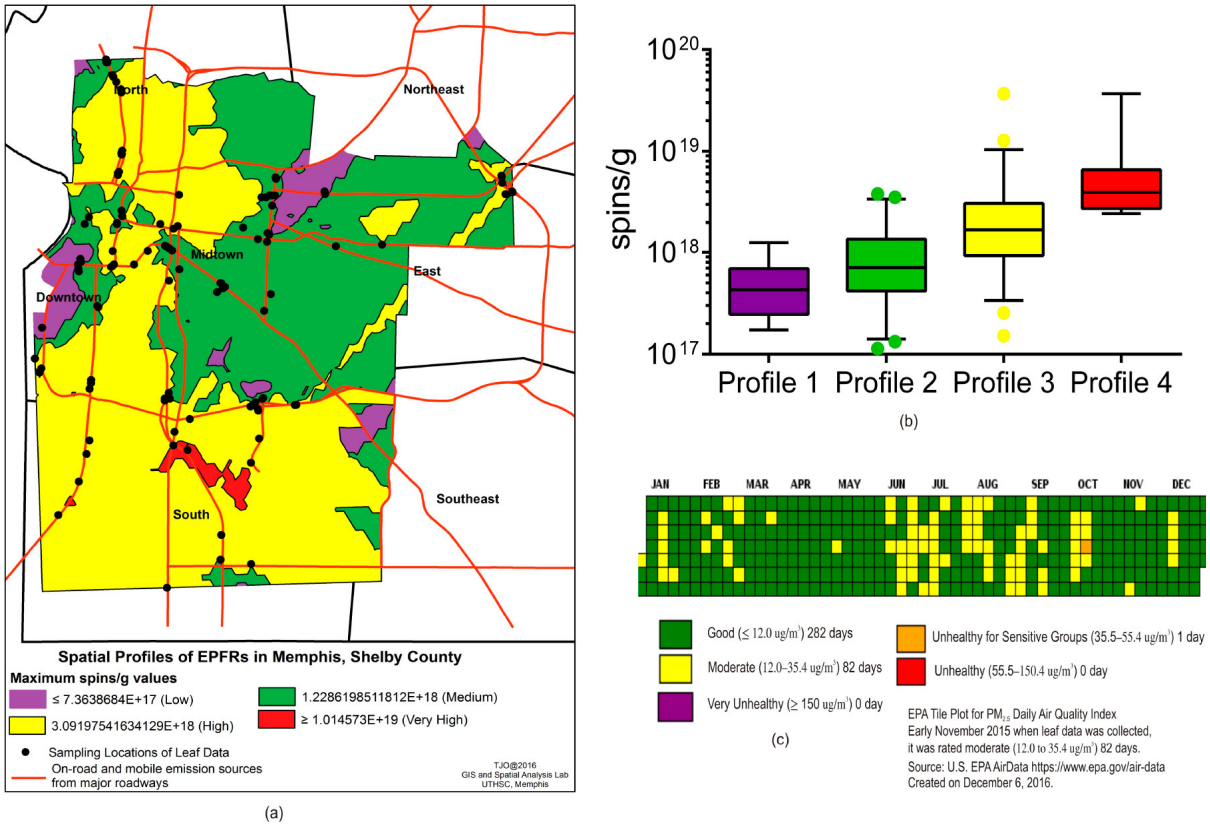

Figure 5.5. Predicted spatial profiles of EPFRs in Memphis, Tennessee derived from the ordinary kriging technique. (a) is the spatial patterns of 4 profiles. (b) is the box plot of EPFRs concentration for each profile. (c) is the tile plot for EPA $PM_{2.5}$ Daily Air Quality Index in early November 2015.

Phytosampling cannot assess the PM concentration in the air at a specific site because it is a static deposition, namely, the PM is the accumulation of a period of time. (However, if refer to known PM concentration data, e.g., by satellite, and when integrating data together, we found that the PM concentration in ambient air does not necessarily follow the overall concentration of these radicals in the air). The PM concentration in the whole city does not have too much difference, but radical concentration varies a lot. These differences can cause a potential epidemiological effect. This combined map shows that there is an area in the city (marking red) that the population lives there has a much higher exposure risk to PM-associated EPFRs. This area is an industrial area, as well as a heavy transportation area. Correlations have been found between g-factor and the concentration of the EPFRs that more oxygen-centered radicals, the higher the radical

concentrations. This study is the first effort to apply the phytosampling method to acquire spatial distributions of EPFRs in a city. Although there still exist some limitations such as limited sampling sites and some inherent drawbacks of the method, the study reveals the EPFRs spatial variations and potential exposure risk, especially in the “hotspots” area, which in turn, provides important information for a possibly better epidemiological understanding.

5.2. Field Study Concerning PM Emissions from a Ship Cargo Terminal in New Orleans, LA

5.2.1. Introduction

The ship cargo terminal in midstream next to the River Ridge area in New Orleans has raised the concern of PM exposure to the residents in this area. A Tisch high volume air sampler has been set up in the residential area to collect $PM_{2.5}$ and PM_{10}. The phytosampling method has also been applied. Leaves from *Pittosporum tobira* in the front yard have been collected four times and PM smaller than 3.0 μm (P_3) and PM larger than 3.0μm ($P_{>3}$) have been retrieved. Retrieved PM from both sampler and leaves have been weighed, and the signal of EPFRs, element composition, metal concentration, and polycyclic aromatic hydrocarbons (PAHs) concentration have been analyzed. PM_{10} are coarse particles that can be filtered out by nose, so it is not a big concern while the fine particles $PM_{2.5}$ and P_3, in this case, can reach lower parts of the respiratory tract, thus are more dangerous. PM_{10} and $P_{>3}$ were analyzed for references.

5.2.2. Sample Collection

A Tisch High Volume Air Sampler (TE-6070V, Tisch Environmental, Inc. Figure 5.6.) was set up in the backyard of 133 Rex Dr., River Ridge, LA, 70123, (29.945889, -90.215581). The sampler could be operated in the flow rate range 1000-1700 L/min. This sampler is also a cascade impactor for PM_{10} collection, but the substrate for PM_{10} collection makes a filter size cutoff for $PM_{2.5}$ collection. We used cellulose slotted collection substrates for PM_{10} collections and polyurethane filters (PUF) for $PM_{2.5}$ collections. Figure 5.7 shows the sampling location in Google Earth. A 6-day continuous collection and a total 5-day 24 hrs on and off shift collection had been done in June and July. And at both start time and finish time of each sampler collection, 300 leaves (13.5-14 cm^2/leaf) from *Pittosporum tobira* in the front yard had been collected.

Figure 5.6. Tisch high volume air sampler on site.

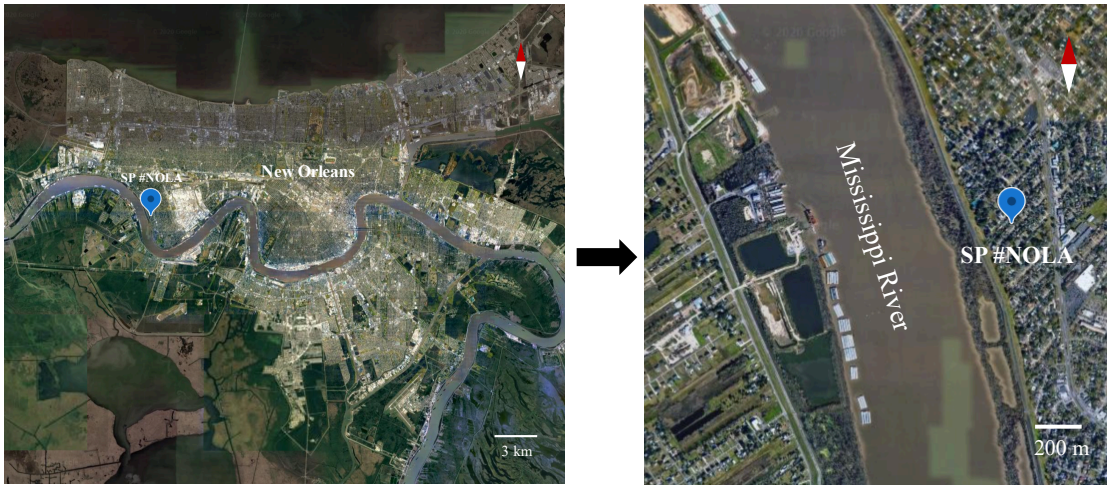

Figure 5.7. Sampling location for the field study in New Orleans showed in Google Earth.

The collection dates are summarized in Table 5.2. High volume PM samples are indicated by HV and phytosamples are indicated by SP. And the numbers in the sample ID are the order of collection time.

Table 5.2. Summary of sample collection dates.

	Start	Finish	Collection Pattern
HV #NOLA-1	05/01/19	05/07/19	Continuous
HV #NOLA-2	06/11/19	06/22/19	24-hr on/off shift
SP # NOLA-1	05/01/19		/
SP # NOLA-2	05/07/19		/
SP # NOLA-3	06/11/19		/
SP # NOLA-4	06/22/19		/

After collections, PM from leaves was retrieved using the method described before. Particles that cannot be filtered through 3.0 μm were also freeze dried to retrieve $P_{>3}$. PUF filter with $PM_{2.5}$ was cut into 1 cm^2 pieces and sonicated in deionized water for 20 mins, and water suspension was freeze dried to retrieve $PM_{2.5}$. Cellulose slotted substrates were cut into single slots and froze separately for further analysis. Table 5.3 is a mass summary of all retrievable particles. Table 5.4 estimates the concentration of PM_{10} and $PM_{2.5}$ in the air based on the mass change of the collection substrates and the sampled air volume in second collection by HV PM sampler. Comparing the calculated PM concentration in the air from this study to the NAAQS ($PM_{2.5}$:12 $\mu g/m^3$ (annual), 35 $\mu g/m^3$ (24 hr), and PM_{10}: 150 $\mu g/m^3$ (24 hr))[14], concentrations of both $PM_{2.5}$ and PM_{10} are within the standards.

Table 5.3. Mass summary of retrievable PM.

Sample ID	PM size	Mass(mg)
HV #NOLA-1	$PM_{2.5}$	1.4
HV #NOLA-2	$PM_{2.5}$	2
SP # NOLA-1	P_3	6.7
	$P_{>3}$	17
SP # NOLA-2	P_3	7
	$P_{>3}$	20
SP # NOLA-3	P_3	9.7
	$P_{>3}$	22
SP # NOLA-4	P_3	10
	$P_{>3}$	26

Table 5.4. Estimation of PM concentration of PM in the air based on the mass change of collection substrates.

	Flow rate	Duration	Weight	PM concentration in air
PM_{10}	$1m^3$ /min	7787 mins	50mg	$0.006mg/m^3$
$PM_{2.5}$	$1m^3$ /min	7787 mins	10mg	$0.001mg/m^3$

5.2.3. Environmentally Persistent Free Radicals Analysis

Retrieved PM samples from both HV PM sampler and phytosampling were measured by EPR for EPFRs signals. The results of EPFRs measurements from all retrievable samples are summarized in Figure 5.8. Phytosamples SP 050119 and SP 050719 are corresponding to HV PM sample HV 050719, while phytosamples SP 061119 and SP 062219 are corresponding to HV PM sample HV 062219. Panel A shows the g-factor of radicals and phytosamples turn to have higher g-factor than HV PM sampler samples, which indicates more oxygen-centered radicals in phytosamples. This finding is consistent with the results showed in radicals on PM collected from Baton Rouge. Panel B shows the peak width of the radical spectra. The peak width of HV PM sampler samples has a big difference between the two collections, so the data is not reliable to represent the sampling area. But the very narrow peak is indicative of a more specific radical species. Within the phytosampling group, P_3 shows broader peaks than corresponding $P_{>3}$ in all collections indicating that smaller PM, which is mainly from combustion processes, contains more radical species. In panel C, $P_{>3}$ carries around ten times higher concentration of radicals than the corresponding P_3 from phytosampling and $PM_{2.5}$ from the sampler. $P_{>3}$ counted all bigger particles that are in the non-respirable range on the surface of leaves, and the detection of such high EPFRs concentration is abnormal in bigger particles.

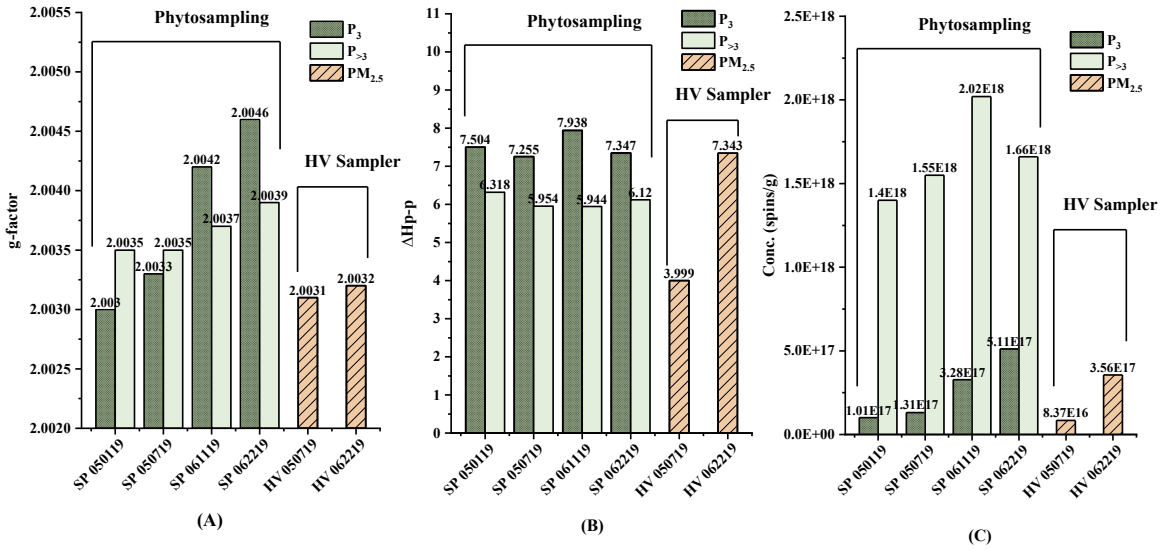

Figure 5.8. Comparisons of EPFRs g-factor (A), ΔHp-p (B) and spins concentration (C) between PM collected by phytosampling and HV PM sampler in New Orleans.

Figure 5.9 compares the average EPFRs characteristics on PM from New Orleans (NOLA) with the same size PM samples from Baton Rouge (BTR). P_3 is collected by the phytosampling method, while $PM_{2.5}$ is from HV PM samplers. Panel A shows that g-factor from samples in BTR is significantly higher than in NOLA ($p=0.01$ for $PM_{2.5}$ and $p=0.001$ for P_3 from ANOVA). The higher g-factor, which characterizes more oxygen-centered radicals found in the samples from BTR, could be due to the different sources of PM in two cities. In BTR, the main source is vehicle emissions while in NOLA, the source we were monitoring for the PM is the ship cargo terminal and potentially some industrial factories, and the particle types depend on it. The range of peak width (Panel B) of samples from NOLA is comparable with data collected in BTR. More samples in BTR results in wider EPFRs concentration ranges in both $PM_{2.5}$ and P_3. The results of ANOVA show that there is no significant difference in radical concentrations between samples in NOLA and BTR.

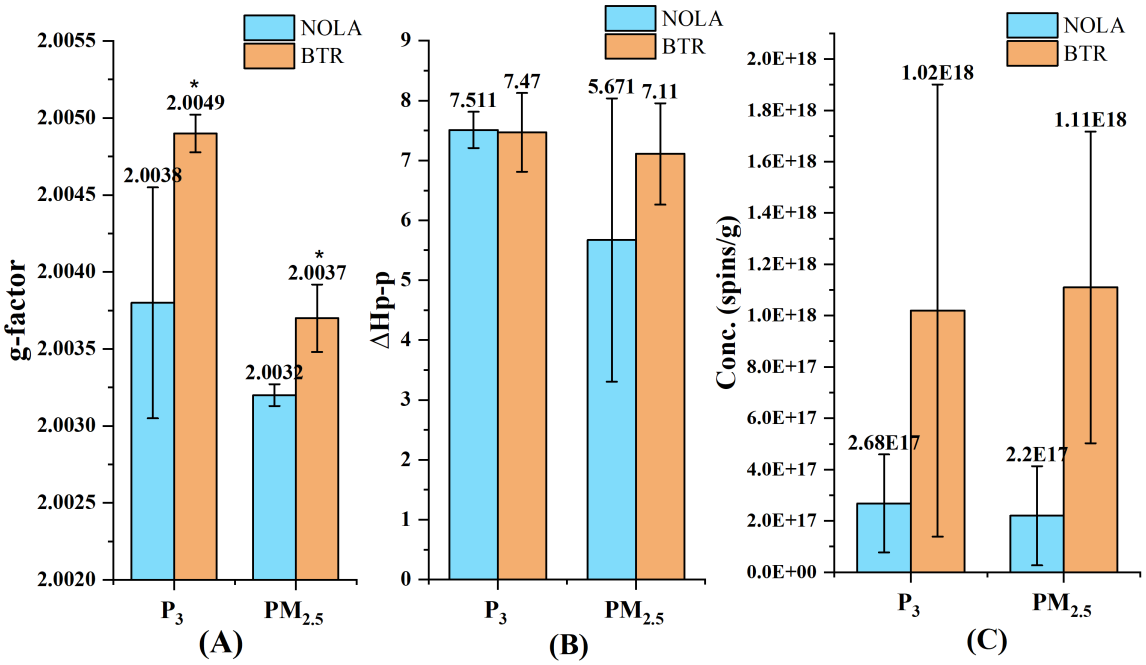

Figure 5.9. Comparison of EPFRs' average g-factor (A), ΔHp-p (B) and spins concentration (C) on PM with same sizes collected from New Orleans (NOLA) and Baton Rouge (BTR). * is indicating the significant difference by ANOVA ($p<0.01$).

5.2.4. PM Surface Element Analysis

Retrieved PM samples and a 1 cm^2 piece of cellulose slotted substrates with PM_{10} were analyzed by the SEM-EDS. Figure 5.10 shows the typical aggregated morphology of PM.

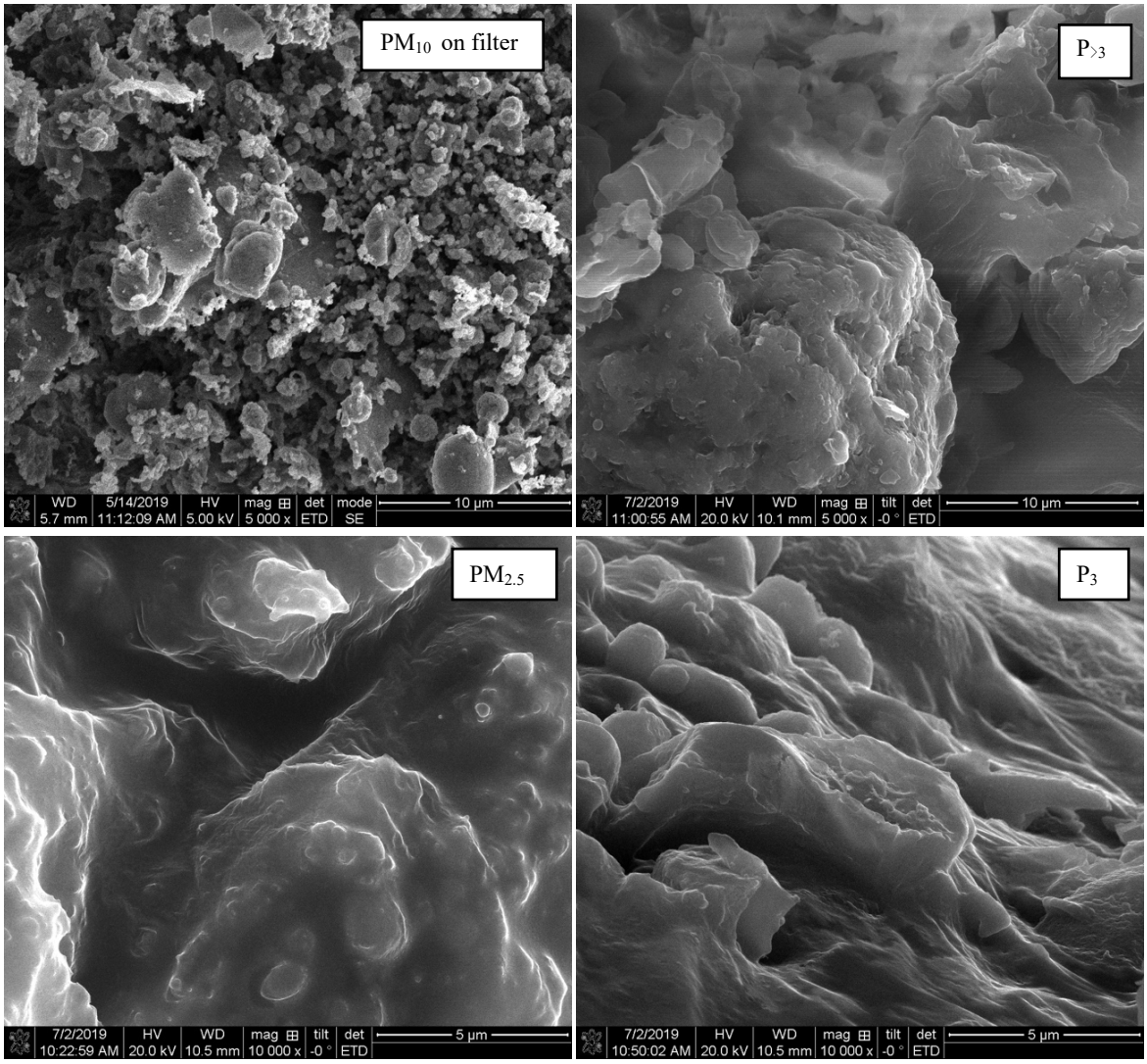

Figure 5.10. SEM images of PM_{10}, $PM_{2.5}$ from HV PM sampler and P_3, $P_{>3}$ from phytosampling.

Figure 5.11 shows the EDS spectra from PM samples with different sizes. Elemental carbon and oxygen accounted for the majority of elements in the samples, and the atomic percentage of other elements are normalized without C and O and are shown in the histograms with the average from several samples in analysis areas. PM_{10} shows a very high content of copper; $PM_{2.5}$ shows a high content of fluorine; and P_3 contains a lot of nitrogen. The difference of the relative element contents would be a result of PM source of different sizes, and higher nitrogen in

phytosampling PM is related to the nitrate deposition. The results are in line with what we saw in phytosamples from Baton Rouge.

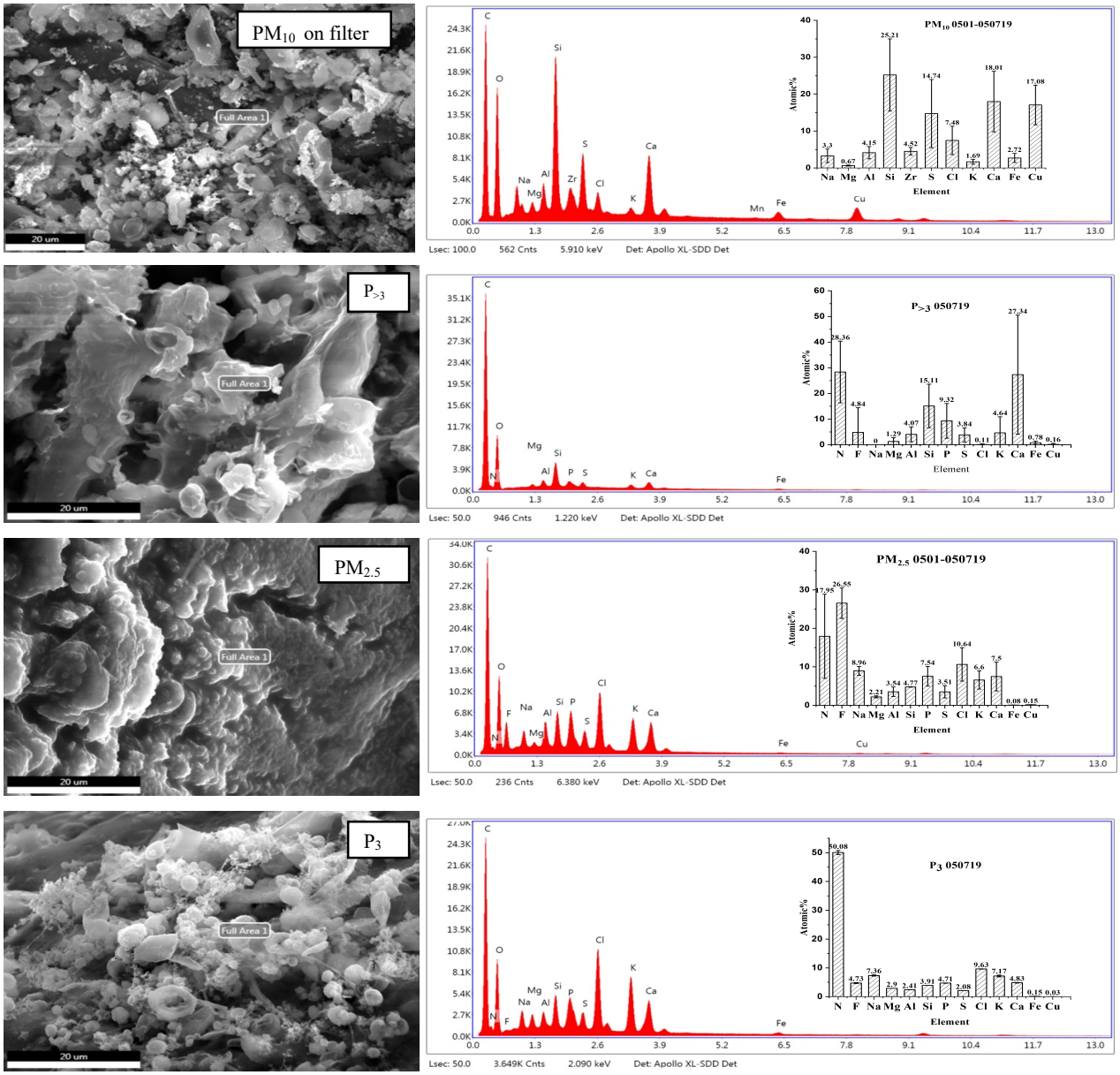

Figure 5.11. The EDS spectra and the normalized relative elements contents from PM samples with different sizes (PM_{10}, $P_{>3}$, $PM_{2.5}$ and P_3).

5.2.5. Polycyclic Aromatic Hydrocarbons Analysis

Due to the limited sample size of PM retrieved from HV air sampler, only PM from two phytosampling collection and a slot of cellulose collection substrate with PM_{10} were extracted for PAHs analysis. A blank cellulose collection substrate slot was subjected to the PAHs extraction

and analyzed for references. Samples were extracted by the vortex-sonication method introduced before, and the cellulose filter slot was cut into small pieces to ensure the immersion to the extraction solvent (DCM, (≥99.9%, MilliporeSigma)). 27 PAHs in extracted PM solutions have been analyzed by GC-MS/MS (Agilent 7980B GC system/ Agilent 7000C GC/MS Triple Quad system) to obtain PAHs data. Figure 5.12 shows the concentration percentage of individual PAH to the total PAHs in the sample. A spike of Phenanthrene in one of the two phytosamples and PM_{10} was detected. This value is more than five times higher than the other PAHs, but since Phenanthrene was only present in one sample, it is not reliable to draw any conclusion from it, and more data is needed. Considering about all other PAHs, only Fluoranthene and Pyrene from two phytosamples shows the concentration percentage over 10% of total PAHs while all other PAHs have a nearly even distribution.

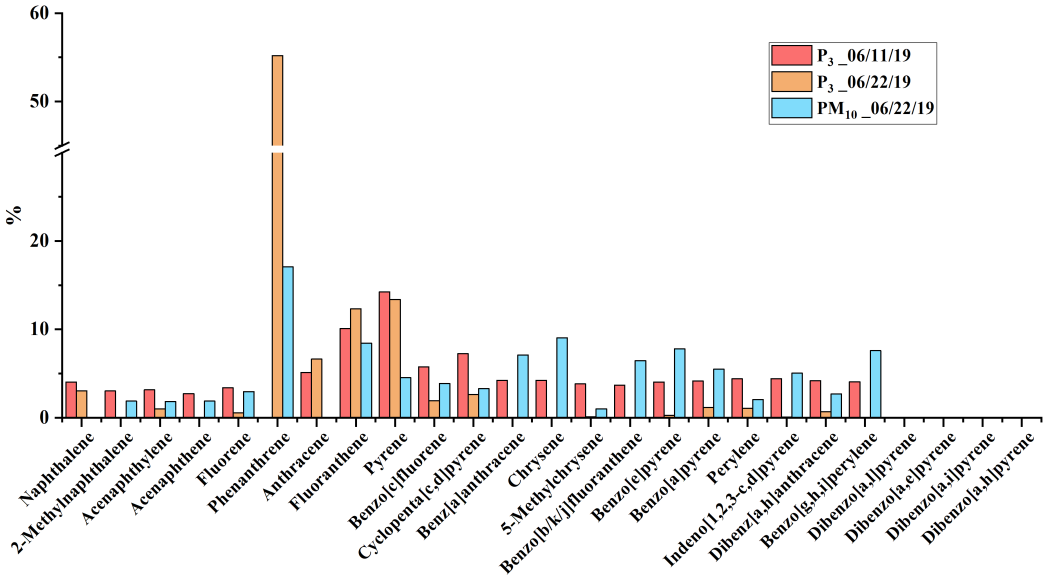

Figure 5.12. PAH concentration percentages in P_3 and PM_{10} collected from NOLA.

Figure 5.13 compares the total PAHs concentration in P_3 from NOLA to P_3 from BTR. PAHs concentration in NOLA samples is much lower than in BTR samples. Since combustion processes are important sources of PAHs generation, these results also support our speculation that the PM sources from two cities are not the same.

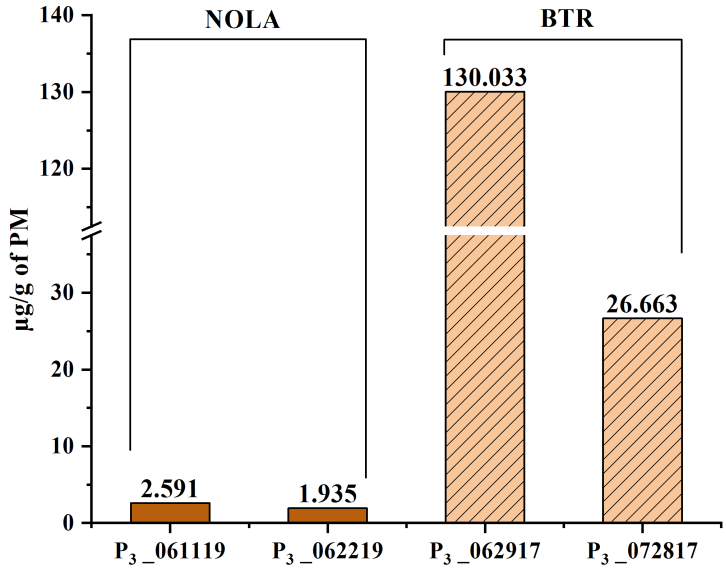

Figure 5.13. Comparison of total PAHs concentrations on P_3 between NOLA and BTR.

5.2.6. Metal and Element Analysis

Samples were also subjected to metal and element analysis. Due to limited retrieved $PM_{2.5}$ mass, only PM_{10} on cellulose filter, retrieved P_3 and $P_{>3}$ were treated and analyzed (two samples each). Samples were digested with a mixture of HNO_3 and H_2O_2 in a microwave digester (MDS-6G, Sineo) and analyzed by VISTA-MPS CCD Simultaneous ICP-OES.

Figure 5.14 shows the distribution of each element in the P_3, $P_{>3}$ and PM_{10} samples. Al, Ca, Fe, K, Mg, Na, Si are relative high concentration elements in PM_{10}, P_3 and $P_{>3}$ samples that we analyzed. However, Cu is very high on the PM_{10} but low on P_3 and $P_{>3}$. This result indicates that Cu is mainly carried by particles that are bigger than 3.0 µm and smaller than 10 µm.

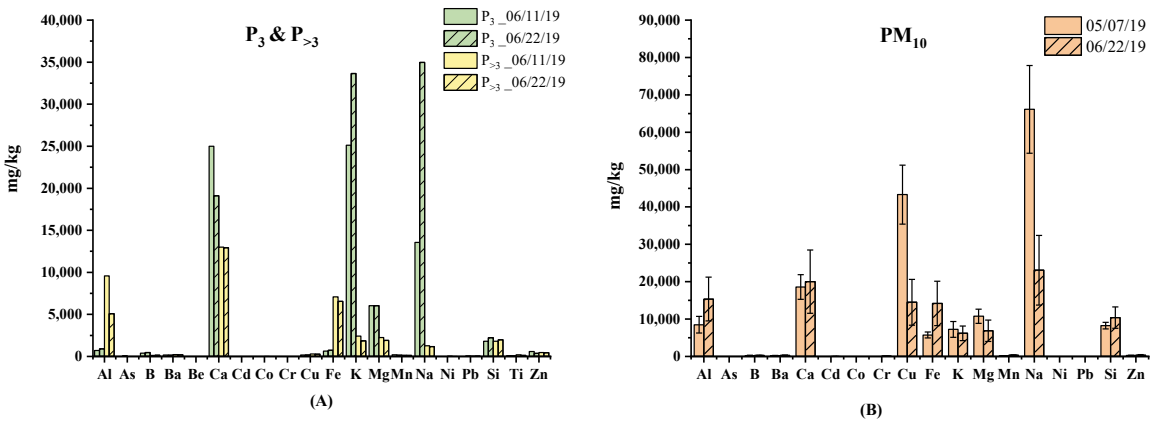

Figure 5.14. Element concentration distribution in the P_3, $P_{>3}$ (A) and PM_{10} (B) collected in NOLA.

Figure 5.15 compares the individual concentration of these eight elements individually among P_3, $P_{>3}$ and PM_{10} samples. Except for Cu, which is almost exclusively present in PM_{10} samples, Al, Fe, Mg, Na and Si are elements with relatively higher contents carried on PM_{10}. Comparing P_3 with $P_{>3}$ samples, two metals, Al and Fe, have a much higher concentration on $P_{>3}$, while Ca, K, Mg and Na are dominant in P_3 samples. This result could be partially attributed to soluble components carried on the particles. When retrieving PM by washing and sonicating leaves in water, soluble components would dissolve in water and concentrate on P_3 once the sample gets dried. So, this may lead to an overestimation of soluble compounds on smaller particles collected from the phytosampling, and extra caution is needed when reporting such results. The abnormally high concentration of Cu and Fe observed in PM_{10} samples could be an indicator that it is possible that particles from the refinery factory were blown away to reach this residential area. Considering the high EPFRs concentration in the $P_{>3}$ and the high Cu and Fe contents in PM_{10}, the exposure risk in this study area is mainly from non-respirable particles. Although the inhalation risk of the residents living in this area to EPFRs and metals are low, the chance of exposure through other routes, such as ingestion, are increased and should draw more attention.

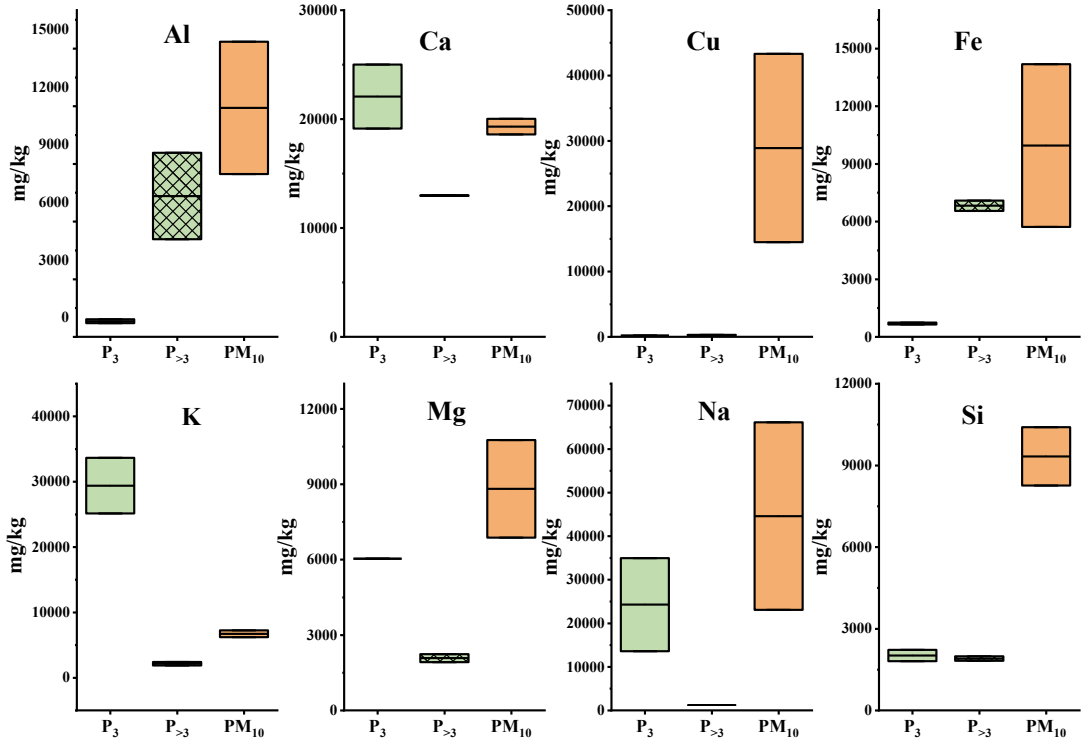

Figure 5.15. Comparison of individual element concentrations among P_3, $P_{>3}$ and PM_{10} collected in NOLA.

CHAPTER 6. TAILGATE-ASSOCIATED PM EMISSION ANALYSIS

As a university with unique football culture, the tailgate party before games is an important part of football seasons. Tailgating usually takes place in the parking lot around the stadium before a game and involves a lot of meat grilling and using of gasoline generator, which will contribute to the PM-associated pollutant emissions.

6.1. Sample Collections

In the 2019 football season, five PM sample collections had been done during the home game on the campus of Louisiana State University. The phytosampling method was not applied due to the reasons that there is limited availability of leaves, and the sampling period cannot be specified to tailgating. The Tisch High Volume Air sampler (TE-6070V, Tisch Environmental, Inc.) was set up near the parking lots (location is shown in Figure 6.1.). Since the game is on Saturdays, sample collections started at 6:00 pm on Friday evenings and stopped at 8:00 am on Sunday mornings (38 hrs in total) to cover the whole game period. Four collections had been conducted during gamedays with one collection that had been done when there was no game, and the data was used as a background control. Cellulose slotted collection substrates were used for PM_{10} collections, while polyurethane foam (PUF) filters were cleaned and used for $PM_{2.5}$ collections. Filters were weighed before and after the collections. Table 6.1 summarized the mass change on the filters, estimated PM concentrations in the air (based on the mass change and collection air volume), and the mass of retrievable PM.

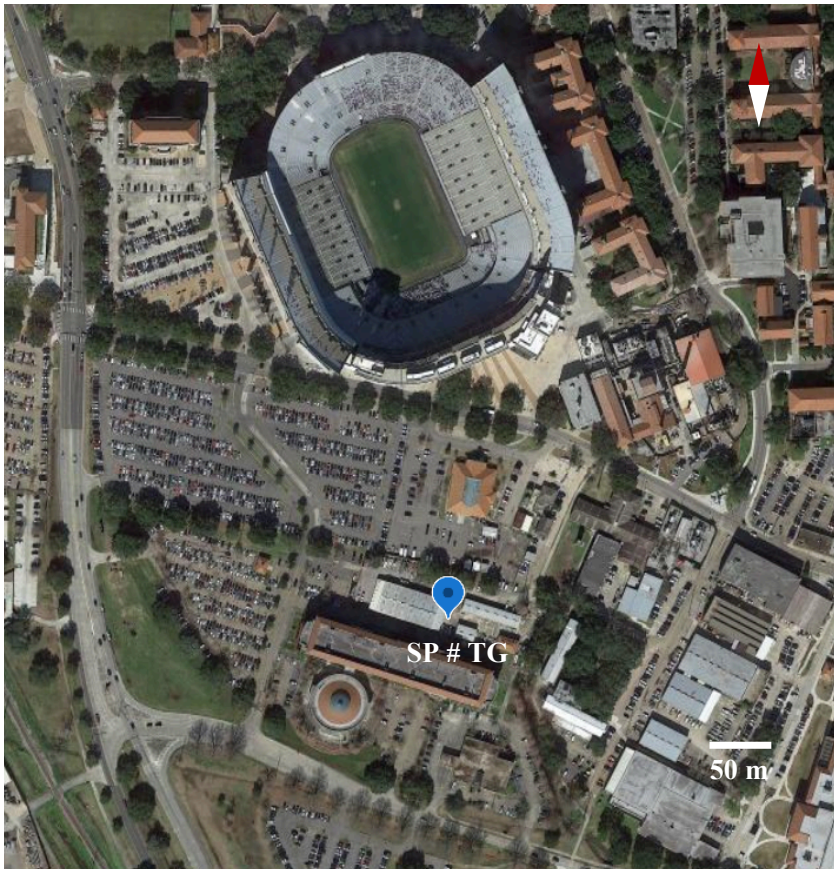

Figure 6.1. Sampling location for tailgating in Google Earth.

Table 6.1. Sample mass summary.

Collection #	Collection Date	Filter type	Mass Change (mg)	Average PM Concentration in Air ($\mu g/m^3$)	Retrieved Mass(mg)
1	8/30/19-9/1/19 (kickoff: 6: 30pm)	Cellulose Slotted (PM_{10})	42	18	/
		PUF ($PM_{2.5}$)	51	22	3.3
2	9/13/19-9/15/19 (kickoff: 6: 39pm)	Cellulose Slotted (PM_{10})	47.44	21	/
		PUF ($PM_{2.5}$)	41.38	18	2.6
3*	9/27/19-9/29/19 (no game)	Cellulose Slotted (PM_{10})	52.5	23	/
		PUF ($PM_{2.5}$)	22.02	10	2
4†	10/4/19-10/6/19 (kickoff: 11: 00am)	Cellulose Slotted (PM_{10})	43.48	19	/
		PUF ($PM_{2.5}$)	25	11	1.2
5‡	10/11/19-10/13/19 (kickoff: 7: 00pm)	Cellulose Slotted (PM_{10})	17.34	8	/
		PUF ($PM_{2.5}$)	1.52	0.7	N/A

*This collection was done in a weekend without football game as a control experiment.
†This collection was done in a football game weekend with early kickoff time (11:00 am).
‡There was a heavy rain lasted for around 1 hr right before this collection started.

The first two collections (#1&#2) were done at a regular football kickoff schedule (08/31/19 kickoff at 6:30 pm and 09/14/19 kickoff at 6:39 pm). The third collection (#3) was done at the weekend without football games as a collection control. The kickoff time for the fourth collection (#4) was earlier (10/05/19 kickoff at 11:00 am). The earlier kickoff results in decreased incidents and short time for meat grilling and using gasoline generators. The last collection was done during a game with regular kickoff time, but there was a heavy rain last for around 1 hr right before the collection started. From Table 6.1, #1 and #2 collections show similar mass change on

both PM_{10} and $PM_{2.5}$ collection filters. Collections #3 and #4 show around half of the mass for $PM_{2.5}$ collection compared to #1 and #2 but similar mass change for PM_{10}. Figure 6.2 plotted the PM concentration in air of these five collections based on the sampled air volume and the mass change of collection matrixes. This result indicates that activities during a regular gameday tailgate contribute to almost twice more $PM_{2.5}$ concentration in the air, and the PM_{10} were not mainly generated from these activities. The distinct mass drop on PM_{10} and $PM_{2.5}$ collection in #5 refer to the significant influence of rain on washing off to the accumulated PM in the ambient air. Comparing the PM concentration in the air from this study to the NAAQS ($PM_{2.5}$:12 $\mu g/m^3$ (annual), 35 $\mu g/m^3$ (24 hr) and PM_{10}: 150 $\mu g/m^3$ (24 hr))[14], no collection exceeded the 24 hr standard for $PM_{2.5}$ and PM_{10}.

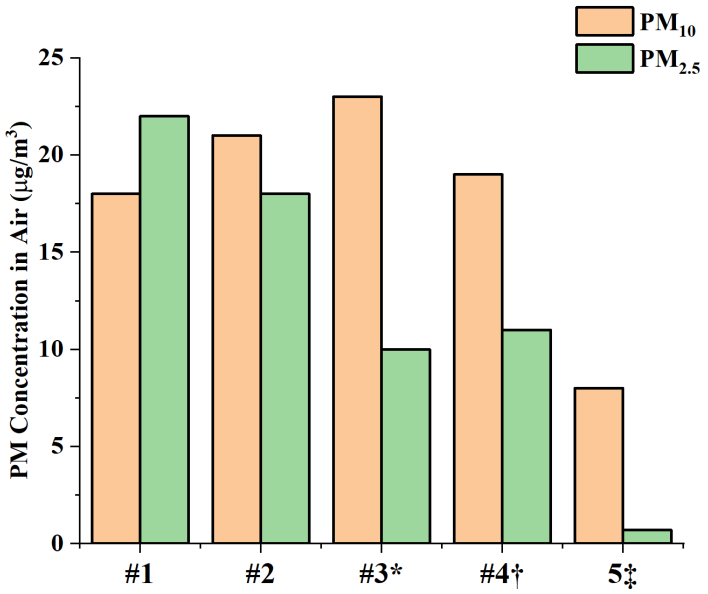

*This collection was done in a weekend without football game as a control experiment.
†This collection was done in a football game weekend with early kickoff time (11:00 am).
‡There was a heavy rain that lasted for around 1hr right before this collection started.

Figure 6.2. Calculated PM concentration in the air for five collections.

6.2. Environmentally Persistent Free Radicals Analysis

Retrieved $PM_{2.5}$ samples from PUF filters were subjected to EPR measurement for EPFRs signal, and the characteristics of EPFRs for four collections (two regular collections, one collection with early kickoff and one control collection) were summarized in Figure 6.3.

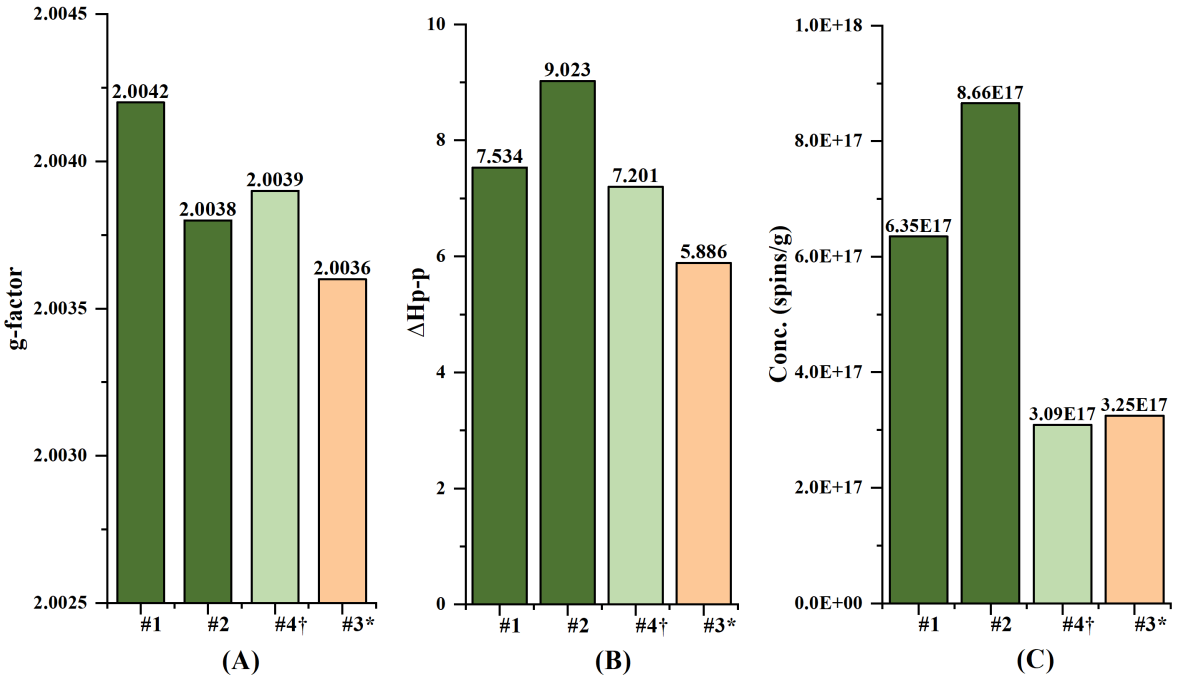

†This collection was done in a football game weekend with early kickoff.
*This collection was done in a weekend without football game as a control experiment.

Figure 6.3. EPFRs g-factor (A), ΔHp-p (B) and spins concentration (C) of four PM collections in the 2019 football season. The collection site numbers are corresponding to the details showed in Table 6.1.

The g-factors of EPFRs from four collections are in the range of 2.0036-2.0042, showing a carbon-centered radical dominated feature, which is consistent with the g-factor range measured from samples in previous studies. The peak width of the radical spectra from samples collected during game day weekends are higher than in the control, and #2 shows an even higher peak width indicating more radical species. And this sample also shows the highest radical concentrations than other samples, but the correlations between peak width and the concentration cannot be identified due to the limited replicates. Samples collected on a regular game day (#1 & #2) contain a high concentration of EPFRs than the sample in an early game day and control. It is noticed that the control sample (#3) shows the lowest number in all three characteristics, namely, it contains more carbon-centered radicals, less radical species, and lower radical concentration compared to all other samples.

6.3. PAHs Extraction and Analysis

Since meat grilling is an important source for the general public exposure to PAHs[135], we assume that our samples collected during tailgating would contain a high PAHs concentration. Due to the limited retrievable $PM_{2.5}$, we adapted our PM vertex-sonication method for PAHs extraction and applied direct PUF filter extraction. After retrieving for PM by cutting PUF filters into 2 cm^2 pieces and sonicated in deionized water, PUF filters were merged into 150 mL of dichloromethane (≥99.9%, MilliporeSigma) and sonicate for 1hr (FS-20 ultrasonic, Fisher Sci.). PUF filter pieces were removed, and the extracted solvent was dried under a gentle flow of nitrogen and redissolved in 1 mL of DCM. A 0.2 μm DCM resistant filter was used to remove any particles in the analyte.

Because the extraction was applied to the whole piece of PUF filter, using the mass change as the final mass of PM to calculate the concentration of PAHs on PM could cause a big error and make the results misleading, we report the concentration data based on the air volume (shown in

Figure 6.4.). The result shows that the total PAHs concentration in the air during the tailgating in a regular kickoff gameday (#1 & 2) is higher than in early kickoff day (#4) and no game day (#3). The same trend has been observed in the individual PAHs concentration shown in Figure 6.5 among collections. And Pyrene, Phenanthrene, and Fluoranthene are the dominant PAHs among the whole sample.

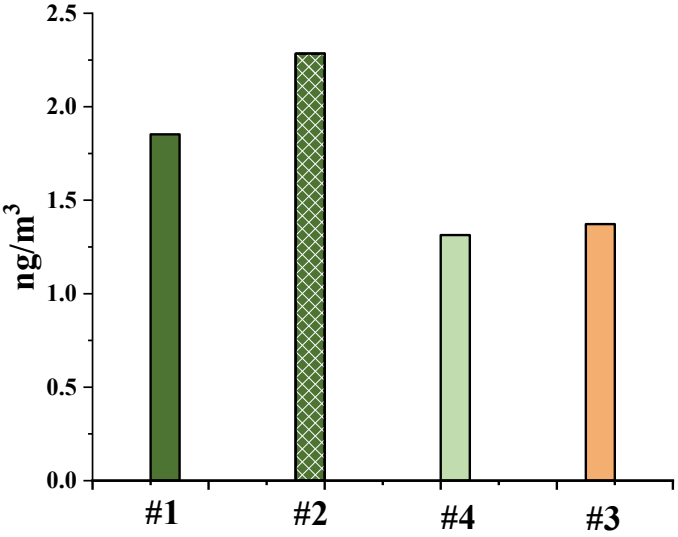

Figure 6.4. Total PAHs concentration from tailgate samples based on sampled air volume.

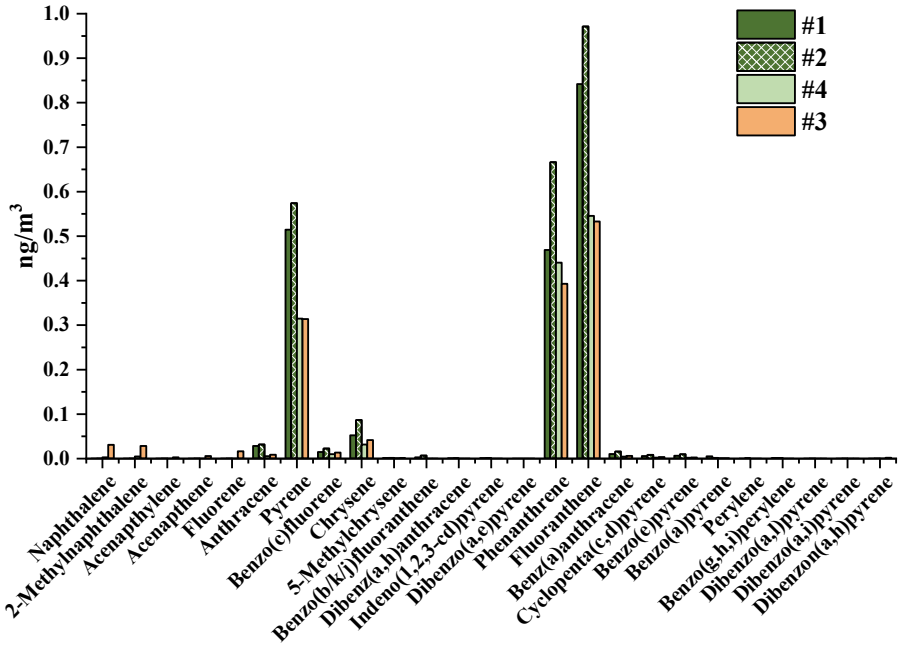

Figure 6.5. Individual PAH concentration from tailgate PM samples.

CHAPTER 7. CONCLUSIONS

In summary, this new "phytosampling" method is an effective method to collect particulate matter from ambient air. And such particles could be retrieved for analysis without compromising the integrity of the leaf surface. After comparing the results from several analyses on the PM collected by the phytosampling method and high volume PM sampler, we found that the sampling method affects the composition of PM. Higher Na, Si, Al, S, and Cl are detected on the HV PM sampler samples, while K, Ca, N, and S were higher in phytosampled samples. This is a result from the different sources of particles collected by two methods and concentrating soluble compounds to smaller particles. The overall g-factor of EPFRs on PM accumulated in natural conditions is higher ($g>2.0045$), indicating that phytosampled PM is dominated by oxygen-centered EPFRs while particles collected from air sampler ($g < 2.0040$) are dominated by carbon-centered radicals. The simulated aging study indicates a long-time high persistency of EPFRs on all samples. The increasing trend of radical concentration at the early stage and the decreasing trend of g-factor for phytosamples provide a valuable direction for studying and understanding EPFRs dynamic changing in the ambient air. However, the HV PM sampler was not able to capture this changing phase. Spin trapping data confirmed the capacity of hydroxyl radical generation in PBS solution by EPFRs-associated PM. Different PAHs profiles between methods and PM sizes were observed, indicating the source distinctions between collection methods and possible analyte loss during sampling. The photosamples tend to induce less toxicological stress than surrogate radical-containing particles and the HV PM samples to the BEAS-2B cells. Although the mechanism behind this phenomenon cannot be interpreted from the limited data in this research, one can speculate that it is related to the composition differences and even components interaction effects between HV PM samples and phytosamples.

There is no perfect method for collecting ambient air PM samples. The proposed phytosampling method shows advantages in the analysis and evaluation of chemical speciation associated with PM. The deposited samples are exposed to natural conditions that prevent the unpredictable changes on some organic fractions of PM during the collection phase in samplers. In particular, this method is very useful to evaluate the EPFRs speciation and content on PM, which are very sensitive to changing conditions and elapsed time from the moment they are removed from ambient. Also, other chemicals (for example, PAHs) present a more accurate description of both their speciation and content in respirable particles. Besides, this method is cheaper and can be handled easily. The major challenge of applying this method is the translation of the results into the ambient air concentration, as phytosamples cannot be used to evaluate an absolute air concentration of PM and their components in the air, but rather relative content of chemicals on PM. This can be overcome by supplementing phytosampling data with other monitoring methods that can provide a local concentration of PM in the air (for example, PurpleAir samplers).

One of the biggest advantages of phytosampling is the ability to sample at almost any location and to create a dense network of sampling sites to achieve a high-resolution data on chemical distribution without high cost of HV samplers.

APPENDIX. COPYRIGHT INFORMATION

Copyright information for materials used in 5.1. Reproduction of published paper as a co-author is granted by American Chemical Society.

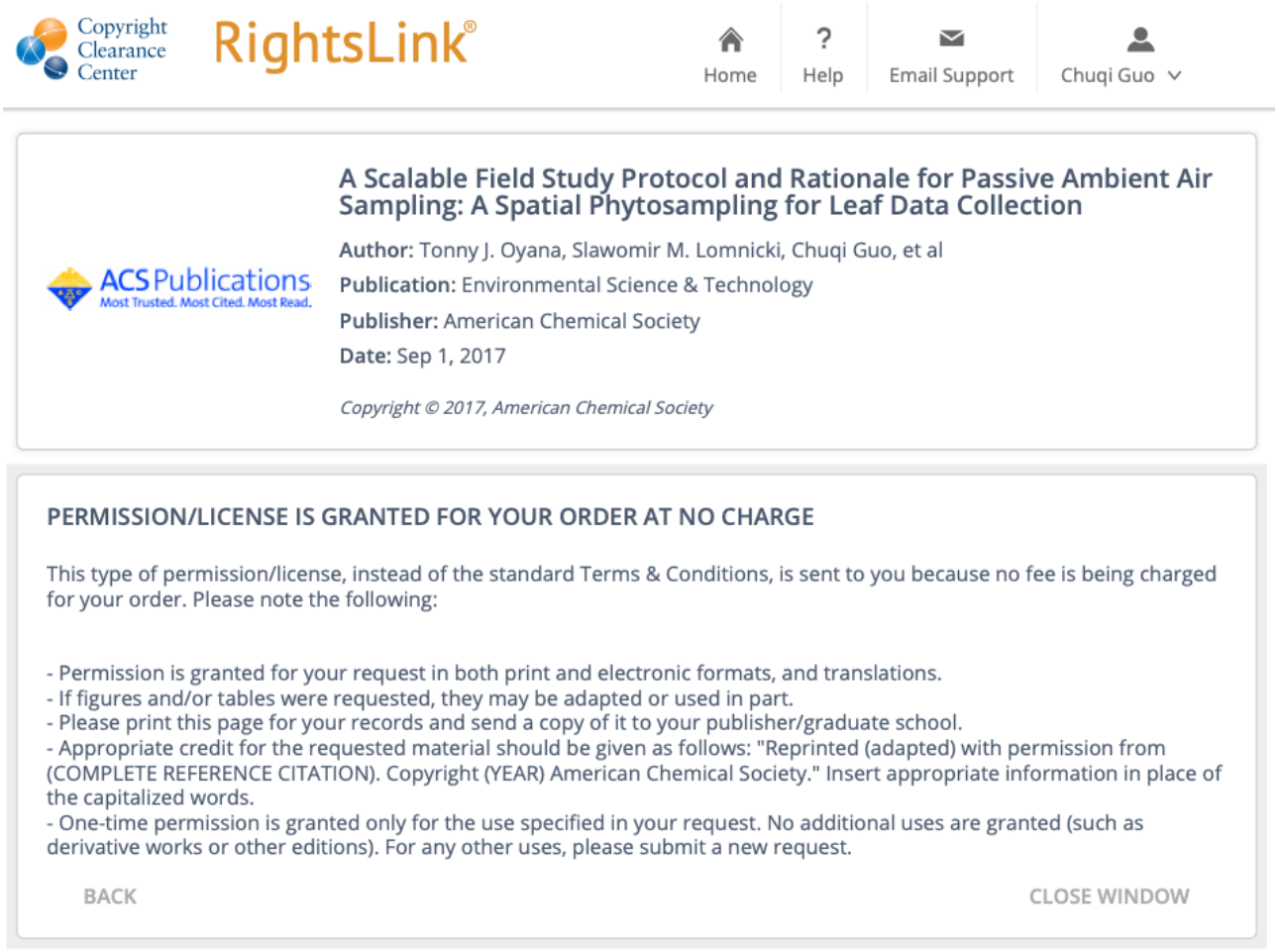

REFERENCES

(1) Beckett, K. P.; Freer-Smith, P. H.; Taylor, G. Urban Woodlands: Their Role in Reducing the Effects of Particulate Pollution. *Environ. Pollut.* **1998**, *99* (3), 347–360. https://doi.org/10.1016/S0269-7491(98)00016-5.

(2) Dzierżanowski, K.; Popek, R.; Gawrońska, H.; Sæbø, A.; Gawroński, S. W. Deposition of Particulate Matter of Different Size Fractions on Leaf Surfaces and in Waxes of Urban Forest Species. *Int. J. Phytoremediation* **2011**, *13* (10), 1037–1046. https://doi.org/10.1080/15226514.2011.552929.

(3) Oberdörster, G.; Oberdörster, E.; Oberdörster, J. Nanotoxicology: An Emerging Discipline Evolving from Studies of Ultrafine Particles. *Environmental Health Perspectives*. 2005. https://doi.org/10.1289/ehp.7339.

(4) Chen, R.; Hu, B.; Liu, Y.; Xu, J.; Yang, G.; Xu, D.; Chen, C. Beyond PM2.5: The Role of Ultrafine Particles on Adverse Health Effects of Air Pollution. *Biochim. Biophys. Acta - Gen. Subj.* **2016**. https://doi.org/10.1016/j.bbagen.2016.03.019.

(5) Health Effect Institute. *Understanding the Health Effects of Ambient Ultrafine Particles*; 2013.

(6) Li, D.; Li, Y.; Li, G.; Zhang, Y.; Li, J.; Chen, H. Fluorescent Reconstitution on Deposition of PM 2.5 in Lung and Extrapulmonary Organs. *Proc. Natl. Acad. Sci. U. S. A.* **2019**. https://doi.org/10.1073/pnas.1818134116.

(7) World Health Organization. Ambient Air Pollution: A Global Assessment of Exposure and Burden of Disease. *World Heal. Organ.* **2016**.

(8) Brook, R. D.; Rajagopalan, S.; Pope, C. A.; Brook, J. R.; Bhatnagar, A.; Diez-Roux, A. V.; Holguin, F.; Hong, Y.; Luepker, R. V.; Mittleman, M. A.; et al. Particulate Matter Air Pollution and Cardiovascular Disease: An Update to the Scientific Statement from the American Heart Association. *Circulation*. 2010. https://doi.org/10.1161/CIR.0b013e3181dbece1.

(9) Kim, K. H.; Kabir, E.; Kabir, S. A Review on the Human Health Impact of Airborne Particulate Matter. *Environment International*. 2015. https://doi.org/10.1016/j.envint.2014.10.005.

(10) Katanoda, K.; Sobue, T.; Satoh, H.; Tajima, K.; Suzuki, T.; Nakatsuka, H.; Takezaki, T.; Nakayama, T.; Nitta, H.; Tanabe, K.; et al. An Association between Long-Term Exposure to Ambient Air Pollution and Mortality from Lung Cancer and Respiratory Diseases in Japan. *J. Epidemiol.* **2011**. https://doi.org/10.2188/jea.JE20100098.

(11) Xing, Y. F.; Xu, Y. H.; Shi, M. H.; Lian, Y. X. The Impact of PM2.5 on the Human Respiratory System. *Journal of Thoracic Disease*. 2016. https://doi.org/10.3978/j.issn.2072-1439.2016.01.19.

(12) Li, T.; Hu, R.; Chen, Z.; Li, Q.; Huang, S.; Zhu, Z.; Zhou, L.-F. Fine Particulate Matter (PM(2.5)): The Culprit for Chronic Lung Diseases in China. *Chronic Dis. Transl. Med.* **2018**, *4* (3), 176–186. https://doi.org/10.1016/j.cdtm.2018.07.002.

(13) Du, Y.; Xu, X.; Chu, M.; Guo, Y.; Wang, J. Air Particulate Matter and Cardiovascular Disease: The Epidemiological, Biomedical and Clinical Evidence. *J. Thorac. Dis.* **2016**, *8* (1), E8–E19. https://doi.org/10.3978/j.issn.2072-1439.2015.11.37.

(14) EPA. NAAQS Table | Criteria Air Pollutants | US EPA https://www.epa.gov/criteria-air-pollutants/naaqs-table (accessed Feb 9, 2020).

(15) WHO. Ambient (outdoor) air pollution https://www.who.int/news-room/fact-sheets/detail/ambient-(outdoor)-air-quality-and-health (accessed Feb 9, 2020).

(16) Standards - Air Quality - Environment - European Commission https://ec.europa.eu/environment/air/quality/standards.htm (accessed Feb 9, 2020).

(17) MEE, P. Ambient air quality standards http://english.mee.gov.cn/Resources/standards/Air_Environment/quality_standard1/20160 5/t20160511_337502.shtml (accessed Feb 9, 2020).

(18) Barker, T.; Bashmakov, I.; Bernstein, L.; Bogner, J. E.; Bosch, P. R.; Dave, R.; Metz, B.; Nabuurs, G. J. Contribution of Working Group III to the Fourth Assessment Report of the IPCC: Technical Summary. In *Climate Change 2007: Mitigation contribution of Working Group III to the Fourth Assessment Report of the Intergovernmental Panel on Climate Change, Intergovernmental Panel on Climate Change*; Cambridge University Press, 2009; pp 27–93.

(19) He, L.; Chen, H.; Rangognio, J.; Yahyaoui, A.; Colin, P.; Wang, J.; Daële, V.; Mellouki, A. Fine Particles at a Background Site in Central France: Chemical Compositions, Seasonal Variations and Pollution Events. *Sci. Total Environ.* **2018**. https://doi.org/10.1016/j.scitotenv.2017.08.273.

(20) Razak, I. S.; Latif, M. T.; Jaafar, S. A.; Khan, M. F.; Mushrifah, I. Surfactants in Atmospheric Aerosols and Rainwater around Lake Ecosystem. *Environ. Sci. Pollut. Res.* **2015**, *22* (8), 6024–6033.

(21) Cass, G. R.; Hughes, L. A.; Bhave, P.; Kleeman, M. J.; Allen, J. O.; Salmon, L. G. The Chemical Composition of Atmospheric Ultrafine Particles. *Philos. Trans. R. Soc. A Math. Phys. Eng. Sci.* **2000**. https://doi.org/10.1098/rsta.2000.0670.

(22) Lomnicki, S.; Truong, H.; Vejerano, E.; Dellinger, B. Copper Oxide-Based Model of Persistent Free Radical Formation on Combustion-Derived Particulate Matter. *Environ. Sci. Technol.* **2008**, *42* (13), 4982–4988. https://doi.org/10.1021/es071708h.

(23) Kennedy, I. M. The Health Effects of Combustion-Generated Aerosols. *Proc. Combust. Inst.* **2007**. https://doi.org/10.1016/j.proci.2006.08.116.

(24) Xu, M.; Wu, T.; Tang, Y.-T.; Chen, T.; Khachatryan, L.; Iyer, P. R.; Guo, D.; Chen, A.; Lyu, M.; Li, J.; et al. Environmentally Persistent Free Radicals in PM2.5: A Review. *Waste Dispos. Sustain. Energy* **2019**. https://doi.org/10.1007/s42768-019-00021-z.

(25) Nowakowski, M.; Rostkowski, P.; Andrzejewski, P. Oxidized Forms of Polycyclic Aromatic Hydrocarbons (Oxy-PAHs): Determination in Suspended Particulate Matter (SPM). In *15th International Conference on Environmental Science and Technology*; 2017.

(26) Cormier, S. A.; Lomnicki, S.; Backes, W.; Dellinger, B. Origin and Health Impacts of Emissions of Toxic By-Products and Fine Particles from Combustion and Thermal Treatment of Hazardous Wastes and Materials. *Environ. Health Perspect.* **2006**, *114* (6), 810–817.

(27) Yang, L.; Liu, G.; Zheng, M.; Jin, R.; Zhu, Q.; Zhao, Y.; Wu, X.; Xu, Y. Highly Elevated Levels and Particle-Size Distributions of Environmentally Persistent Free Radicals in Haze-Associated Atmosphere. *Environ. Sci. Technol.* **2017**, *51* (14), 7936–7944. https://doi.org/10.1021/acs.est.7b01929.

(28) Gehling, W.; Dellinger, B. Environmentally Persistent Free Radicals and Their Lifetimes in PM 2.5. *Environ. Sci. Technol.* **2013**, *47* (15), 8172–8178. https://doi.org/10.1021/es401767m.

(29) Dellinger, B.; Lomnicki, S.; Khachatryan, L.; Maskos, Z.; Hall, R. W.; Adounkpe, J.; McFerrin, C.; Truong, H. Formation and Stabilization of Persistent Free Radicals. *Proc. Combust. Inst.* **2007**, *31 I*, 521–528. https://doi.org/10.1016/j.proci.2006.07.172.

(30) Kiruri, L. W.; Khachatryan, L.; Dellinger, B.; Lomnicki, S. Effect of Copper Oxide Concentration on the Formation and Persistency of Environmentally Persistent Free Radicals (EPFRs) in Particulates. *Environ. Sci. Technol.* **2014**, *48* (4), 2212–2217. https://doi.org/10.1021/es404013g.

(31) Kelley, M. A.; Hebert, V. Y.; Thibeaux, T. M.; Orchard, M. A.; Hasan, F.; Cormier, S. A.; Thevenot, P. T.; Lomnicki, S. M.; Varner, K. J.; Dellinger, B.; et al. Model Combustion-Generated Particulate Matter Containing Persistent Free Radicals Redox Cycle to Produce Reactive Oxygen Species. *Chem. Res. Toxicol.* **2013**, *26* (12), 1862–1871. https://doi.org/10.1021/tx400227s.

(32) Khachatryan, L.; Vejerano, E.; Lomnicki, S.; Dellinger, B. Environmentally Persistent Free Radicals (EPFRs). 1. Generation of Reactive Oxygen Species in Aqueous Solutions. *Environ. Sci. Technol.* **2011**, *45* (19), 8559–8566. https://doi.org/10.1021/es201309c.

(33) Dellinger, B.; Pryor, W.; Cueto, R.; Squadrito, G.; Hegde, V.; Deutsch, W. Role of Free Radicals in the Toxicity of Airborne Fine Particulate Matter. *Chem. Res. Toxicol.* **2001**, *14* (10), 1371–1377. https://doi.org/10.1021/tx010050x.

(34) Ayres, J. G.; Borm, P.; Cassee, F. R.; Castranova, V.; Donaldson, K.; Ghio, A.; Harrison, R. M.; Hider, R.; Kelly, F.; Kooter, I. M.; et al. Evaluating the Toxicity of Airborne

Particulate Matter and Nanoparticles by Measuring Oxidative Stress Potential - A Workshop Report and Consensus Statement. In *Inhalation Toxicology*; 2008; Vol. 20, pp 75–99. https://doi.org/10.1080/08958370701665517.

(35) Nel, A.; Xia, T.; Mädler, L.; Li, N. Toxic Potential of Materials at the Nanolevel. *Science*. 2006, pp 622–627. https://doi.org/10.1126/science.1114397.

(36) Bährle, C.; Nick, T. U.; Bennati, M.; Jeschke, G.; Vogel, F. High-Field Electron Paramagnetic Resonance and Density Functional Theory Study of Stable Organic Radicals in Lignin: Influence of the Extraction Process, Botanical Origin, and Protonation Reactions on the Radical g Tensor. *J. Phys. Chem. A* **2015**, *119* (24), 6475–6482.

(37) Liu, J.; Jiang, X.; Shen, J.; Zhang, H. Chemical Properties of Superfine Pulverized Coal Particles. Part 1. Electron Paramagnetic Resonance Analysis of Free Radical Characteristics. *Adv. Powder Technol.* **2014**, *25* (3), 916–925.

(38) Zhao, S.; Gao, P.; Miao, D.; Wu, L.; Qian, Y.; Chen, S.; Sharma, V. K.; Jia, H. Formation and Evolution of Solvent-Extracted and Nonextractable Environmentally Persistent Free Radicals in Fly Ash of Municipal Solid Waste Incinerators. *Environ. Sci. Technol.* **2019**, *53* (17), 10120–10130.

(39) Wang, P.; Pan, B.; Li, H.; Huang, Y.; Dong, X.; Ai, F.; Liu, L.; Wu, M.; Xing, B. The Overlooked Occurrence of Environmentally Persistent Free Radicals in an Area with Low-Rank Coal Burning, Xuanwei, China. *Environ. Sci. Technol.* **2018**, *52* (3), 1054–1061.

(40) Cormier, S. A.; Lomnicki, S.; Backes, W.; Dellinger, B. Origin and Health Impacts of Emissions of Toxic By-Products and Fine Particles from Combustion and Thermal Treatment of Hazardous Wastes and Materials. *Environmental Health Perspectives*. 2006, pp 810–817. https://doi.org/10.1289/ehp.8629.

(41) Ingram, D. J. E.; Tapley, J. G.; Jackson, R.; Bond, R. L.; Murnaghan, A. R. Paramagnetic Resonance in Carbonaceous Solids. *Nature* **1954**, *174* (4434), 797–798.

(42) Pryor, W. A. Free Radicals in Biological Systems. *Sci. Am.* **1970**, *223* (2), 70–83.

(43) Pryor, W. A.; Terauchi, K.; Davis Jr, W. H. Electron Spin Resonance (ESR) Study of Cigarette Smoke by Use of Spin Trapping Techniques. *Environ. Health Perspect.* **1976**, *16*, 161–176.

(44) Lomnicki, S.; Dellinger, B. A Detailed Mechanism of the Surface-Mediated Formation of PCDD/F from the Oxidation of 2-Chlorophenol on a CuO/Silica Surface. *J. Phys. Chem. A* **2003**. https://doi.org/10.1021/jp026045z.

(45) Weber, P.; Dinjus, E.; Stieglitz, L. The Role of Copper(II) Chloride in the Formation of Organic Chlorine in Fly Ash. *Chemosphere* **2001**. https://doi.org/10.1016/S0045-6535(00)00230-7.

(46) Okeson, C. D.; Riley, M. R.; Fernandez, A.; Wendt, J. O. L. Impact of the Composition of Combustion Generated Fine Particles on Epithelial Cell Toxicity: Influences of Metals on Metabolism. In *Chemosphere*; 2003. https://doi.org/10.1016/S0045-6535(02)00721-X.

(47) Fahmy, B.; Ding, L.; You, D.; Lomnicki, S.; Dellinger, B.; Cormier, S. A. In Vitro and in Vivo Assessment of Pulmonary Risk Associated with Exposure to Combustion Generated Fine Particles. *Environ. Toxicol. Pharmacol.* **2010**. https://doi.org/10.1016/j.etap.2009.12.007.

(48) Nganai, S.; Lomnicki, S.; Dellinger, B. Ferric Oxide Mediated Formation of PCDD/Fs from 2-Monochlorophenol. *Environ. Sci. Technol.* **2009**, *43* (2), 368–373. https://doi.org/10.1021/es8022495.

(49) Alderman, S. L.; Farquar, G. R.; Poliakoff, E. D.; Dellinger, B. An Infrared and X-Ray Spectroscopic Study of the Reactions of 2-Chlorophenol, 1, 2-Dichlorobenzene, and Chlorobenzene with Model CuO/Silica Fly Ash Surfaces. *Environ. Sci. Technol.* **2005**, *39* (19), 7396–7401.

(50) Thevenot, P. T.; Saravia, J.; Jin, N.; Giaimo, J. D.; Chustz, R. E.; Mahne, S.; Kelley, M. A.; Hebert, V. Y.; Dellinger, B.; Dugas, T. R.; et al. Radical-Containing Ultrafine Particulate Matter Initiates Epithelial-to-Mesenchymal Transitions in Airway Epithelial Cells. *Am. J. Respir. Cell Mol. Biol.* **2013**. https://doi.org/10.1165/rcmb.2012-0052OC.

(51) Balakrishna, S.; Saravia, J.; Thevenot, P.; Ahlert, T.; Lominiki, S.; Dellinger, B.; Cormier, S. A. Environmentally Persistent Free Radicals Induce Airway Hyperresponsiveness in Neonatal Rat Lungs. *Part. Fibre Toxicol.* **2011**. https://doi.org/10.1186/1743-8977-8-11.

(52) Vejerano, E. W.; Rao, G.; Khachatryan, L.; Cormier, S. A.; Lomnicki, S. M. Environmentally Persistent Free Radicals: Insights on a New Class of Pollutants. *Environ. Sci. Technol.* **2018**, acs.est.7b04439. https://doi.org/10.1021/acs.est.7b04439.

(53) Borrowman, C. K.; Zhou, S.; Burrow, T. E.; Abbatt, J. P. D. Formation of Environmentally Persistent Free Radicals from the Heterogeneous Reaction of Ozone and Polycyclic Aromatic Compounds. *Phys. Chem. Chem. Phys.* **2016**. https://doi.org/10.1039/c5cp05606c.

(54) Dela Cruz, A. L. N.; Gehling, W.; Lomnicki, S.; Cook, R.; Dellinger, B. Detection of Environmentally Persistent Free Radicals at a Superfund Wood Treating Site. *Environ. Sci. Technol.* **2011**. https://doi.org/10.1021/es2012947.

(55) Penning, T. M.; Burczynski, M. E.; Hung, C. F.; McCoull, K. D.; Palackal, N. T.; Tsuruda, L. S. Dihydrodiol Dehydrogenases and Polycyclic Aromatic Hydrocarbon Activation: Generation of Reactive and Redox Active o-Quinones. *Chemical Research in Toxicology*. 1999. https://doi.org/10.1021/tx980143n.

(56) Dellinger, B.; Khachatryan, L.; Masko, S.; Lomnicki, S. Free Radicals in Tobacco Smoke. *Mini. Rev. Org. Chem.* **2011**, *8* (4), 427–433. https://doi.org/10.2174/157019311797440281.

(57) Gehling, W.; Khachatryan, L.; Dellinger, B. Hydroxyl Radical Generation from Environmentally Persistent Free Radicals (EPFRs) in PM2.5. *Environ. Sci. Technol.* **2014**, *48* (8), 4266–4272. https://doi.org/10.1021/es401770y.

(58) Donaldson, K.; Beswick, P. H.; Gilmour, P. S. Free Radical Activity Associated with the Surface of Particles: A Unifying Factor in Determining Biological Activity? *Toxicol. Lett.* **1996**, *88* (1–3), 293–298.

(59) Borish, E. T.; Cosgrove, J. P.; Church, D. F.; Deutsch, W. A.; Pryor, W. A. Cigarette Tar Causes Single-Strand Breaks in DNA. *Biochem. Biophys. Res. Commun.* **1985**, *133* (2), 780–786.

(60) Chuang, G. C.; Xia, H.; Mahne, S. E.; Varner, K. J. Environmentally Persistent Free Radicals Cause Apoptosis in HL-1 Cardiomyocytes. *Cardiovasc. Toxicol.* **2017**, *17* (2), 140–149. https://doi.org/10.1007/s12012-016-9367-x.

(61) Balakrishna, S.; Lomnicki, S.; Mcavey, K. M.; Cole, R. B.; Dellinger, B.; Cormier, S. A. Environmentally Persistent Free Radicals Amplify Ultrafine Particle Mediated Cellular Oxidative Stress and Cytotoxicity. **2009**. https://doi.org/10.1186/1743-8977-6-11.

(62) Burn, B. R.; Varner, K. J. Environmentally Persistent Free Radicals Compromise Left Ventricular Function during Ischemia/Reperfusion Injury. *Am. J. Physiol. - Hear. Circ. Physiol.* **2015**. https://doi.org/10.1152/ajpheart.00891.2014.

(63) Lord, K.; Moll, D.; Lindsey, J. K.; Mahne, S.; Raman, G.; Dugas, T.; Cormier, S.; Troxlair, D.; Lomnicki, S.; Dellinger, B.; et al. Environmentally Persistent Free Radicals Decrease Cardiac Function before and after Ischemia/Reperfusion Injury in Vivo. *J. Recept. Signal Transduct.* **2011**. https://doi.org/10.3109/10799893.2011.555767.

(64) Mahne, S.; Chuang, G. C.; Pankey, E.; Kiruri, L.; Kadowitz, P. J.; Dellinger, B.; Varner, K. J. Environmentally Persistent Free Radicals Decrease Cardiac Function and Increase Pulmonary Artery Pressure. *AJP Hear. Circ. Physiol.* **2012**. https://doi.org/10.1152/ajpheart.00545.2012.

(65) Filep, Á.; Fodor, G. H.; Kun-Szabó, F.; Tiszlavicz, L.; Rázga, Z.; Bozsó, G.; Bozóki, Z.; Szabó, G.; Peták, F. Exposure to Urban PM1 in Rats: Development of Bronchial Inflammation and Airway Hyperresponsiveness. *Respir. Res.* **2016**. https://doi.org/10.1186/s12931-016-0332-9.

(66) Wang, P.; Thevenot, P.; Saravia, J.; Ahlert, T.; Cormier, S. A. Radical-Containing Particles Activate Dendritic Cells and Enhance Th17 Inflammation in a Mouse Model of Asthma. *Am. J. Respir. Cell Mol. Biol.* **2011**. https://doi.org/10.1165/rcmb.2011-0001OC.

(67) Wang, Y.; Xiong, L.; Tang, M. Toxicity of Inhaled Particulate Matter on the Central Nervous System: Neuroinflammation, Neuropsychological Effects and Neurodegenerative Disease. *Journal of Applied Toxicology*. 2017. https://doi.org/10.1002/jat.3451.

(68) Allen, J. L.; Oberdorster, G.; Morris-Schaffer, K.; Wong, C.; Klocke, C.; Sobolewski, M.;

Conrad, K.; Mayer-Proschel, M.; Cory-Slechta, D. A. Developmental Neurotoxicity of Inhaled Ambient Ultrafine Particle Air Pollution: Parallels with Neuropathological and Behavioral Features of Autism and Other Neurodevelopmental Disorders. *Neurotoxicology* **2017**. https://doi.org/10.1016/j.neuro.2015.12.014.

(69) Lucio G. Costa; Toby B. Cole; Jacki Coburn; Yu-Chi Chang; Khoi Dao; Pamela J. Roqué. Neurotoxicity of Traffic-Related Air Pollution. *Neurotox. traffic-related air Pollut.* **2015**. https://doi.org/10.1016/j.neuro.2015.11.008.

(70) Solaimani, P.; Saffari, A.; Sioutas, C.; Bondy, S. C.; Campbell, A. Exposure to Ambient Ultrafine Particulate Matter Alters the Expression of Genes in Primary Human Neurons. *Neurotoxicology* **2017**. https://doi.org/10.1016/j.neuro.2016.11.001.

(71) Ljubimova, J. Y.; Braubach, O.; Patil, R.; Chiechi, A.; Tang, J.; Galstyan, A.; Shatalova, E. S.; Kleinman, M. T.; Black, K. L.; Holler, E. Coarse Particulate Matter (PM2.5–10) in Los Angeles Basin Air Induces Expression of Inflammation and Cancer Biomarkers in Rat Brains. *Sci. Rep.* **2018**, *8* (1), 5708. https://doi.org/10.1038/s41598-018-23885-3.

(72) Abdel-Shafy, H. I.; Mansour, M. S. M. A Review on Polycyclic Aromatic Hydrocarbons: Source, Environmental Impact, Effect on Human Health and Remediation. *Egyptian Journal of Petroleum*. 2016. https://doi.org/10.1016/j.ejpe.2015.03.011.

(73) Zhang, Y.; Tao, S. Global Atmospheric Emission Inventory of Polycyclic Aromatic Hydrocarbons (PAHs) for 2004. *Atmos. Environ.* **2009**. https://doi.org/10.1016/j.atmosenv.2008.10.050.

(74) Lee, B.-K. Sources, Distribution and Toxicity of Polyaromatic Hydrocarbons (PAHs) in Particulate Matter. In *Air Pollution*; 2010. https://doi.org/10.5772/10045.

(75) Ravindra, K.; Sokhi, R.; Van Grieken, R. Atmospheric Polycyclic Aromatic Hydrocarbons: Source Attribution, Emission Factors and Regulation. *Atmospheric Environment*. 2008. https://doi.org/10.1016/j.atmosenv.2007.12.010.

(76) Zhang, Y.; Zhang, L.; Huang, Z.; Li, Y.; Li, J.; Wu, N.; He, J.; Zhang, Z.; Liu, Y.; Niu, Z. Pollution of Polycyclic Aromatic Hydrocarbons (PAHs) in Drinking Water of China: Composition, Distribution and Influencing Factors. *Ecotoxicol. Environ. Saf.* **2019**, *177*, 108–116. https://doi.org/10.1016/J.ECOENV.2019.03.119.

(77) Masiol, M.; Hofer, A.; Squizzato, S.; Piazza, R.; Rampazzo, G.; Pavoni, B. Carcinogenic and Mutagenic Risk Associated to Airborne Particle-Phase Polycyclic Aromatic Hydrocarbons: A Source Apportionment. *Atmos. Environ.* **2012**, *60*, 375–382. https://doi.org/10.1016/J.ATMOSENV.2012.06.073.

(78) Unwin, J.; Cocker, J.; Scobbie, E.; Chambers, H. An Assessment of Occupational Exposure to Polycyclic Aromatic Hydrocarbons in the UK. *Ann. Occup. Hyg.* **2006**. https://doi.org/10.1093/annhyg/mel010.

(79) Armstrong, B.; Hutchinson, E.; Unwin, J.; Fletcher, T. Lung Cancer Risk after Exposure

to Polycyclic Aromatic Hydrocarbons: A Review and Meta-Analysis. *Environmental Health Perspectives*. 2004. https://doi.org/10.1289/ehp.6895.

(80) Xia, Z.; Duan, X.; Tao, S.; Qiu, W.; Liu, D.; Wang, Y.; Wei, S.; Wang, B.; Jiang, Q.; Lu, B.; et al. Pollution Level, Inhalation Exposure and Lung Cancer Risk of Ambient Atmospheric Polycyclic Aromatic Hydrocarbons (PAHs) in Taiyuan, China. *Environ. Pollut.* **2013**, *173*, 150–156. https://doi.org/10.1016/J.ENVPOL.2012.10.009.

(81) Clark, J. D.; Serdar, B.; Lee, D. J.; Arheart, K.; Wilkinson, J. D.; Fleming, L. E. Exposure to Polycyclic Aromatic Hydrocarbons and Serum Inflammatory Markers of Cardiovascular Disease. *Environ. Res.* **2012**, *117*, 132–137. https://doi.org/10.1016/J.ENVRES.2012.04.012.

(82) Alshaarawy, O.; Elbaz, H. A.; Andrew, M. E. The Association of Urinary Polycyclic Aromatic Hydrocarbon Biomarkers and Cardiovascular Disease in the US Population. *Environ. Int.* **2016**, *89–90*, 174–178. https://doi.org/10.1016/J.ENVINT.2016.02.006.

(83) Huo, X.; Wu, Y.; Xu, L.; Zeng, X.; Qin, Q.; Xu, X. Maternal Urinary Metabolites of PAHs and Its Association with Adverse Birth Outcomes in an Intensive E-Waste Recycling Area. *Environ. Pollut.* **2019**, *245*, 453–461. https://doi.org/10.1016/J.ENVPOL.2018.10.098.

(84) Nethery, E.; Wheeler, A. J.; Fisher, M.; Sjödin, A.; Li, Z.; Romanoff, L. C.; Foster, W.; Arbuckle, T. E. Urinary Polycyclic Aromatic Hydrocarbons as a Biomarker of Exposure to PAHs in Air: A Pilot Study among Pregnant Women. *J. Expo. Sci. Environ. Epidemiol.* **2012**. https://doi.org/10.1038/jes.2011.32.

(85) Campo, L.; Rossella, F.; Pavanello, S.; Mielzynska, D.; Siwinska, E.; Kapka, L.; Bertazzi, P. A.; Fustinoni, S. Urinary Profiles to Assess Polycyclic Aromatic Hydrocarbons Exposure in Coke-Oven Workers. *Toxicol. Lett.* **2010**, *192* (1), 72–78. https://doi.org/10.1016/J.TOXLET.2008.12.018.

(86) Xue, W.; Warshawsky, D. Metabolic Activation of Polycyclic and Heterocyclic Aromatic Hydrocarbons and DNA Damage: A Review. *Toxicol. Appl. Pharmacol.* **2005**. https://doi.org/10.1016/j.taap.2004.11.006.

(87) Shimada, T.; Fujii-Kuriyama, Y. Metabolic Activation of Polycyclic Aromatic Hydrocarbons to Carcinogens by Cytochromes P450 1A1 and 1B1. *Cancer Science*. 2004. https://doi.org/10.1111/j.1349-7006.2004.tb03162.x.

(88) Androutsopoulos, V. P.; Tsatsakis, A. M.; Spandidos, D. A. Cytochrome P450 CYP1A1: Wider Roles in Cancer Progression and Prevention. *BMC Cancer*. 2009. https://doi.org/10.1186/1471-2407-9-187.

(89) Jouraeva, V. A.; Johnson, D. L.; Hassett, J. P.; Nowak, D. J. Differences in Accumulation of PAHs and Metals on the Leaves of Tiliaxeuchlora and Pyrus Calleryana. *Environ. Pollut.* **2002**, *120* (2), 331–338. https://doi.org/10.1016/S0269-7491(02)00121-5.

(90) Allan, I. J.; O'Connell, S. G.; Meland, S.; Bæk, K.; Grung, M.; Anderson, K. A.; Ranneklev, S. B. PAH Accessibility in Particulate Matter from Road-Impacted Environments. *Environ. Sci. Technol.* **2016**. https://doi.org/10.1021/acs.est.6b00504.

(91) Wang, J.; Geng, N. B.; Xu, Y. F.; Zhang, W. D.; Tang, X. Y.; Zhang, R. Q. PAHs in PM2.5 in Zhengzhou: Concentration, Carcinogenic Risk Analysis, and Source Apportionment. *Environ. Monit. Assess.* **2014**. https://doi.org/10.1007/s10661-014-3940-1.

(92) Chen, Y.; Li, X.; Zhu, T.; Han, Y.; Lv, D. PM2.5-Bound PAHs in Three Indoor and One Outdoor Air in Beijing: Concentration, Source and Health Risk Assessment. *Sci. Total Environ.* **2017**. https://doi.org/10.1016/j.scitotenv.2017.01.214.

(93) Wu, D.; Wang, Z.; Chen, J.; Kong, S.; Fu, X.; Deng, H.; Shao, G.; Wu, G. Polycyclic Aromatic Hydrocarbons (PAHs) in Atmospheric PM2.5 and PM10 at a Coal-Based Industrial City: Implication for PAH Control at Industrial Agglomeration Regions, China. *Atmos. Res.* **2014**. https://doi.org/10.1016/j.atmosres.2014.06.012.

(94) Pehnec, G.; Jakovljević, I. Carcinogenic Potency of Airborne Polycyclic Aromatic Hydrocarbons in Relation to the Particle Fraction Size. *Int. J. Environ. Res. Public Health* **2018**. https://doi.org/10.3390/ijerph15112485.

(95) Schauer, C.; Niessner, R.; Pöschl, U. Polycyclic Aromatic Hydrocarbons in Urban Air Particulate Matter: Decadal and Seasonal Trends, Chemical Degradation, and Sampling Artifacts. *Environ. Sci. Technol.* **2003**. https://doi.org/10.1021/es034059s.

(96) Callén, M. S.; De La Cruz, M. T.; López, J. M.; Mastral, A. M. PAH in Airborne Particulate Matter.: Carcinogenic Character of PM10 Samples and Assessment of the Energy Generation Impact. In *Fuel Processing Technology*; 2011. https://doi.org/10.1016/j.fuproc.2010.05.019.

(97) Xu, S.; Liu, W.; Tao, S. Emission of Polycyclic Aromatic Hydrocarbons in China. *Environ. Sci. Technol.* **2006**, *40* (3), 702–708. https://doi.org/10.1021/es0517062.

(98) Wang, X.; Cheng, H.; Xu, X.; Zhuang, G.; Zhao, C. A Wintertime Study of Polycyclic Aromatic Hydrocarbons in PM2.5 and PM2.5-10 in Beijing: Assessment of Energy Structure Conversion. *J. Hazard. Mater.* **2008**. https://doi.org/10.1016/j.jhazmat.2007.12.092.

(99) Yang, M.; Wang, Y.; Li, H.; Li, T.; Nie, X.; Cao, F.; Yang, F.; Wang, Z.; Wang, T.; Qie, G.; et al. Polycyclic Aromatic Hydrocarbons (PAHs) Associated with PM2.5 within Boundary Layer: Cloud/Fog and Regional Transport. *Sci. Total Environ.* **2018**, *627*, 613–621. https://doi.org/10.1016/J.SCITOTENV.2018.01.014.

(100) Saxena, S. C.; Jotshi, C. K. Management and Combustion of Hazardous Wastes. *Prog. Energy Combust. Sci.* **1996**, *22* (5), 401–425.

(101) EPA. *Environmental Protection Agency 40 CFR Part 63 NESHAP: National Emission*

Standards for Hazardous Air Pollutants: Standards for Hazardous Waste Combustors: Reconsideration; Final Rule; 2008.

(102) Goldstein, J. I.; Newbury, D. E.; Michael, J. R.; Ritchie, N. W. M.; Scott, J. H. J.; Joy, D. C. *Scanning Electron Microscopy and X-Ray Microanalysis*; 2017. https://doi.org/10.1007/978-1-4939-6676-9.

(103) Wertz, J. *Electron Spin Resonance: Elementary Theory and Practical Applications*; Springer Science & Business Media, 2012.

(104) Bruker. EPR Detection of the Superoxide Free Radical with the Nitrone Spin Traps DMPO and BMPO. *Bruker* **2008**, 5–8.

(105) Zhao, H.; Joseph, J.; Zhang, H.; Karoui, H.; Kalyanaraman, B. Synthesis and Biochemical Applications of a Solid Cyclic Nitrone Spin Trap: A Relatively Superior Trap for Detecting Superoxide Anions and Glutathiyl Radicals. *Free Radic. Biol. Med.* **2001**. https://doi.org/10.1016/S0891-5849(01)00619-0.

(106) Sparkman, O. D.; Penton, Z.; Kitson, F. G. *Gas Chromatography and Mass Spectrometry: A Practical Guide*; 2011. https://doi.org/10.1016/C2009-0-17039-3.

(107) Hites, R. A. Development of Gas Chromatographic Mass Spectrometry. *Analytical Chemistry*. 2016. https://doi.org/10.1021/acs.analchem.6b01628.

(108) Domon, B.; Aebersold, R. Mass Spectrometry and Protein Analysis. *Science (80-.).* **2006**, *312* (5771), 212–217.

(109) Thevenot, P. T.; Saravia, J.; Jin, N.; Giaimo, J. D.; Chustz, R. E.; Mahne, S.; Kelley, M. A.; Hebert, V. Y.; Dellinger, B.; Dugas, T. R.; et al. Radical-Containing Ultrafine Particulate Matter Initiates Epithelial-to-Mesenchymal Transitions in Airway Epithelial Cells. *Am. J. Respir. Cell Mol. Biol.* **2013**. https://doi.org/10.1165/rcmb.2012-0052OC.

(110) Balakrishna, S.; Lomnicki, S.; McAvey, K. M.; Cole, R. B.; Dellinger, B.; Cormier, S. A. Environmentally Persistent Free Radicals Amplify Ultrafine Particle Mediated Cellular Oxidative Stress and Cytotoxicity. *Part. Fibre Toxicol.* **2009**. https://doi.org/10.1186/1743-8977-6-11.

(111) Charles, B.; Fredeen, K. J. Concepts, Instrumentation and Techniques in Inductively Coupled Plasma Optical Emission Spectrometry. *Perkin Elmer Corp.* **1997**.

(112) Hou, X.; Amais, R. S.; Jones, B. T.; Donati, G. L. Inductively Coupled Plasma Optical Emission Spectrometry. *Encycl. Anal. Chem. Appl. Theory Instrum.* **2006**, 1–25.

(113) Lamble, K. J.; Hill, S. J. Microwave Digestion Procedures for Environmental Matrices. Critical Review. *Analyst* **1998**, *123* (7), 103R-133R.

(114) Moran, P. A. P.; Smith, C. A. B. The Correlation Between Relatives on the Supposition of Mendelian Inheritance. *Trans. R. Soc. Edinburgh* **1918**, *52*, 438–899.

(115) Sauvé, S.; Desrosiers, M. A Review of What Is an Emerging Contaminant. *Chemistry Central Journal*. 2014. https://doi.org/10.1186/1752-153X-8-15.

(116) Nowak, D. J.; Crane, D. E.; Stevens, J. C. Air Pollution Removal by Urban Trees and Shrubs in the United States. *Urban For. Urban Green.* **2006**, *4* (3), 115–123. https://doi.org/https://doi.org/10.1016/j.ufug.2006.01.007.

(117) Terzaghi, E.; Wild, E.; Zacchello, G.; Cerabolini, B. E. L.; Jones, K. C.; Di Guardo, A. Forest Filter Effect: Role of Leaves in Capturing/Releasing Air Particulate Matter and Its Associated PAHs. *Atmos. Environ.* **2013**, *74*, 378–384. https://doi.org/https://doi.org/10.1016/j.atmosenv.2013.04.013.

(118) Yin, S.; Shen, Z.; Zhou, P.; Zou, X.; Che, S.; Wang, W. Quantifying Air Pollution Attenuation within Urban Parks: An Experimental Approach in Shanghai, China. *Environ. Pollut.* **2011**. https://doi.org/10.1016/j.envpol.2011.03.009.

(119) McDonald, A. G.; Bealey, W. J.; Fowler, D.; Dragosits, U.; Skiba, U.; Smith, R. I.; Donovan, R. G.; Brett, H. E.; Hewitt, C. N.; Nemitz, E. Quantifying the Effect of Urban Tree Planting on Concentrations and Depositions of PM10 in Two UK Conurbations. *Atmos. Environ.* **2007**, *41* (38), 8455–8467. https://doi.org/10.1016/j.atmosenv.2007.07.025.

(120) Yang, J.; McBride, J.; Zhou, J.; Sun, Z. The Urban Forest in Beijing and Its Role in Air Pollution Reduction. *Urban For. Urban Green.* **2005**, *3* (2), 65–78. https://doi.org/https://doi.org/10.1016/j.ufug.2004.09.001.

(121) Sæbø, A.; Popek, R.; Nawrot, B.; Hanslin, H. M.; Gawronska, H.; Gawronski, S. W. Plant Species Differences in Particulate Matter Accumulation on Leaf Surfaces. *Sci. Total Environ.* **2012**, *427–428*, 347–354. https://doi.org/10.1016/j.scitotenv.2012.03.084.

(122) Chen, L.; Liu, C.; Zhang, L.; Zou, R.; Zhang, Z. Variation in Tree Species Ability to Capture and Retain Airborne Fine Particulate Matter (PM2.5). *Sci. Rep.* **2017**. https://doi.org/10.1038/s41598-017-03360-1.

(123) Song, Y.; Maher, B. A.; Li, F.; Wang, X.; Sun, X.; Zhang, H. Particulate Matter Deposited on Leaf of Five Evergreen Species in Beijing, China: Source Identification and Size Distribution. *Atmos. Environ.* **2015**. https://doi.org/10.1016/j.atmosenv.2015.01.032.

(124) Sun, X.; Li, H.; Guo, X.; Sun, Y.; Li, S. Capacity of Six Shrub Species to Retain Atmospheric Particulates with Different Diameters. *Environ. Sci. Pollut. Res.* **2018**. https://doi.org/10.1007/s11356-017-0549-2.

(125) Liu, J.; Cao, Z.; Zou, S.; Liu, H.; Hai, X.; Wang, S.; Duan, J.; Xi, B.; Yan, G.; Zhang, S.; et al. An Investigation of the Leaf Retention Capacity, Efficiency and Mechanism for Atmospheric Particulate Matter of Five Greening Tree Species in Beijing, China. *Sci. Total Environ.* **2018**, *616–617*, 417–426. https://doi.org/10.1016/j.scitotenv.2017.10.314.

(126) *Guidance Manual BGI 900 High Volume Cascade Impactor*, 1.0.0.; BGI Incorporated:

Waltham, MA, 2008.

(127) Tian, L.; Koshland, C. P.; Yano, J.; Yachandra, V. K.; Yu, I. T. S.; Lee, S. C.; Lucas, D. Carbon-Centered Free Radicals in Particulate Matter Emissions from Wood and Coal Combustion. *Energy & Fuels* **2009**, *23* (5), 2523–2526. https://doi.org/10.1021/ef8010096.

(128) Chen, Q.; Sun, H.; Wang, M.; Mu, Z.; Wang, Y.; Li, Y.; Wang, Y.; Zhang, L.; Zhang, Z. Dominant Fraction of EPFRs from Nonsolvent-Extractable Organic Matter in Fine Particulates over Xi'an, China. *Environ. Sci. Technol.* **2018**. https://doi.org/10.1021/acs.est.8b01980.

(129) Antipova, A.; Ozdenerol, E. Using Longitudinal Employer Dynamics (LED) Data for the Analysis of Memphis Aerotropolis, Tennessee. *Appl. Geogr.* **2013**. https://doi.org/10.1016/j.apgeog.2013.04.013.

(130) Jia, C.; Foran, J. Air Toxics Concentrations, Source Identification, and Health Risks: An Air Pollution Hot Spot in Southwest Memphis, TN. *Atmos. Environ.* **2013**. https://doi.org/10.1016/j.atmosenv.2013.09.006.

(131) Jia, C.; James, W.; Kedia, S. Relationship of Racial Composition and Cancer Risks from Air Toxics Exposure in Memphis, Tennessee, USA. *Int. J. Environ. Res. Public Health* **2014**. https://doi.org/10.3390/ijerph110807713.

(132) Oyana, T. J.; Margai, F. *Spatial Analysis: Statistics, Visualization, and Computational Methods*; CRC Press, 2015.

(133) Brus, D. J.; Heuvelink, G. B. M. Optimization of Sample Patterns for Universal Kriging of Environmental Variables. *Geoderma* **2007**. https://doi.org/10.1016/j.geoderma.2006.10.016.

(134) Subramanian, R.; Donahue, N. M.; Bernardo-Bricker, A.; Rogge, W. F.; Robinson, A. L. Insights into the Primary-Secondary and Regional-Local Contributions to Organic Aerosol and PM2.5 Mass in Pittsburgh, Pennsylvania. *Atmos. Environ.* **2007**. https://doi.org/10.1016/j.atmosenv.2007.05.058.

(135) Cross, A. J.; Sinha, R. Meat-related Mutagens/Carcinogens in the Etiology of Colorectal Cancer. *Environ. Mol. Mutagen.* **2004**, *44* (1), 44–55.

(136) Lomnicki, S.; Dellinger, B. A Detailed Mechanism of the Surface-Mediated Formation of PCDD/F from the Oxidation of 2-Chlorophenol on a CuO/Silica Surface. *J. Phys. Chem. A* **2003**, *107* (22), 4387–4395. https://doi.org/10.1021/jp026045z.

VITA

Chuqi Guo was born in Qingyang, Gansu, China, in 1992. She attended Tianjin University of Technology and received the Bachelor of Science in Environmental Sciences in June 2014. She began her graduate study and worked as a Research Assistant in Dr. Slawo Lomnicki's research group at Louisiana State University, Baton Rouge, LA, since August 2014. At the same time, she worked as a trainee of LSU Superfund Research Center. She is a candidate to receive a Ph.D in Environmental Sciences in May 2020.